Modelling offshore sand waves

Samenstelling promotiecommissie:

prof. dr. ir. H.J. Grootenboer	Universiteit Twente, voorzitter/secretaris
prof. dr. S.J.M.H. Hulscher	Universiteit Twente, promotor
prof. dr. ir. H.J. de Vriend	Universiteit Twente, promotor
dr. R.M.J van Damme	Universiteit Twente
dr. A. Falqués	Universitat Politècnica de Catalunya
prof. dr. A. van Harten	Universiteit Twente
dr. A.J.F. van der Spek	Nederlands Instituut voor Toegepaste Geowetenschappen TNO
prof. dr. ir. G.S. Stelling	Technische Universiteit Delft
dr. A. Trentesaux	Université des Sciences et Technologies de Lille

ISBN 90-365-1931-4

Cover: Bed forms covered by ice in Lake Balaton, Hungary, Image courtesy by Fruzsi Török

Printed by PrintPartners Ipskamp BV, Enschede, The Netherlands

Modelling offshore sand waves

PROEFSCHRIFT

ter verkrijging van

de graad van doctor aan de Universiteit Twente,

op gezag van de rector magnificus,

prof. dr. F.A. van Vught,

volgens besluit van het College voor Promoties

in het openbaar te verdedigen

op vrijdag 20 juni 2003 om 16.45 uur

door

Attila Alexander Németh

geboren op 26 maart 1976

te Haskerland

Dit proefschrift is goedgekeurd door de promotoren:

prof. dr. S.J.M.H. Hulscher
prof. dr. ir. H.J. de Vriend

Contents

Acknowledgements **9**

Summary **11**

Samenvatting **15**

1 Introduction **19**
1.1 General 19
1.2 Sand waves and alluvial sand dunes 20
1.3 State-of-the art of modelling sand waves 21
1.4 Central research theme of this thesis 23
1.5 Keywords 25
1.6 Outline of this thesis 25
1.7 Acknowledgements 26

2 Offshore sand wave dynamics, engineering problems and future solutions **27**
2.1 Introduction 28
2.2 Seabed topography charts 29
2.2.1 Echo soundings 30
2.2.2 Satellite images 30
2.2.3 Bathymetry Assessment System 31
2.3 Pipelines and Cables 31
2.3.1 Free spans 32
2.3.2 Survey before, during and after use 33
2.4 Channels and navigational routes 34
2.5 Sand extraction 34
2.6 Burial of objects 35
2.7 Discussion and conclusions 36
2.8 Acknowledgements 37

3 Sand wave migration, a stability approach **39**
3.1 Introduction . . . 39
3.2 Description of the analytical model . . . 42
3.2.1 Scaling . . . 42
3.2.2 Flow model . . . 44
3.2.3 Boundary conditions and assumptions . . . 45
3.2.4 Sediment transport and seabed behaviour . . . 45
3.3 Linear stability analysis . . . 46
3.3.1 Basic state . . . 47
3.3.2 Perturbed state . . . 48
3.4 Results . . . 49
3.5 Sensitivity analysis . . . 52
3.6 Conclusions and Discussion . . . 54
3.7 Acknowledgements . . . 55
3.8 Appendix: Solution vertical flow structure . . . 56
3.9 Epilogue: Sand wave migration along a pipeline in the North Sea . . . 57
3.9.1 Bathymetric surveys along a North Sea pipeline . . . 57
3.9.2 Data pre-processing . . . 58
3.9.3 Application stability analysis . . . 60
3.9.4 Results stability analysis . . . 60
3.9.5 Conclusions . . . 61
3.10 Acknowledgements . . . 61

4 A sand wave simulation model **63**
4.1 Introduction . . . 63
4.2 2DV morphological model . . . 66
4.2.1 Flow model . . . 66
4.2.2 Sediment transport and seabed behaviour . . . 67
4.2.3 Boundary conditions and assumptions . . . 67
4.2.4 Discussion boundary conditions . . . 68
4.3 Numerical approximation . . . 70
4.3.1 Spatial discretisation . . . 70
4.3.2 Coordinate transformation . . . 71
4.3.3 Partial derivatives . . . 72
4.3.4 Temporal discretisation flow model and grid . . . 72
4.3.5 Initial values and time stepping . . . 74
4.4 Results . . . 75
4.4.1 Steady flow and sand waves in stability analysis . . . 76
4.4.2 Mathematical validation simulation model . . . 77
4.5 Discussion . . . 82
4.6 Conclusions . . . 83
4.7 Acknowledgements . . . 83
4.8 Appendix . . . 84

5 Finite amplitude sand waves **87**
5.1 Introduction . . . 88
5.2 Description of the model set up . . . 90
5.2.1 2DV Flow model . . . 90
5.2.2 Sediment transport and seabed behaviour . . . 91
5.2.3 Boundary conditions at the free surface and seabed . . . 92
5.2.4 Inflow and outflow boundary conditions . . . 93
5.3 Sand waves of finite extent, a morphostatic approach . . . 95
5.3.1 Unidirectional steady current . . . 96
5.3.2 Block current . . . 99
5.3.3 Discussion . . . 101
5.4 Sand wave evolution, a morphodynamic approach . . . 102
5.4.1 Unidirectional steady flow - The Gulf of Cadiz . . . 103
5.4.2 Periodic water motion - The North Sea . . . 108
5.5 Sand wave migration . . . 109
5.6 Sensitivity analysis . . . 110
5.6.1 Slope term . . . 110
5.6.2 Viscosity and resistance at the seabed . . . 112
5.6.3 Sand wave height and average water depth . . . 113
5.7 Dredging . . . 115
5.8 Conclusions . . . 118
5.9 Appendix . . . 120
5.9.1 Numerical considerations . . . 120

6 Conclusions **121**

7 Recommendations **123**
7.1 Data and validation . . . 123
7.1.1 Migrating sand waves . . . 123
7.1.2 Sand wave evolution . . . 123
7.2 Calculation time and use . . . 124
7.3 Stochastic variations and reality . . . 124
7.4 Sediment grain size . . . 124
7.5 Additional processes . . . 125

Bibliography **127**

Nomenclature **135**

About the author **141**

Acknowledgements

This work is supported by Technology Foundation STW, the applied science division of NWO and the technology programme of the Ministry of Economic Affairs and performed within the EU-sponsored project HUMOR (HUman interaction with large-scale coastal MORphologic evolution; EVK3-CT-2000-00037).

First of all, I would like to thank Suzanne Hulscher and Huib de Vriend. They have provided me with the opportunity to do this research and further develop myself. Looking back until the start of my masters thesis, I cannot imagine a place where I could have learned more. Thank you for your support, discussions and the obtained experiences. Furthermore, Ruud van Damme, thank you for your support, focus and critical insight. It was and is inspiring working with you.

Also, I would like to thank the members of the STW Users-Group for the inspiring meetings bringing (theoretical) research closer to real life issues: F.T.M. van den Berg and P. Beckers from STW, H. Keyser and A. Stolk from the North Sea Directorate, C. Laban and A.J.F. van der Spek from TNO - National Geological Survey, G.J. Wensink from ARGOSS, J. Appelman, L.L. Dorst, M.R. Gerding and W. Korbijn from The Hydrographic Service of the Royal Netherlands Navy, J. Dronkers and M. Boers from the National institute for Coastal and Marine Management (RIKZ) and R. Bijker.

From the University of Twente, mainly Department of Civil Engineering, I would like to thank: Frans Tillema, Mascha van der Voort, Henriette Otter, Astrid Blom, Mark Zuidgeest, Wendy Weijermars, Jebbe van der Werf, Cornelie van Driel, Joost van der Weide, Jeroen van den Adel, Marjolein Dohmen-Janssen and Michiel Knaapen for their discussions at the lunchtable, their opposition on the squashcourt and other good times.

Of course many thanks for the support throughout the years by: Anke Groothuijs, René Buijsrogge, Anne-Marie Klijnstra, Maureen Hendrikx, Dorette Alink-Olthof, Suse Engberts, Joke Meijer-Lentelink and Martijn Elferink.

I would like to thank my paranimfen Liliane Németh (coincidentally also my sister) and Pieter Roos on the piano, thanks Pieter. Thanks a lot for your help in organising the final day and standing by me during the defense. My parents Françoise Németh-Bresson and György Németh have always supported me unconditionally. They endured the ups and downs probably as much as I did. So this thesis can also be seen as an achievement for them. Finally, Valentina, whom I want to thank for her patience this last year. You helped me keep my feet on the ground and focus on my work.

Attila A. Németh

Enschede, 18th of May 2003

Summary

Sand waves form a prominent regular pattern in the offshore seabed of sandy shallow seas such as the North Sea. They can be found at water depths of 10 to 50 m. Their wavelengths can lead up to 500 m and their heights are typically several metres. The positions of sand wave crests and troughs slowly change in time. Sand waves are assumed to migrate in the direction of the asymmetry in the water motion, with typical velocities of up to several metres per year.

Practical relevance Several offshore activities are affected by sand waves. Based on interviews with managers and engineers from several institutions in the Netherlands, an overview of the sand wave problems and the ways in which they are handled is presented. Firstly, these sand waves decrease the least navigable depths and so they pose a threat to navigation routes and access channels. To avoid unsafe situations, continuous monitoring and, if necessary, dredging are required. Now, seabed topography charts are made using echo soundings. Combining such sounding techniques with satellite images may lead to more efficient ways to create bathymetry charts. Insight into the dynamics of sand waves can further reduce monitoring costs. Due to the movement of sand waves, pipelines and cables may become exposed. This may result in free spans, which in turn may cause the pipeline to buckle or break. Moreover, anchors and fishing nets may cause damage to the exposed pipelines and cables. In addition, exposed objects may be covered by a sand wave, making it difficult to locate them. Knowledge of sand wave behaviour will enable better management strategies and provide information supporting the design of offshore activities.

Linear stability analysis Hulscher [1996] investigated sand waves with a linear stability analysis, assuming they are free instabilities of the seabed-water system. In such an analysis, we start with a flat seabed over which water is flowing. Next, a range of wavy bed patterns is applied disturbing the water motion. Subsequently, the influence of the change in water motion over the seabed is investigated. If there is a net amount of sediment transported to the top of the bedform, the seabed is unstable and the bedform is growing. If there is a net flux towards the trough of the bedform, the seabed is stable. Based on linear theory, the bedform with a wavelength having the largest growth rate will dominate over the rest of the patterns. The analysis showed that for a certain range of wavelengths coinciding with observed sand waves, a net sediment flux exists oriented towards the crest over a tidal cycle, leading to

their development.

Here, we extended this linear analysis to investigate the physical mechanisms that may cause sand waves to migrate. We used a morphological model with one horizontal and one vertical direction (2DV). It contains the 2DV shallow water equations, with a general bed load formula taking the sediment transport into account. The water movement is coupled to the seabed evolution equation, based on a mass balance, with the sediment transport equation.

We introduced an asymmetry in the water motion by choosing a unidirectional steady current (M_0) together with (symmetrical) tidal motion (M_2). The results show sand waves migrating slowly in the direction of the asymmetry of the flow. The rates of migration and wavelengths found with this linear analysis agree with theoretical and empirical values reported in the literature. Furthermore, we compared the results with data of sand waves along a pipeline in the North Sea, showing good agreement.

However, this linear analysis is only valid for sand waves having small amplitudes and does not say anything about sand waves having larger finite amplitudes.

Numerical simulation To investigate the intermediate term behaviour of sand waves having finite amplitudes, we developed a numerical simulation model (2DV). This model allows us to investigate the evolutionary processes of sand waves after their initial evolution. The simulation model is validated mathematically by comparing the results for small amplitude sand waves with the performed linear stability analysis. The results show that the numerical model is able to reproduce the initial evolution of sand waves, as was found in the linear stability analysis.

Next, we used the developed simulation model to investigate the behaviour of offshore sand waves for finite values of their amplitude. We investigated a unidirectional steady current and unidirectional block current simulating tidal motion. Initially the sand waves develop exponentially, as follows from the linear stability analysis. Next, the growth rate diminishes, resulting in the stabilisation of the sand wave. The sand waves reach a maximum height of about 10-30% of the average water depth in a matter of decades. The mechanism causing sand waves to saturate is based on the increased importance for larger amplitudes of the principle that sediment is transported easier downhill than uphill. This process counteracts the shear stress at the seabed transporting sediment upwards towards the crest. The order of magnitudes found of the time and spatial scales coincide with observations.

For a unidirectional steady flow in an offshore setting we find sand waves with wavelengths in the order of hundreds of metres when the resistance at the seabed is relatively large based on linear theory. These sand waves migrate and become asymmetrical in the horizontal direction, as has been found for dunes in rivers. The migration rate of the sand waves decreases slightly during their evolution. For a unidirectional block current we find slightly elongated troughs and coinciding shortened crests. Similar features are found in data from the North Sea. Finally, the recovery of dredged sand waves is investigated. Sand waves are able to recover after they are dredged. The timescale and resulting maximum height depend on the amount of sand

dredged and where the sand is dumped.

Discussion The here developed models form tools to obtain insight and a framework to perform further research into the dynamics of sand waves. Moreover, the obtained knowledge and the models themselves can be used to optimise management strategies and provide information supporting the design of offshore activities.

Samenvatting

Zandgolven vormen een prominent regelmatig patroon in de offshore zeebodem in ondiepe zeeën zoals de Noordzee. Zij komen voor in waterdieptes van 10 tot 50 m. Hun golflengtes liggen in de orde van enkele honderden meters en de typische waarden van hun hoogten zijn enkele meters. De positie van de toppen en dalen van zandgolven veranderen langzaam in de tijd. Verondersteld wordt dat zandgolven migreren in de richting van de asymmetrie van de waterbeweging, waarbij migratiesnelheden van enkele meters per jaar bereikt kunnen worden.

Praktische relevantie Verschillende offshore activiteiten ondervinden hinder van zandgolven. Op basis van interviews met managers en technici van verschillende organisaties en bedrijven in Nederland wordt een overzicht van de problemen omtrent zandgolven en de manieren waarop met deze problemen wordt omgegaan gepresenteerd. Zo verminderen zandgolven de minimale diepte beschikbaar voor scheepvaart en vormen daardoor een gevaar voor scheepvaartroutes en vaargeulen. Om gevaarlijke situaties te vermijden wordt er continu gemeten en indien noodzakelijk wordt de waterdiepte vergroot door de toppen van zandgolven te baggeren. Op dit moment worden kaarten met daarop de ligging van de zeebodem gemaakt met behulp van echolodingen. Het combineren van zulke lodingtechnieken met satellietbeelden kan leiden tot meer efficiënte manieren om bathymetrische kaarten te maken. Inzicht in het dynamische gedrag van zandgolven zal leiden tot verdere reductie van de kosten verbonden aan het meten van de positie van de zeebodem. Verder kunnen zandgolven, doordat ze migreren, pijpleidingen en kabels blootleggen. Dit kan resulteren in vrije overspanningen die op hun beurt het breken of buigen van pijpleidingen tot gevolg kunnen hebben. Daarnaast kunnen ankers en visnetten de blootliggende kabels en pijpleidingen beschadigen. Bovendien kunnen objecten op de zeebodem bedekt worden door zandgolven, wat het moeilijk maakt om ze te vinden. Kennis omtrent het gedrag van zandgolven baant de weg naar betere managementstrategieën en kan gebruikt worden bij het ontwerp van offshore activiteiten.

Lineaire stabiliteitsanalyse Hulscher [1996] heeft zandgolven onderzocht aan de hand van een lineaire stabiliteitsanalyse, waarbij aangenomen wordt dat zandgolven vrije instabiliteiten zijn van het zeebodem-water systeem. In een dergelijke analyse beginnen we met een vlakke zeebodem, waarover water stroomt. Vervolgens worden er verschillende verstoringen op aangebracht met verschillende golflengtes, die de wa-

terbeweging verstoren. Daarna wordt de invloed van de veranderde waterbeweging op de zeebodem onderzocht. Wanneer er een netto hoeveelheid sediment getransporteerd wordt richting de top van de bodemvorm, wordt de zeebodem gezien als instabiel waardoor de bodemvorm groeit. Wanneer er een netto hoeveelheid sediment wordt getransporteerd richting het dal van de bodemvorm, wordt de zeebodem gezien als stabiel. Op basis van de lineaire theorie veronderstellen we dat de bodemvorm met de golflengte die het hardst groeit zal domineren over de rest van de golflengtes. Deze verwachten we daarmee aan te treffen in de werkelijkheid. De analyse laat zien dat voor een scala van golflengtes, die overeenkomen met geobserveerde zandgolven, er gemiddeld over een getij-periode een netto sediment flux bestaat richting de toppen van de bodemvormen, wat leidt tot hun ontwikkeling.

Hier hebben we deze lineaire analyse uitgebreid om de fysische mechanismen te onderzoeken die leiden tot migratie van zandgolven. Hiervoor hebben we gebruik gemaakt van een morfologisch model met een horizontale en een verticale richting (2DV). Het omvat de 2DV ondiepwatervergelijkingen en een algemene bodemtransportformule, die het sedimenttransport beschrijft. De waterbeweging is middels de sediment transportformule gekoppeld aan de zeebodemevolutievergelijking, die gebaseerd is op een massabalans.

Wij introduceerden een asymmetrie in de waterbeweging door een unidirectionele constante stroom (M_0) te beschouwen samen met (symmetrische) getijbeweging (M_2). De resultaten laten zien dat de zandgolven langzaam migreren in de richting van de asymmetrie van de waterbeweging. De gevonden migratiesnelheden en de golflengtes komen overeen met de theoretische en empirische waarden gepubliceerd in de literatuur. Verder hebben we de resultaten vergeleken met data van zandgolven langs een pijpleiding in de Noordzee en deze komen goed overeen.

Echter, deze lineaire analyse is slechts geldig voor zandgolven die een kleine amplitude hebben ten opzichte van de waterdiepte. De analyse zegt daarom niets over zandgolven met grotere eindige amplitudes.

Numerieke simulatie Om het middellange termijn gedrag van zandgolven met eindige amplitudes te beschrijven hebben we een numeriek simulatiemodel ontwikkeld. Dit model maakt het mogelijk de processen gedurende de evolutie van zandgolven ook na hun initiële ontstaan te onderzoeken. Het simulatiemodel is mathematisch gevalideerd door de resultaten te vergelijken voor kleine amplitude zandgolven met de uitgevoerde lineaire stabiliteitsanalyse. De resultaten laten zien dat het numerieke simulatiemodel in staat is om de initiële vorming van zandgolven, zoals gevonden middels de lineaire analyse te reproduceren.

Vervolgens hebben we het ontwikkelde simulatiemodel gebruikt om het gedrag van offshore zandgolven te onderzoeken voor eindige waarden van hun amplitude. Hierbij hebben we een unidirectionele constante stroming en een unidirectionele blokstroming die getijbeweging simuleert onderzocht. Initieel ontwikkelen de zandgolven zich exponentieel, zoals volgt uit de lineaire analyse. Vervolgens vermindert de groeisnelheid tijdens de evolutie van de zandgolf, wat resulteert in de stabilisatie van de zand-

golf. De maximale hoogte, die in enkele decennia wordt bereikt, bedraagt 10-30% van de gemiddelde waterdiepte. Het mechanisme dat er voor zorgt dat zandgolven stoppen met groeien is gebaseerd op het principe dat zand eenvoudiger bergafwaarts dan bergopwaarts wordt getransporteerd. Dit proces neutraliseert de bodemschuifspanning aan de zeebodem die ervoor zorgt dat sediment bergopwaarts wordt getransporteerd richting de top van de zandgolf. De orde van grootte van de tijd- en ruimteschalen komen overeen met observaties.

Voor een unidirectionele constante stroming in een offshore omgeving vinden we, gebaseerd op lineaire theorie, zandgolven met golflengtes in de orde van enkele honderden meters wanneer de weerstand aan de bodem relatief groot is. Deze zandgolven migreren en worden asymmetrisch in de horizontale richting (analoog aan rivierduinen). De migratiesnelheid vermindert licht gedurende de evolutie van de zandgolf. Voor een unidirectionele blokstroming vinden we langgerektere troggen en daarbij behorende kortere toppen. Soortgelijke patronen zijn gevonden in data van de Noordzee. Tenslotte is het herstel van zandgolven na baggeractiviteiten bestudeerd. De simulaties laten zien dat zandgolven in staat zijn om te herstellen nadat ze zijn gebaggerd. De tijdschaal en resulterende maximum hoogte hangen af van de hoeveelheid zand die word gebaggerd en waar het zand wordt gestort.

Discussie De in dit proefschrift ontwikkelde modellen vormen gereedschap om inzicht te verkrijgen in *en* een raamwerk om verder onderzoek te verrichten naar het gedrag van zandgolven. Bovendien kunnen de modellen en het verkregen inzicht gebruikt worden om de management strategieën te optimaliseren *en* voorzien in informatie nodig voor het ontwerpen van offshore activiteiten.

Chapter 1

Introduction

1.1 General

Shallow seas, such as the North Sea, with water depths in the order of tens of metres, are often covered with bed features with fascinatingly regular properties. In fact, several different types of bed features can be distinguished, each with different length and timescales.

Sand waves — the topic of this thesis — form a prominent bed pattern with crests spaced about 500 metres apart. They are generally found in areas where sand is abundant [Fenster *et al.*, 1990]. Their heights can be up to 30% of the water depth in which they are found, being in the order of 30 metres [Hulscher, 1996] (see Fig. 1.1, Fig. 1.3 and Fig. 1.5). This means that the relative sand wave height is very significant. It is assumed that their crests are oriented largely perpendicular to the prevailing current ([Johnson *et al.*, 1981], [Langhorne, 1981] and [Tobias, 1989]). Sand waves show spatial as well as temporal variations. These changes in shape and position of sand waves take place on a time-scale of a couple of years. In fact, sand waves have been observed to migrate several metres per year ([Allen, 1980a&b], [Lanckneus and De Moor, 1991] and [Van Maren, 1998]) (see Fig. 1.2).

These sand waves can also coexist with other bed forms. For example, sand waves can often be found on sandbanks (see Fig. 1.4), such as the Buiten Ratel bank and the Oostdijk Bank in Belgium (see also Huntley *et al.* [1993]). Tidal sandbanks are elongated sand bodies with wavelengths of about five to ten kilometres. Their heights can lead up to 30 m, which is high compared to the water depth in shallow seas. Characteristic of tidal sandbanks is that their crests are oriented between 5 and 30° anti-clockwise with respect to the principal direction of the water movement. These sandbanks are believed to evolve on a timescale of hundreds of years ([Huthnance, 1982a&b], [Van Alphen and Damoiseaux, 1989], [De Vriend, 1991] and [Hulscher, 1996]). Furthermore, analytical and numerical studies have shown that they can migrate at a velocity of about 1 m yr^{-1} ([Németh, 1998], [Idier and Astruc, 2001], [Roos *et al.*, 2001] and [Roos and Hulscher, 2002]).

On top of these sand waves, mega-ripples are sometimes found migrating towards the crests of sand waves [Houthuys, 1990]. Mega-ripples are an order of magnitude

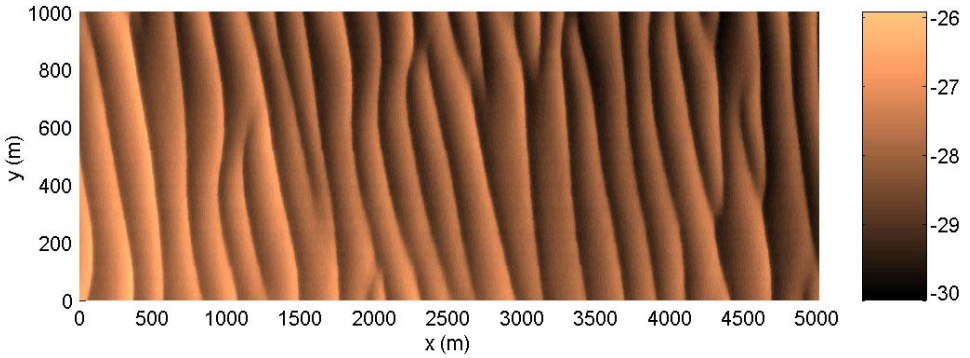

Figure 1.1: Regular sand waves with wavelengths of about 250 m and wave heights in the order of 10% of the water depth in the North Sea in front of the Dutch coast near IJmuiden. The horizontal and vertical scales depict distance in metres. The color scale is based on the depth below the sea surface. The data is provided by the North Sea Directorate.

smaller, having heights of up to a metre and wavelengths in the order of tens of metres. Wever and Stender [2000] measured migration rates of 0.5 m day^{-1}, which equates to almost 200 m yr^{-1}.

A new rhythmic pattern, larger than sand waves, was found by Knaapen *et al.* [2002]. This bed pattern has a wavelength of about 1.6 km and a height in the order of one metre. Based on their length and height, we could place these new bed forms — named long bed waves — in between the long sandbanks and the smaller sand waves. Their orientation is about 50 to 60° anticlockwise with respect to the direction of the tidal motion. The mechanism leading to this type of bed pattern is not yet understood.

1.2 Sand waves and alluvial sand dunes

Sand waves are often compared with alluvial sand dunes. The main difference in origin is that alluvial dunes are caused by time-independent flow, whereas sand waves are generated by periodic water motion. In the current literature, the term sand wave is used for a large variety of bed forms with different shapes and dimensions at various locations and for several distinct conditions. In this thesis, the aim is to investigate sand waves in an offshore environment under the effect of time dependent water motion.

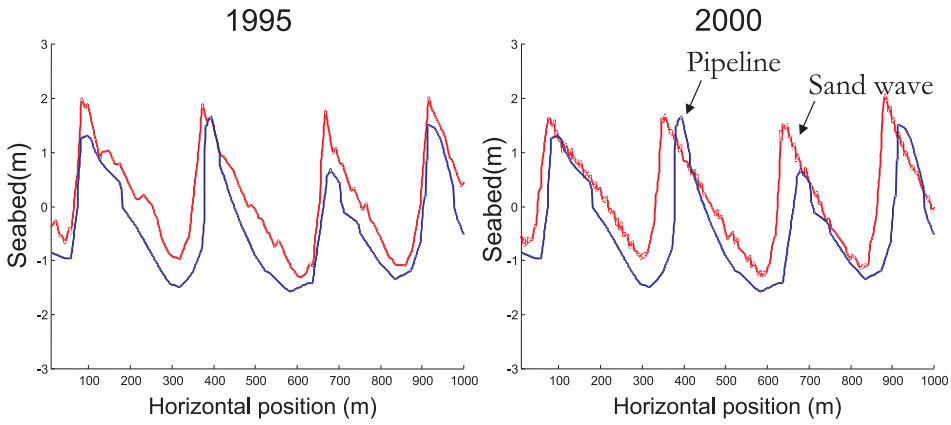

Figure 1.2: Sand wave migration and pipelines. The upper line denotes the position of the seabed. The lower line shows the position of the estimated pipeline. The measurements for two years (1995 and 2000) are shown. We can see that the sand wave is migrating to the left here, thereby exposing the buried pipeline.

1.3 State-of-the art of modelling sand waves

Johns *et al.* [1990] and Stansby [1998] discussed unidirectional water movement over dune-like features with steep slopes. Richards and Taylor [1981] discussed sediment transport characteristics for more sand wave like bed forms in a unidirectional flow, with milder slopes compared to river dunes. Idier [2003] investigated sinusoidal sand waves for various amplitudes with a numerical model for unidirectional flow conditions.

Fredsøe and Deigaard [1992] describe dunes having their equilibrium heights and wavelengths. Dune migration is described as a function of sediment transport parameters. Therefore, the model does not give insight into the evolutionary process of dunes. Sand waves under the influence of tidal movement are modelled with this model as being under the influence of a unidirectional current and only slightly modified by the tidal movement.

Hulscher [1996], Gerkema [2000] and Komarova and Hulscher [2000] investigated sand waves by considering the seabed and water motion as a dynamically coupled system. The results of their analytical studies gave insight into the actual mechanisms for the initial formation of sand waves. For a certain range of wavelengths, similar to sand waves, residual circulation cells appear in the water column. These cells induce a net sediment flux towards the crest of sand waves, leading to their initial evolution. Furthermore, with these models predictions can be made about the occurrence of sand waves at certain locations in, for instance, the North Sea [Hulscher and Van den Brink, 2001]. However, these studies are only valid for infinitely small amplitude

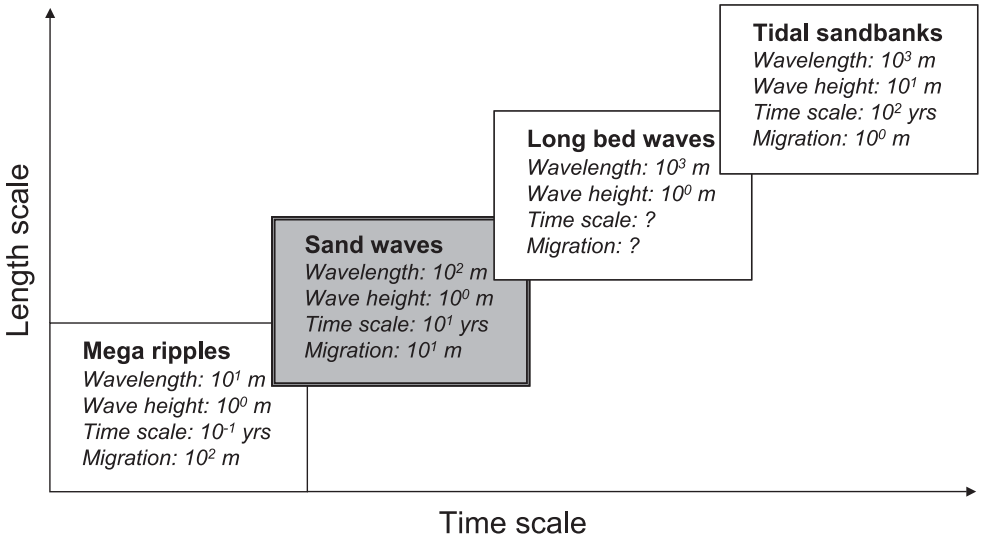

Figure 1.3: Characteristics of typical offshore bed patterns. The wavelength is defined as the separation between crests and the wave height is the distance from the trough to the top. Furthermore, the migration rate is the horizontal displacement of an entire wavelength of a bed form. The timescale is the period on which significant changes are expected to occur. Based on the concept of De Vriend [1991].

sand waves and do not give insight into the behaviour of finite amplitude sand waves. Furthermore, they only describe regular sinusoidal sand waves and migration is not considered.

Komarova and Newell [2000] investigated the model by Hulscher [1996] combined with the viscosity parameterisation from Komarova and Hulscher [2000] with a weakly non-linear analysis. This analysis led to coupled spatial variations of sand waves and the average bed level, of which the latter seems to have similarities with tidal sandbanks. This analysis only describes regular bed forms based on the assumption that the system is weakly non-linear. Furthermore, the model does not describe sand wave migration.

Knaapen and Hulscher [2002] used an amplitude evolution model based on the Landau equation, to make predictions of the intermediate term evolution of (dredged) sand waves. This method, based on measured data, gives first estimates that are very useful. Morelissen *et al.* [2002] extended this work by allowing sand waves to migrate in the model using a modified Landau equation and applied the model in a pipeline case study. However, insight into the actual physical mechanisms is limited. Furthermore, large data sets over several years are needed, which are rarely available.

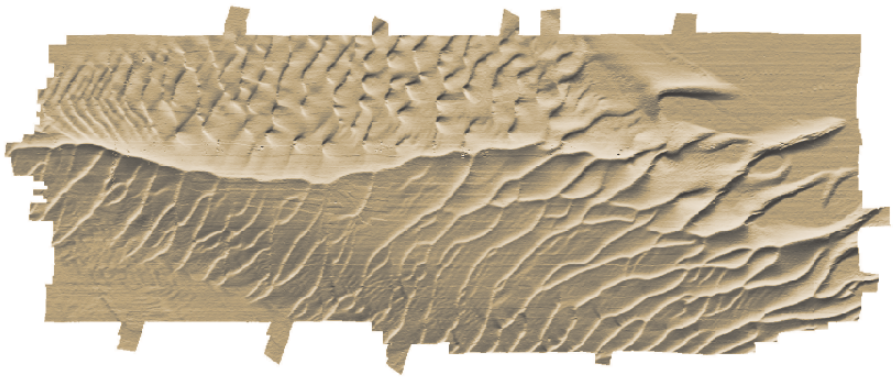

Figure 1.4: Banc de la Schôle. Sandbank of the coast of Normandy (the long elongated crest), covered with sand waves (smaller features), after [Bisquay and Ledu, 1999].

1.4 Central research theme of this thesis

The main aim of this thesis is to identify the key practical problems due to sand waves, and to obtain insight into the intermediate term behaviour with respect to their migration, evolution and changes in shape. This information — obtained with a model-oriented approach — can then be used to optimise management strategies.

The main research questions are formulated as follows:

- What are the key practical problems concerning sand waves and their coinciding time and length scales?
- What processes can cause sand waves to migrate?
- Can the processes determining the initial sand wave formation be simulated by a numerical model?
- What processes are responsible for the stabilisation of sand wave evolution?
- How do the migration rates and shape of a sand wave change in the intermediate term?
- What data do we need to validate and apply the developed models in reality?

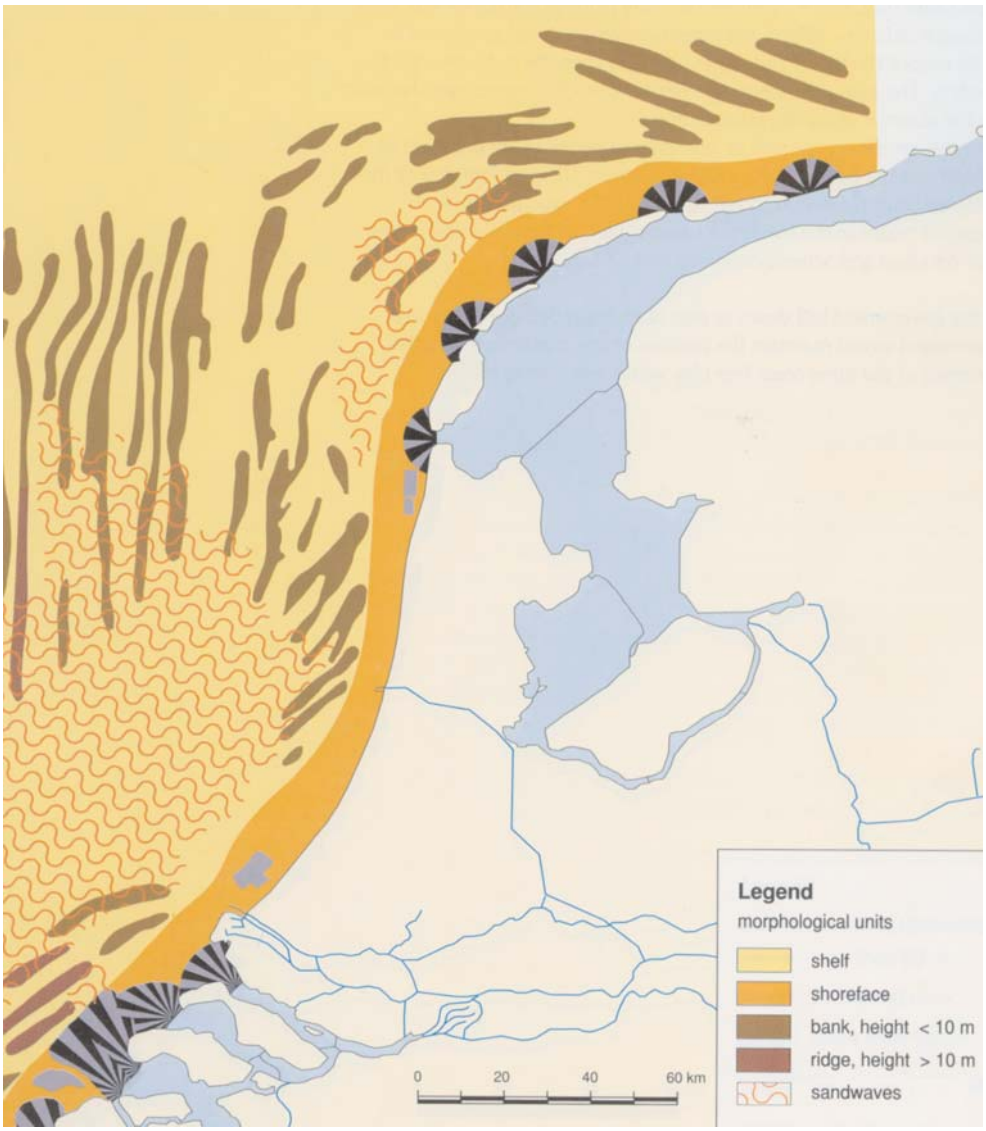

Figure 1.5: Location sand waves and other bed patterns such as sandbanks in the North Sea in front of the Dutch coast, after [Van Alphen and Damoiseaux, 1989].

1.5 Keywords

Offshore, Sand waves, Tidal current, Steady current, Bed load transport, Stability analysis, Spectral methods, 2DV, Morphodynamic modelling, Pipelines, Navigational routes, Cables, Charts, Buried objects.

1.6 Outline of this thesis

Chapter 2 discusses the practical relevance of research into the dynamics of sand waves. It gives an overview of the variety of problems encountered by companies and institutions which are involved in offshore seabed morphology. The main topics are pipelines, navigation and sand extraction. The problems are coupled to the state of the art literature.

Chapter 3 presents a morphodynamic model for the formation and migration of sand waves. It is based on the 2DV shallow water equations taking the flow in the vertical into account. The model describes the initial sand wave evolution by solving the system with a linear stability analysis. This analysis is valid for infinitely small amplitude sand waves. Furthermore, it describes sand wave migration due to an asymmetry in the water motion. This asymmetry is forced by a wind stress applied at the sea surface or by a pressure gradient, which can be combined with symmetrical tidal motion. The model results show good agreement with observations.

Chapter 4 shows the structure of the developed non-linear simulation model which is able to describe the behaviour of finite amplitude sand waves on the intermediate term. The simulation model is based on the model presented in Chapter 3. However, the system is solved using a spectral approximation method using Chebyshev polynomials on a non-periodic grid. Furthermore, we applied an implicit time stepping method. We validated the simulation model mathematically with the help of the results from the linear stability analysis discussed in Chapter 3. For both the models we also investigated bed forms induced by a steady current only.

Chapter 5 discusses the behaviour of finite amplitude sand waves using the simulation model discussed in Chapter 4. We focus on the evolution of sand waves, the saturation mechanisms and their saturation height. A unidirectional current is investigated, the results of which we compare with observations made in the Gulf of Cadiz in Spain. Subsequently, we investigate periodic water motion, to investigate North Sea conditions. Furthermore, the migration rates and changes in shape of sand waves of finite amplitude are discussed. Finally, the recovery of dredged sand waves is investigated.

Chapter 6 presents the main conclusions of this thesis, referring to the central research theme stated above.

Chapter 7 gives some directions for future research.

1.7 Acknowledgements

We thank the North Sea Directorate, Clyde Petroleum Exploratie, Holland Offshore Consulting and the State Supervision of Mines for providing the data supporting the Figs. 1.1 and Figs. 1.2.

Chapter 2

Offshore sand wave dynamics, engineering problems and future solutions

Abstract: Offshore activities often encounter large scale sand patterns, such as sand waves. Sand waves are offshore bed forms occurring at water depths of 10 to 50 m. Their wavelengths can lead up to 500 m and their heights are typically several metres. Furthermore, sand waves have been shown to migrate, with typical velocities of up to metres per year. These dynamic sand waves decrease the least navigable depths and so they pose a threat to navigation routes and access channels. To avoid unsafe situations, continuous monitoring and, if necessary, dredging are required. Now, seabed topography charts are made using echo soundings. Combining such sounding techniques with satellite images may lead to more efficient ways to create bathymetry charts. Insight into the dynamics of sand waves can further reduce monitoring costs. Due to the movement of sand waves, pipelines and cables may become exposed. This may result in free spans, which in turn may cause the pipeline to buckle or break. Moreover, anchors and fishing nets may cause damage to the exposed pipelines and cables. In addition, exposed objects may be covered by a sand wave, making it difficult to locate them. Recently, new insight into the migration of sand waves and data-based predictions concerning sand wave amplitude evolution, have been explored. Despite this progress, a number of questions concerning sand wave behaviour remain. It is shown that further knowledge of sand wave behaviour will enable better management strategies and provide information supporting the design of offshore activities[1].

Keywords: sand waves, shelf seas, pipelines, navigation, dredging, monitoring, burial.

[1]Németh, A.A., Hulscher, S.J.M.H. and De Vriend, H.J., 2003, Offshore sand wave dynamics, engineering problems and future solutions, Pipeline & Gas Journal, Vol. 230 (4), pp. 67-69.

Figure 2.1: Observed sand wave occurrence in the southern part of the North Sea (adapted after Hulscher and Van den Brink [2001]).

2.1 Introduction

On the seabed of The North Sea, and many other shallow shelf seas, a variety of regular patterns can be found. These have different spatial and temporal scales, as shown in Table 2.1. These large-scale seabed patterns are often strikingly regular.

Quantity	Ripples	Sand waves	Sandbanks
Wavelength (m)	10^{-2}	10^{2}	10^{3}
Wave height (m)	10^{-2}	10	30
Timescale	minutes	years	millenia

Table 2.1: Characteristics of typical offshore bed patterns.

Sand waves (Fig. 2.1) are bed forms with wavelengths of about 500 m and heights up to about 10 m in water depths of about 30 m [Hulscher, 1996]. It is usually assumed that their crests are oriented perpendicular to the dominant current ([Johnson *et al.*, 1981], [Langhorne, 1981] and [Tobias, 1989]).

Some decades ago, scientists concluded that the migration rate of sand waves was quite high (100 m y^{-1}). More recently, migration rate estimates have become lower (of the order of metres per year). The main reason for this discrepancy is that the migration rates used to be smaller than the location errors in the measurements.

Nowadays, positioning has become more precise and the location errors now lie in the order of magnitude of the distance over which sand waves migrate in a year (also see Németh *et al.* [2002]). This margin makes it difficult to accurately determine the migration rates from data that are only a few years apart.

Sand waves often have asymmetrical shapes. Furthermore, observed asymmetries may change over a relatively short period of time, e.g. one season. Harris [1989] reported a reversal of the asymmetry of the sand waves in the Adolphus Channel of Australia within a period of five months, due to wind-driven currents during the Monsoon season.

Modelling sand wave dynamics is still far from perfect. Recently, the evolution of sand waves has been investigated by Knaapen and Hulscher [2002] and Morelissen *et al.* [2002]. Data assimilation was used to estimate the amplitude evolution. Based on a set of measurements in time and space, estimates of the evolution of a sand wave pattern can be made in a certain area. This leads to a locally validated sand wave behaviour model. This knowledge can be used to develop more efficient dredging strategies. Despite its success, this empirical method does not include the full knowledge of sand wave physics. This makes it less suited to reveal the mechanics of sand wave formation.

Sand waves have a significant effect on the activities taking place in shallow shelf seas such as the North Sea. This paper will focus on questions about the behaviour of sand waves in relation to a number of matters: navigational safety, pipelines and cables, sand extraction and the burial of objects.

Managers and engineers from several institutions in the Netherlands, all dealing with sand waves from a different point of view, have been interviewed to help address this question. Backed up with literature, this paper provides an overview of the sand wave problems and their ways in which they are handled, and suggests possible improvements based on recent scientific progress.

We will first address the issue of seabed topography charting (Section 2) and how this could be improved with more knowledge on sand wave dynamics. Next, we will consider the effects of sand waves on pipelines and cables (Section 3), and on navigation routes and access channels (Section 4). Sand extraction from sand wave fields is discussed in Section 5 and Section 6 goes into the issue of sand wave induced covering and uncovering of objects on the seabed. Finally, we will summarize the conclusions and discussion (Section 7).

2.2 Seabed topography charts

Navigational charts are probably the most common seabed topography charts. For safe navigation, it is sufficient if nautical charts give minimum depths. As the seabed is likely to change over time, it is expected that the accuracy of a chart will decrease with time. Apart from long-term influences, such as sea level rise and overall sedimentation or erosion, the combined effects of moving sandbanks, sand waves and mega-ripples form the major source of change in the least depths.

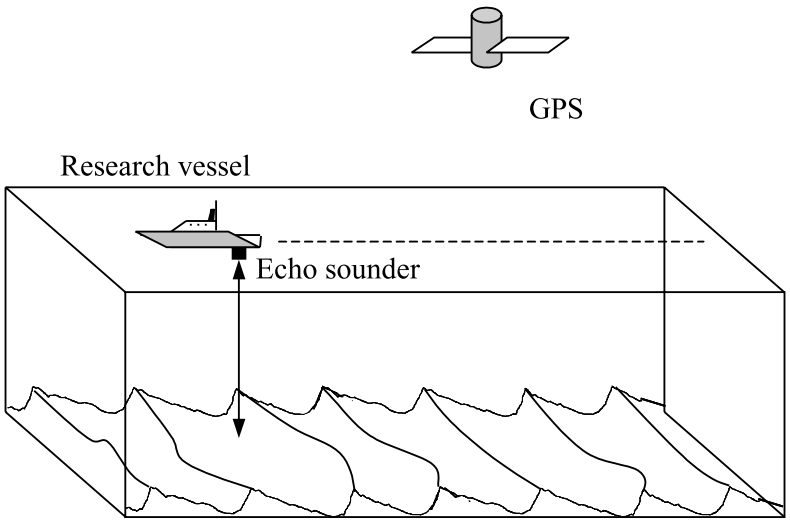

Figure 2.2: Echo soundings, satellite imagery and GPS are techniques used to obtain bathymetric data.

2.2.1 Echo soundings

Nowadays, topographic data is mostly obtained using single-beam echo sounders, which are attached to ships sailing over the area to be charted. They measure the depth directly below the device (Fig. 2.2). Recently, multi-beam echo sounders enable measurements not only directly under the ship, but also in a swath (strip) with a width of several times the water depth on either side of the ship. Although these systems are expensive and the processing of the obtained data takes a lot of time [Calkoen *et al.*, 2001], the results are quite revealing if it comes to the spatial pattern of bed forms ([Schüttenhelm, 2000] and [Knaapen *et al.*, 2002]).

2.2.2 Satellite images

Remote sensing may be an alternative way of obtaining data on the seabed topography. Satellite images are inexpensive and provide snapshots of the sea-surface. Techniques to translate satellite images into seabed topography are being developed at this moment [Calkoen *et al.*, 2001].

The ERS-1 (European Remote Sensing) satellite is equipped with a Synthetic Aperture Radar. The horizontal accuracy of its images is quite low, in the order of hundreds of metres, due to the lack of good landmarks. If good landmarks (characteristic features on land) are available, satellite images can be positioned more precisely in the horizontal. In practice, this means that images taken near the coast are much

more accurate than images taken farther offshore. Near the coast, the accuracy of the horizontal positioning can then be as good as ± 25 m.

2.2.3 Bathymetry Assessment System

The BAS (Bathymetry Assessment System) is based on the concept of combining the above optical sea surface measurements with a translation model of such sea surface information to seabed topography. This system, which is under development, is meant to produce charts at much lower costs than before. Theoretically, combining the satellite images with additional ship soundings and radar images taken from aircraft can improve the horizontal and vertical accuracy down to the order of metres or less. Ship soundings will therefore probably remain necessary, to make accurate charts. One may expect however, that, once the BAS technique is fully developed, it will reduce the number of soundings considerably, thus reducing the total production costs of charts.

To obtain seabed-data from satellite images, a translation model is used, based on an inverse modelling technique. The model consisting of a flow, wave and radar-backscatter module, use a known chart to create a simulated radar image. Comparing this simulated image with the observed one and adding data from traditional soundings, ultimately leads to a chart of the seabed topography. Accuracy and costs of such a chart are reasonably in balance. Soundings are more accurate, but also more expensive.

Calkoen *et al.* [2001] observed sand wave patterns on SAR images. Combining these images with ship soundings and the BAS system allows the study of sand wave characteristics. However, when exploring this technique in further detail, Middelkoop [1998] found sand waves with wavelengths significantly larger than usually observed in that area. The sand wave spacing estimated from the SAR images was in the range of 900 to 1800 m, whereas sand wave crests in this area are only a few hundred metres apart. Knaapen *et al.* [2002] suggest that what is seen on the SAR images are not sand waves, but another type of seabed feature, due to the interference of bed form modes.

In conclusion, the use of radar imagery for bathymetric mapping is under investigation. Because the flow-dependence of the relationship between sea-surface patterns and seabed topography, we may not expect that this technique is accurate enough for investigating sand wave migration. On the other hand, sand waves influence processes, such as tidal motion, wave motion and sediment sorting. Insight into sand wave behaviour and its relationships with these processes will enable better estimates of the unknowns in the BAS system and improvement of the underlying model components.

2.3 Pipelines and Cables

The costs of offshore pipelines constitute a large portion of the total costs of developing a new oil or gas field. Furthermore, pipeline protection takes up a large part of these

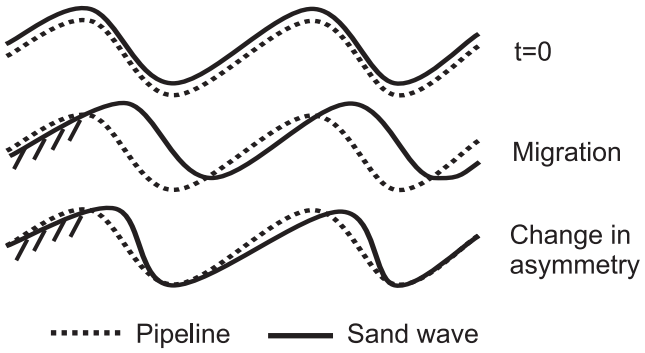

Figure 2.3: Illustration free span pipeline, along a cross section of the seabed, due to the migration and change in asymmetry of sand waves. The solid line denotes the sand wave in which the pipeline, represented by the dotted line is buried. Note the exaggeration of the vertical scale compared to the horizontal scale.

costs [Li and Cheng, 1999].

2.3.1 Free spans

Hundreds of kilometres of pipelines can be found in, for instance, the North Sea. These pipelines sometimes have to cross a sand wave field. The sand waves can form a threat if they migrate and expose the pipelines (Fig. 2.3). Free spans may develop, causing stresses due to gravity. Moreover, the pipelines can start vibrating, due to the turbulence generated under these free spans. The vibration also causes undesirable stresses, which may cause the pipeline to bend, break or buckle. Furthermore, once exposed, a pipeline or cable can be damaged by ship anchors or fishing gear. The height and migration speed of sand waves are therefore important design parameters for pipelines and cables. Mega-ripples are too small to create significant over-exertions and are therefore not considered here.

Free spans may also be caused by changes in sand wave asymmetry, i.e. changes in the shape of the sand waves, irrespective of their migration. Such a change in asymmetry may falsely be identified as migration, due to the large measuring errors. Hence, sand wave migration data in the literature are not always reliable. Such a change in asymmetry may be caused by a change in the water movement across the sand wave field.

One way to overcome the sand wave problem is to lay pipelines around sand wave fields, instead of across them. Often, this is not a very attractive option, because the sand wave field considered is too large and thus requires a much longer pipeline. On the other hand, this solution would reduce the costs of monitoring and maintenance, and decrease the risk.

The most straightforward solution is to lay the pipeline in a trench through the sand wave field, so that sand wave migration will be less of a threat. This solution is effective, but expensive. The main question is: what is the most efficient depth for a trench to place the pipeline in? This optimal depth depends on factors such as dredging costs, pipeline construction costs, monitoring costs and risk.

Under certain conditions, the pipeline may have a 'burial potential' of its own [Bos *et al.*, 1996]:

- Firstly, tunnel erosion takes place. This process removes sand directly beneath the pipeline. This leaves a hole in which the pipeline descends on a timescale of hours to days;
- Next, downstream of the pipeline turbulence is increased, leading to a scour hole on a timescale of weeks to months. This hole develops on both sides of the pipeline due to the oscillatory tidal motion. Thus the pipeline gradually sinks further into the bed. The pipeline can furthermore be equipped with a spoiler on top, increasing the rate at which the pipeline sinks into the seabed;
- Once the pipeline has sunk far enough, the hole in the seabed locally decelerates the flow, reducing the transport capacity. This process, called backfilling, will eventually dominate the scour process and bury the pipeline.

A pipeline laid on top of sand waves is curved, whence it will not sink as easily into the bed as it would in the case of a flat bed. Moreover, the current velocity varies along a sand wave, making it harder to predict the burial behaviour of the pipeline.

Knowledge concerning the behaviour of the seabed and its interaction with a pipeline can help optimise the design such that the total costs are minimized. This requires predictions of the migration rate of sand waves. Since the pipeline follows the contours of the bed, we also need to understand the behaviour of the entire profile of sand waves, not only that of the crests and the troughs. Furthermore, it is necessary to know to what extent the pipeline works itself into the seabed.

2.3.2 Survey before, during and after use

Several bathymetric surveys are made in projects concerning pipelines:

- First, a reconnaissance survey is made to inventory the seabed profile of the area where the pipeline is to be laid;
- Next, the chosen route is measured more precisely;
- Before the pipeline is constructed, the route is surveyed once more in order to have the latest information about the condition of the seabed;
- After the pipeline has been placed, the whole pipeline and its surroundings are checked;

- During the entire life span of the pipeline, this area is monitored on a yearly basis.

Knowledge about sand wave behaviour can reduce the survey effort and thus the costs. It can furthermore improve the accuracy of the measurements and help their interpretation. In addition, this knowledge can be used to cut costs after the pipeline has been decommissioned. Such an object on the seabed may endanger navigation, fisheries and the marine environment.

2.4 Channels and navigational routes

Ships sailing to, for example, Rotterdam harbour enter through the access channel leading to the port. Such a channel has to be wide and deep enough for ships to pass safely. If the channel becomes too shallow, it has to be dredged. Bathymetric information is provided to mariners so that they can navigate safely over the Netherlands Continental Shelf. This is done by publishing nautical charts, depicting the least depths of the seabed together with information about wrecks and other obstructions.

Both migration and seasonal variations in height or asymmetry of sand waves change the topography and possibly affect the minimum water depth. This can be a problem if it happens along these navigation routes and access channels. This is especially true if the clearance is marginal, such as for super tankers in a harbour access channel.

The channel plus its surrounding area therefore has to be monitored in order to decide about where and when sediment has to be extracted. Knowledge about the mobility of sand waves, which are present in a large part of the North Sea, would furthermore allow for a larger interval between the surveys needed to guarantee these least depths.

Instead of using the fictitious chart depth, a model can be used to decide whether or not to allow a ship into the channel. This will result in a combination of increased safety and a larger tidal window.

In the Netherlands, the North Sea Directorate and the Royal Navy are interested in the temporal variations of the seabed within navigation channels. These should be presented in the form of frequency distributions of the position of the seabed together with confidence intervals. Furthermore, they want to know the extreme value statistics of the water depth. Knowledge concerning sand wave dynamics can form useful information for the required statistical analyses.

2.5 Sand extraction

Sand mining in the North Sea is sometimes performed by dredging the crests of sand waves (Fig.2.4) (see also [Hoogewoning, 1997] and [Peters, 2000]). Sand extracted from the seabed can then be used for beach nourishment, land reclamation and the

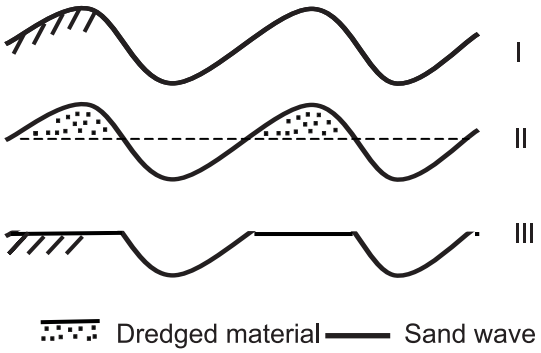

Figure 2.4: Sand mining from sand wave crests. (I) shows initial situation of a cross section of a sand wave pattern, (II) the cross-sectional area to be dredged and (III) the resulting bed profile after dredging.

construction industry. Furthermore, these sand waves also need to be dredged because they form a hazard to navigation (see previous section).

It is still unclear how dredging influences a sand wave field. Do the sand waves regain their original height? If so, how do they recover and how quickly, keeping in mind the overall sand balance of the sand wave field?

Knowledge about the evolution of sand waves will make it possible to determine the depth to which they should be dredged if they form a hazard to navigation. If a sand wave is lowered only marginally, the dredging costs per operation will be relatively low, but the frequency of these operations are expected to be relatively high. Moreover, the sand waves will have to be monitored more frequently, in order to make sure that they do not get higher than acceptable. Knowing the rate at which sand waves evolve will help determine the most efficient monitoring interval and dredging strategy. Such a strategy can be set up using the empirical sand wave model developed by Knaapen and Hulscher [2002]. This model describes the evolution of sand waves in a certain area, based on measurements in time and space in that area.

2.6 Burial of objects

Objects lying on the seabed can get buried, due to the migration and/or growth of sand waves (Fig. 2.5). Here one can think of objects such as shipwrecks, mines and containers possibly containing hazardous materials. Such objects can be buried, after which they lie dormant on the seabed. However, they might become exposed again, forming a direct hazard to the environment (for example leakage of chemical waste). Moreover, these objects can get stuck in fishing gear or inversely.

The time between burial and exposure is called residence time. Not only the

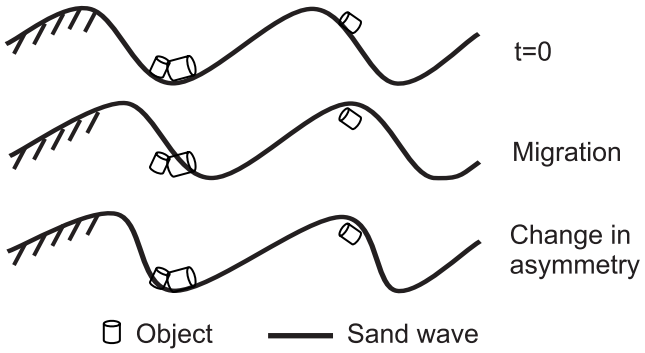

Figure 2.5: Burial of objects due to migration or a change in asymmetry. The figure shows three cross-sections of sand waves with objects located in/on the seabed. These objects can be, for example, chemical waste, mines or shipwrecks.

horizontal displacement of bed forms is important, also the vertical displacement — self-burial — of the objects plays a role in the residence time.

The residence time of these objects is an important factor in setting up a monitoring strategy. There is little point in monitoring an area where the seabed hardly changes. Knowledge about sand wave behaviour can optimise the monitoring strategy and thus reduce the costs.

2.7 Discussion and conclusions

Even though sand waves are not directly visible to the naked eye, they pose a threat to a range of offshore activities. The combination of their timescale (years), length scales (hundreds of metres) and height (metres) make them bed features to be reckoned with.

The questions asked by the institutions and the industries involved in offshore activities can be summarized as: "Under which conditions are sand waves dynamic (horizontal and vertical movement) and what are the typical spatial and temporal scales?" At this moment, several aspects of sand waves can be described and explained. An estimate of the wavelength [Hulscher, 1996] together with the migration rate [Németh *et al.*, 2002] can be obtained. Furthermore, if in a certain area data are available over a period of years, the evolution of sand waves in that area can be described and the position of the seabed in the near future can be predicted ([Knaapen and Hulscher, 2002] and [Morelissen *et al.*, 2002]). However, the latter technique is based on data assimilation, so that the results are only valid for the location from which the data originates. A model based on physical principles describing the non-linear dynamics is not yet available, but is expected in the near future.

Extra insight into sand wave migration is important to estimate the optimal mon-

itoring frequency for navigation channels, pipelines and buried objects. Furthermore, greater insight into the height evolution of sand waves is required, e.g. in order to determine when and how much should be dredged if sand waves get too high and form a threat to navigation. The monitoring frequency and the amount of sand to be dredged can be optimised when knowing the recovery rate of sand waves after they have been dredged.

Looking at the impact of a large-scale intervention in space and time, such as the construction of an island in the sea or large-scale windmill parks, the aspects evolution and migration are both important. This also holds for the further development of sand wave observations, by the Bathymetry Assessment System combining satellite images with ship soundings.

A special point of attention is the irregularity of sand waves in a field. Bed level statistics, and especially extreme value statistics of the seabed, are indispensable information for dealing with the natural dynamics of the seabed.

2.8 Acknowledgements

We would like to thank M.A.F. Knaapen and P.C. Roos (University of Twente); C.J. Calkoen and G.J. Wensink (ARGOSS); S.L. Bicknese A.M. Haksteen, H. Keyser, R.C. Lambij, A. Stolk and W. Verhagen (North Sea Directorate); C. Laban (TNO National Geological Survey); J. Appelman, M.R. Gerding and W. Korbijn (The Hydrographic Service of the Royal Netherlands Navy) and R. Bijker.

Chapter 3

Sand wave migration, a stability approach

Abstract: Sand waves form a prominent regular pattern in the offshore seabed of sandy shallow seas. The positions of sand-wave crests and troughs slowly change in time. Sand waves are usually assumed to migrate in the direction of the residual current. This paper considers the physical mechanisms that may cause sand waves to migrate and methods to quantify the associated migration rates. We carried out a theoretical study based on the assumption that sand waves evolve as free instabilities of the system. A linear stability analysis was then performed on a 2DV morphological model describing the interaction between the vertically varying water motion and an erodible bed in a shallow sea. Here, we disrupted the basic tidal symmetry by choosing a combination of a steady current (M_0) and a sinusoidal tidal motion (M_2) as the basic flow. We allowed for two different physical mechanisms to generate the steady current: a sea surface wind stress and a pressure gradient. The results show that similar sand waves develop for both flow conditions and that these sand waves migrate slowly in the direction of the residual flow. The rates of migration and wavelengths found in this work agree with theoretical and empirical values reported in the literature[1].

Keywords: stability analysis, sand waves, migration, shelf seas, 2DV.

3.1 Introduction

Large parts of shallow seas, such as the North Sea (Fig. 3.1), are covered with bed features that are fascinatingly regular. Sand waves form a prominent bed pattern with a crest spacing of about 500 m. Usually sand waves (also referred to as dunes as

[1]This chapter has been published as: Németh, A.A., Hulscher, S.J.M.H. and De Vriend, H.J., 2002, Modelling sand wave migration in shallow shelf seas, *Continental Shelf Research*, vol. **22**/18-19, pp. 2795-2806. See also the epilogue in paragraph 3.9 which is not part of Németh *et al.* [2002].

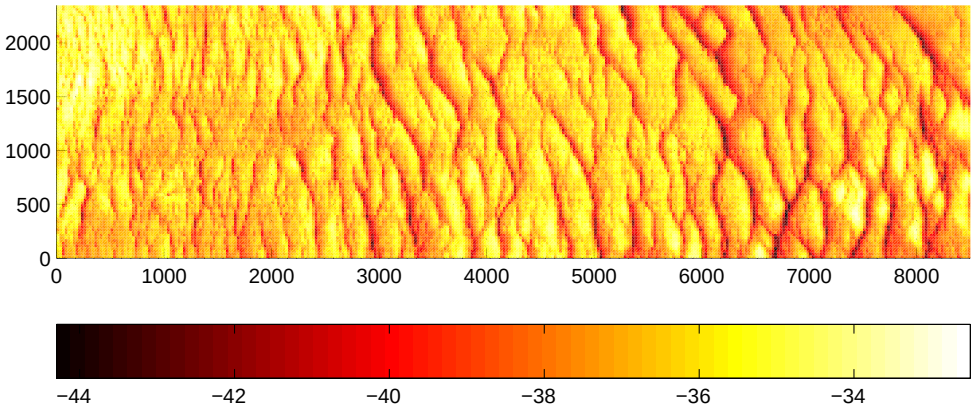

Figure 3.1: Bathymetry measurements made in the North Sea near the Eurogeul, with horizontal coordinates specified in metres and a colorbar denoting the sea bed level below mean sea level (in metres). (Courtesy Rijkswaterstaat, North Sea Directorate; details on measurements and analysis are given in Knaapen *et al.* [2002].)

stated by Ashley [1990]) are observed at a water depth in the order of 30 m and their heights can reach up to several metres. This means that the relative sand wave height can be significant. The crests are often assumed to be perpendicular to the principal current ([Johnson *et al.*, 1981], [Langhorne, 1981] and [Tobias, 1989]). Based on a theoretical analysis, Hulscher [1996] arrived at the conclusion that sand wave crests may deviate up to 10° anti-clockwise from the direction perpendicular to the principal current.

Observations indicate that these sand waves are dynamic ([Van Maren, 1998], [Lanckneus and De Moor, 1991] and [Allen, 1980a & b]) and can migrate with speeds of up to several metres per year. Knowing the spatial and temporal intervals of bed changes will enhance the overall safety of an area [Németh *et al.*, 2003]:

- The North Sea, for example, contains hundreds of kilometres of pipelines and cables. A migrating sand wave can uncover cables and make them susceptible to damage. Furthermore, free spans can develop, which can lead to bending, vibration, buckling or even breaking of pipelines [Whitehouse *et al.*, 2000];

- Migrating sand waves can also cover mines and chemical waste, which consequently may lie hidden within the seafloor, to become exposed in the future.

Sand wave migration has been studied in situ by e.g. Lanckneus and De Moor [1991] and Terwindt [1971]. The current method for quantifying migration has serious limitations, as data tend to be inaccurate (especially older data). Furthermore, often

only the crests are considered, which ignores the major part of the available information. Building long-term data sets and developing objective and accurate methods to process this data will take a considerable amount of time and effort.

To determine sand wave migration in the field, we need bathymetric data on an annual basis and an accurate positioning method, which enables absolute interrelation of the positioning of bathymetric data in the horizontal domain. The latter is an important limiting factor. In recent years, the location accuracy has greatly improved by the use of GPS. Yet, the yearly migration rates are still of the same order of magnitude as the horizontal positioning error. We are working on an objective and accurate method, based on bathymetry data over a number of years, to determine actual migration rates. This will enable us to compare the model results with actual data. This is crucial for understanding sand wave migration and the processes involved. More specifically, it will reveal whether the rather simple model discussed within this paper is sufficient, or whether extensions are needed in order to describe sand wave migration.

Sand wave migration has been modelled in the past as a direct extension of bed form dynamics in rivers [Fredsøe and Deigaard, 1992]. However, the residual current in a tidal environment is much smaller than the steady currents found in rivers. Therefore, the migration velocities of tidal sand waves are one to two orders of magnitude smaller than the velocities attained by dunes in rivers [Allen, 1980]. Fredsøe and Deigaard [1992] describe the behaviour of finite-amplitude dunes under a steady current. They assume the time-dependency of the flow to be negligible when modelling sand waves in a tidal environment.

Huthnance [1982a] was the first to look at a system consisting of depth-averaged tidal flow and an erodible seabed. Within this framework, one can investigate whether certain regular patterns develop as free instabilities of the system. Unstable modes comparable to tidal sandbanks were found, whereas smaller modes corresponding to sand waves were not initiated. Hulscher [1996] extended this work by using a model allowing for vertical circulations and found formation of sand waves due to a basic tidal motion that was horizontally uniform and symmetrical in time. Hulscher [1996] showed that net convergence of sand can occur at the top of the sand waves over an entire tidal cycle (see also Gerkema [2000] and Komarova and Hulscher [2000]). In these models, sand waves do not migrate. Hulscher and Van den Brink [2001] showed the predictive ability of their model for sand wave occurrence. Blondeaux *et al.* [1999] introduced forcing due to surface waves on top of the tidal motion. These wind waves accomplish a net transport of energy and the authors found migration of sand waves. However, the numerical treatment left many questions about the specific mechanisms behind migration unanswered. Komarova and Newell [2000] extended a linear analysis [Komarova and Hulscher, 2000] into the weakly non-linear regime to investigate the behaviour of finite-amplitude sand waves. The latter model does not include migration, either.

We can conclude that cause and migration of sand waves are not fully understood yet. This paper is based upon a model in which sand wave migration by a residual

Scaling parameters	Symbol	Default value	Dimension
Tidal frequency	σ	$1.4 \cdot 10^{-4}$	s^{-1}
Maximum current velocity	U	1	$\mathrm{m\,s}^{-1}$
Average water depth	H	30	m
Stokes layer thickness	δ	12	m
Kinematic viscosity	A_v	$1 \cdot 10^{-2}$	$\mathrm{m}^2\mathrm{s}^{-1}$
Gravitational acceleration	g	9.8	$\mathrm{m\,s}^{-2}$
Morphological length scale	ℓ_m	500	m

Table 3.1: Scaling parameters and variables.

flow is allowed. The paper tests the hypothesis that tidal movement is responsible for the evolution of sand waves and that steady currents cause these features to migrate. It also discusses prediction of migration rates.

In section 2 we present a scaling method appropriate for sand waves. Furthermore, a non-dimensional idealised model is presented. It is based on the two-dimensional vertical shallow water equations combined with a simple sediment transport equation, describing bed load transport. The morphological changes are calculated over a longer timescale than the water movement. This makes it possible to average the bottom evolution over the tidal period. In section 3 we show the results of a linear stability analysis. We start with a basic state, which consists of a steady current, on top of symmetrical tidal movement (M_2). This steady current is either induced by a wind stress applied at the sea surface or by a pressure gradient. The initial behaviour of the system is then investigated by looking at the feedback of small-amplitude sand waves. Also, a sensitivity analysis is performed on this linear stability analysis. In section 4 we will discuss the results. The fifth and final section contains the conclusions and generalisations of the results.

3.2 Description of the analytical model

The model presented in this paper is based on analytical models constructed by Hulscher [1996], Gerkema [1998], Gerkema [2000] and Komarova and Hulscher [2000]. The Coriolis force only slightly affects sand waves. The behaviour of sand waves can therefore be described with the help of the two-dimensional vertical (2DV) shallow water equations.

3.2.1 Scaling

Before a particular choice is made concerning the method of scaling, we will first summarise the variables and parameters that are assumed to play an important role in sand wave behaviour (Table 3.1). The values chosen in Table 3.1 represent a typical

Variable	Hulscher [1996]	Gerkema [2000]	Kom. & Hulsch. [2000]	This paper
u/u_*	U	U	U	U
w/w_*	σH	$UH\hat{k}$	U	$\frac{1}{10}U$
x/x_*	$U\sigma^{-1}$	$\hat{k}^{-1}$	δ	10δ
z/z_*	H	H	δ	δ
t/t_*	σ^{-1}	σ^{-1}	σ^{-1}	σ^{-1}
ζ/ζ_*	$UL\sigma g^{-1}$	.	$U^2 g^{-1}$	$UL\sigma g^{-1}$
τ_b/τ_{b*}	$UH\sigma$	.	$A_v U\delta^{-1}$	$A_v U\delta^{-1}$
h/h_*	H	H	H	H

Table 3.2: Overview scaling methods (blank means not discussed or not appropriate for comparison). The asterisk $*$ denotes a nondimensional quantity.

North Sea location. Next, typical scaling methods used in the past are summarised in Table 3.2. The last column of Table 3.2 shows the scaling method used in this paper.

The symbols g and A_v indicate the acceleration due to gravity and the constant vertical eddy viscosity, respectively. Time is represented by t and is scaled with the tidal frequency represented by σ. This is because tidal movement is assumed to be the main forcing mechanism of the large-scale bed forms. The velocities in the x- and z- directions are u, respectively w. The horizontal velocity (x) is scaled with the tidal velocity amplitude (U). The vertical co-ordinate is denoted by z and h represents the amplitude of the bottom perturbation. They are both scaled with the Stokes depth (δ). The thickness of the tidal boundary layer is related to δ defined by:

$$\delta = \sqrt{\frac{2A_v}{\sigma}}. \tag{3.1}$$

The vertical velocity (w) and the horizontal length scale (x) is scaled with the Stokes depth. They are furthermore divided and multiplied by a factor 10, respectively, so as to make it possible to scale the variables with physically relevant scales, combined with a correct order of magnitude. This value is obtained by looking at the balance between the shear stress and the slope term in the sediment transport formula [Komarova and Hulscher, 2000]. Gerkema [2000] uses a wave number defined by:

$$\tilde{k} = \frac{2\pi}{\text{length sand wave}}. \tag{3.2}$$

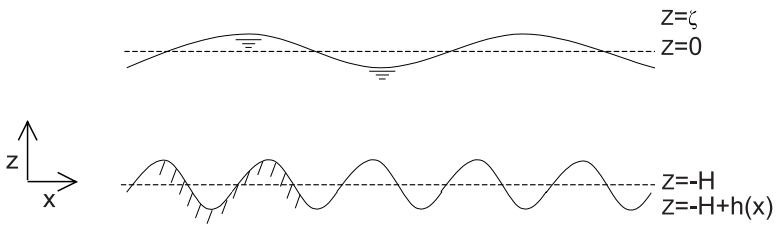

Figure 3.2: Definition sketch of the dimensional model geometry. The horizontal and vertical direction are denoted by x and z. The water surface is defined by ζ relative the $z = 0$. The seabed is defined as h and is relative to the average seabed position, $-H$.

The water level ($z = \zeta$) is scaled with the length over which the tidal wave varies (L). τ_b is the bottom shear stress and scaled analogous to the definition of shear stress giving:

$$\tau_b = A_v \left.\frac{\partial u}{\partial z}\right|_{z=-1+h}. \tag{3.3}$$

3.2.2 Flow model

Starting from the 2DV shallow water equations, neglecting the horizontal viscosity and using the scaling presented in Table 3.2, last column (for convenience $*$ is dropped) we arrive at (see Fig. 3.2):

$$\frac{\partial u}{\partial t} + Ru\frac{\partial u}{\partial x} + Rw\frac{\partial u}{\partial z} = -R\frac{L\sigma}{U}\frac{\partial \zeta}{\partial x} + \frac{\partial}{\partial z}\left(E_v\frac{\partial u}{\partial z}\right), \tag{3.4}$$

$$\frac{\partial u}{\partial x} + \frac{\partial w}{\partial z} = 0, \tag{3.5}$$

with:

$$E_v = \frac{A_v}{\delta^2\sigma}, \qquad R = \frac{U}{10\delta\sigma}. \tag{3.6}$$

E_v can be seen as a measure for the influence of the viscosity on the water movement (by definition the tidal movement) in the water column. R is a function of the square root of the Reynolds number.

3.2.3 Boundary conditions and assumptions

The boundaries in the horizontal plane are located infinitely far away. The boundary conditions at the water surface ($z = \zeta$) are defined as follows:

$$\frac{L\sigma^2 10}{g}\frac{\partial \zeta}{\partial t} + \frac{UL\sigma}{g\delta}u\frac{\partial \zeta}{\partial x} = w, \tag{3.7}$$

$$\frac{\partial u}{\partial z} = \hat{\tau}_w, \tag{3.8}$$

with:

$$\hat{\tau_w} = \frac{\delta}{UA_v}\tau_w, \tag{3.9}$$

in which τ_w describes the wind induced stress at the sea surface. The horizontal flow components at the bottom are described with the help of a partial slip condition (S is the resistance parameter controlling the resistance at the seabed). Models, using a z-independent eddy viscosity formulation and a no-slip condition tend to overestimate the bottom shear stress. The shear stress determines directly the amount of sediment transported. Therefore a partial-slip model with a finite value of the resistance parameter S is needed in order to produce realistic results. The vertical velocity component at the bed ($z = -1 + h$) is described by the kinematic condition:

$$\frac{\partial h}{\partial t} + u\frac{\partial h}{\partial x} = w, \tag{3.10}$$

$$E_v\frac{\partial u}{\partial z} = \hat{S}u, \tag{3.11}$$

with:

$$\hat{S} = \frac{S}{\sigma\delta}. \tag{3.12}$$

3.2.4 Sediment transport and seabed behaviour

The sediment transport model only describes bed load transport. This mode of transport is assumed to be dominant in offshore tidal regimes. As the velocity distribution over the water column is calculated explicitly, bed load transport can be modelled here as a direct function of the bottom shear stress. The following general bed load formula is used [Komarova and Hulscher, 2000]:

$$S_b = \alpha\left(\frac{A_v U}{\sigma}\right)^{1+b}|\tau_b|^b\left[\tau_b - \hat{\lambda}\frac{\partial h}{\partial x}\right]. \tag{3.13}$$

S_b is the volumetric sediment transport. The power of transport, represented by b is set at 1/2. The proportionality constant α can be computed from Van Rijn [1993]. It is set at a value of about $0.3\,\mathrm{m}^{-2}\,\mathrm{s}$ and incorporates the porosity of the bed. The scale factor for the bed slope mechanism is λ. It takes into account that sand is transported more easily downward than upward. The default value is set at 0.0085 in this study [Komarova and Hulscher, 2000]. The effects of the critical shear stress on the slope effects are incorporated herein.

The net inflow of sediment is assumed to be zero. This results in the following sediment balance, which couples the flow model Eqns. (3.4)-(3.12) with the sediment transport model Eq. (3.13) (see Fig. 3.2):

$$\frac{\partial h}{\partial T_m} = -\frac{\partial}{\partial x}\left(|\tau_b|^b\left[\tau_b - \hat{\lambda}\frac{\partial h}{\partial x}\right]\right), \tag{3.14}$$

in which:

$$\hat{\lambda} = \frac{\delta}{10A_vU}\lambda, \qquad T_m = \hat{\alpha}t, \qquad \hat{\alpha} = \frac{\alpha}{10\delta^2\sigma}\left(\frac{A_vU}{\delta}\right)^{1+b} \equiv \frac{1}{\sigma T_{\mathrm{long}}}. \tag{3.15}$$

The bed level will hardly vary on a tidal timescale. The behaviour of the bed is therefore evaluated on a larger time-scale by considering tidally averaged values for the sediment transport.

3.3 Linear stability analysis

The solution of the problem can formally be presented by the vector $\psi = (u, w, \zeta, h)$. The sand wave amplitude to water depth ratio is denoted by ϵ. Starting from an exact solution of the problem, a certain basic state ψ_0 can be perturbed by a small amplitude ($\epsilon \ll 1$) perturbation. The solution can be expanded as follows:

$$\psi = \psi_0 + \epsilon\psi_1 + \epsilon^2\psi_2 + \epsilon^3\psi_3 + \ldots \tag{3.16}$$

For $\epsilon < 1$ and $||\psi_i|| = \mathcal{O}(1)$, the successive terms decrease in magnitude. This means that the one but largest contribution is fully given by the term ψ_1 being linear in ϵ. Therefore, the instability of the basic state ψ_0 can be tested by determining the initial behaviour of ψ_1. Amplification of ψ_1 in time implies that the basic state is unstable and decay means stability.

3.3.1 Basic state

The basic state describes a tidal current together with a steady current over a flat bottom (horizontally uniform flow). The basic vertical velocity turns out to be equal to zero, i.e. $w_0 = 0$. The horizontal basic flow, u_0, satisfies the following equation:

$$\frac{\partial u_0}{\partial t} = -R\frac{L\sigma}{U}\frac{\partial \zeta_0}{\partial x} + \frac{\partial}{\partial z}\left(E_v \frac{\partial u_0}{\partial z}\right). \tag{3.17}$$

The boundary condition at the free water surface $z = 0$ is given by:

$$\frac{\partial u_0}{\partial x} = \tau_w, \tag{3.18}$$

and the boundary conditions at the seabed $z = -1$:

$$E_v \frac{\partial u_0}{\partial z} = \hat{S} u_0, \qquad w_0 = 0. \tag{3.19}$$

The velocity in the horizontal direction consists firstly of a periodic part, which represents M_2 tidal motion. The periodic part of the water motion has a depth-averaged amplitude of $1\,\mathrm{m\,s^{-1}}$ [Hulscher, 1996]. Secondly, we furthermore disrupt the symmetry by adding a steady current ($u_r(z)$). The basic state can now be formulated as follows:

$$u_0 = \beta u_r(z) + (1-\beta)\left\{u_s(z)\sin t + u_c(z)\cos t\right\}, \tag{3.20}$$

in which β enables us to vary the ratio of the steady part and the periodic part, in such a way that the maximum velocity always coincides with the velocity used to scale the system. Two possible types of steady flow components have been investigated. These are (I) a wind driven current and (II) a current induced by a pressure gradient. The vertical structure for each of these cases follows from Eq. (3.17):

$$\text{I}: \quad u_r = \hat{\tau_w}\left(1 + \frac{E_v}{S} + z\right) \tag{3.21}$$

$$\text{II}: \quad u_r = P\left(\frac{1}{2}z^2 - \frac{E_v}{S} - \frac{1}{2}\right), \quad \text{with} \quad P = \frac{L}{10\delta E_v}\zeta. \tag{3.22}$$

Note that in the wind driven case (I), the shear stress at the bottom is equal to the wind stress at the sea surface. This is only the case if the wind-driven current encounters no obstacles.

3.3.2 Perturbed state

The stability of the basic state can be tested by determining the initial behaviour of the first order perturbation. Using Eq. (3.16) and using the basic state solution Eqns. (3.17)-(3.19) gives:

$$\frac{\partial u_1}{\partial t} + Ru_0\frac{\partial u_1}{\partial x} + Rw_1\frac{\partial u_0}{\partial z} = -R\frac{L\sigma}{U}\frac{\partial \zeta_1}{\partial x} + \frac{\partial}{\partial z}\left(E_v\frac{\partial u_1}{\partial z}\right), \tag{3.23}$$

$$\frac{\partial u_1}{\partial x} + \frac{\partial w_1}{\partial z} = 0. \tag{3.24}$$

A Taylor expansion in the small parameter ϵ enables us to transfer the free surface boundary condition from $z = \zeta$ to $z = 0$ and the bottom boundary condition from $z = -1 + h$ to $z = -1$. The boundary conditions at the free surface are then given by:

$$\frac{\partial u_1}{\partial z} = w_1, \tag{3.25}$$

and at the bottom:

$$\frac{\partial u_1}{\partial z} = \frac{\hat{S}}{E_v}u_1 + h_1\frac{\hat{S}}{E_v}\frac{\partial u_0}{\partial z} - h_1\frac{\partial^2 u_0}{\partial z^2}. \tag{3.26}$$

The unknowns are Fourier transformed as follows with $\psi_1 = (u_1, w_1, \zeta_1, h_1)$:

$$\psi_1 = \int \tilde{\psi}(t)\mathrm{e}^{-\mathrm{i}kx}\mathrm{d}k + c.c. \tag{3.27}$$

in which *c.c.* means complex conjugate and k is the wave number of the wavy bottom perturbation. Harmonic truncation in time is applied. This means that the perturbation is restricted to a finite number of tidal components. In the case of a unidirectional tidal flow, the following truncation will contain the dominant physical processes:

$$\hat{u}_{\mathrm{trunc}}(z,t) = \tilde{h}\left[\mathrm{i}a_0(z) + a_s(z)\sin t + a_c(z)\cos t\right], \tag{3.28}$$

$$\hat{w}_{\mathrm{trunc}}(z,t) = \tilde{h}\left[c_0(z) + \mathrm{i}c_s(z)\sin t + \mathrm{i}c_c(z)\cos t\right], \tag{3.29}$$

$$\hat{\zeta}_{\mathrm{trunc}}(z,t) = \tilde{h}\left[d_0 + \mathrm{i}d_s\sin t + \mathrm{i}d_c\cos t\right]. \tag{3.30}$$

The vertical structure (functions $a_s(z)$, etc.)) can now be solved numerically. Subsequently, the shear stress can be calculated and imported into the bottom evolution equation. The evolution of the seabed can best be described by averaging the sediment fluxes over the tidal period, because the seabed will hardly vary on a tidal timescale. The solution for the bottom evolution equation reads:

$$\tilde{h} = h_0\mathrm{e}^{\omega_r T_m}\cos\left(kx - \omega_i T_m\right). \tag{3.31}$$

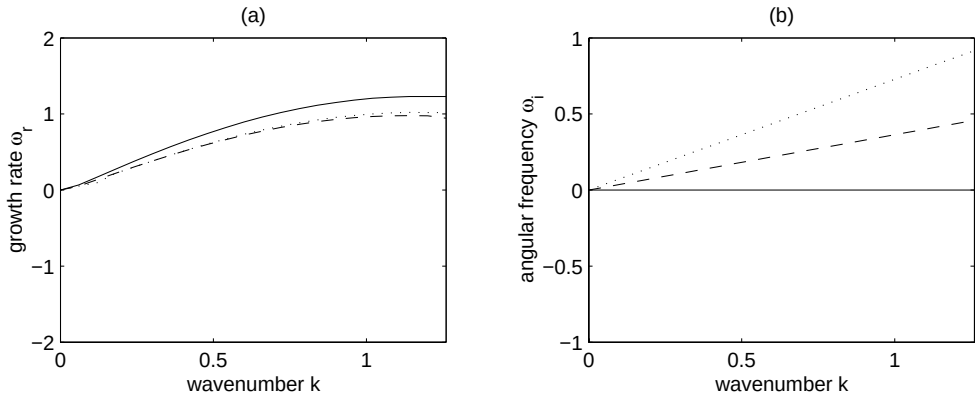

Figure 3.3: Growth characteristics as a function of the wave number k: (a) growth rate ω_r and (b) angular frequency ω_i, both for three cases: M_2 (solid), M_2 plus wind (dashed) and M_2 plus pressure gradient (dotted).

This expression represents a progressive wave, the amplitude of which changes in time, starting from the initial value h_0. The complex growth rate ω is:

$$\begin{aligned}\omega = \omega_r + \mathrm{i}\omega_i \quad = \quad & -k(b+1)a_0'(-1)\left\langle|\tau_{b0}|^b\right\rangle - \hat{\lambda}k^2\left\langle|\tau_{b0}|^b\right\rangle \\ & -\mathrm{i}k(b+1)\left[a_s'(-1)\left\langle|\tau_{b0}|^b\sin t\right\rangle + a_c'(-1)\left\langle|\tau_{b0}|^b\cos t\right\rangle\right], \quad (3.32)\end{aligned}$$

in which the brackets denote the tidal average and τ_{b0} the bottom stress of the basic flow. With this equation the initial response of the bed to the introduced perturbation can be investigated.

3.4 Results

The real part of Eq. (3.32) (ω_r) represents the dimensionless initial growth rate of the sand waves. If the steady current βu_r equals zero, the water motion is symmetric. In Figs. 3.3 (a) and (b) the results are shown for a tidal current with a depth-averaged amplitude of $1\,\mathrm{m\,s^{-1}}$ (M_2, $\beta = 0$). The morphological timescale (T_m) is about 6 years (Eq. (3.15)). This is in line with Hulscher *et al.* [2000] who investigated data sets and found a timescale of 8 years. As was found from previous research ([Gerkema, 2000], [Hulscher, 1996], [Komarova and Hulscher, 2000] and [Blondeaux *et al.*, 1999]) positive growth rates appear for a range of wave numbers k ($\omega_r > 0$). The wavelength having the largest growth rate is the mode we expect to find in nature. The dimensional wavelength follows from:

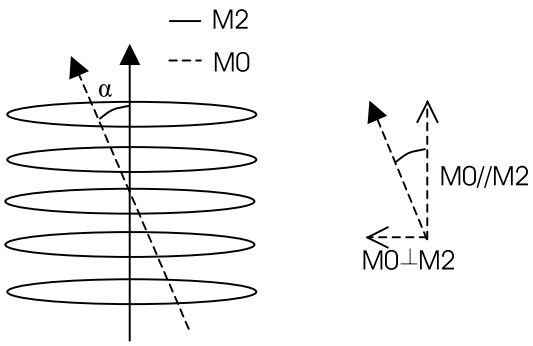

Figure 3.4: Orientation (angle denoted by α) residual current (M_0) with respect to tidal movement (M_2) (crests sand wave oriented perpendicular with respect to the principal current, which is for a typical North Sea location the tidal motion).

$$L_{\mathrm{sw}} = \frac{20\pi}{k}\sqrt{\frac{2A_v}{\sigma}}. \tag{3.33}$$

In this case the fastest growing mode has a wave number $k = 1.25$ (see Fig. 3.3 (a)), which according to Table 3.2, corresponds with a wavelength of about 600 m. In this case, no migration is found.

The phase speed of the sand waves is described by ω_i/k in which ω_i is the imaginary part of Eq. (3.32). These phase speeds are due to the asymmetry in the water motion. The magnitude depends on the nature of the steady part (I or II) and on the magnitude of the asymmetry in the water movement. Fig. 3.3 (a) and (b) show the results for a depth-averaged residual current of $0.1\,\mathrm{m\,s^{-1}}$ (M_0) superimposed on a tidal current of $0.9\,\mathrm{m\,s^{-1}}$ (M_2) ($\beta = 0.1$).

The fastest growing modes have wavelengths in the order of 700 m in both cases (Fig. 3.3 (a)). The angular frequency in case of a net current generated by a pressure gradient and in case of a wind-driven current. The sand waves migrate at a dimensionless rate ω_i/k, in its dimensional form:

$$V_{\mathrm{sw}} = \frac{10\omega_i}{2\pi T_m}\sqrt{\frac{2A_v}{\sigma}}. \tag{3.34}$$

The pressure gradient (case II) induces larger migration rates than a wind stress (case I). For the fastest growing modes, the migration rates for case I become 3 and for case II $10\,\mathrm{m\,yr^{-1}}$. These can be derived from Fig. 3.3 (b) and Eq. 3.34.

In order to assess the sensitivity to the type of driving force of the net current, we combined the velocity profile of case I with the bed shear stress of case II. The

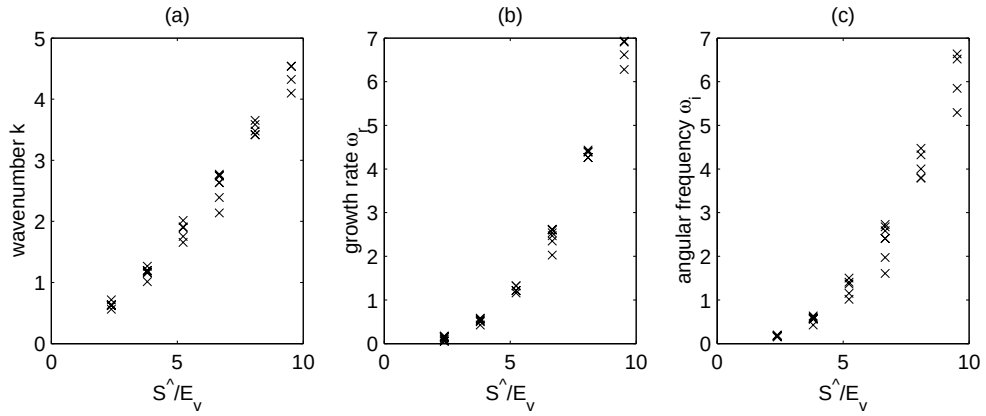

Figure 3.5: Properties of the fastest growing modes a function of $\hat{S}/E_v$: (a) wave number k, (b) growth rate ω_r and (c) angular frequency ω_i.

result was a growth and migration rate close to that of case II. This shows that the bed shear stress is the dominant factor in linear sand wave dynamics. By implication, the parameterisation of the velocity profile is of a lesser importance.

The order of magnitude is similar to values found in the literature ([Van Maren, 1998], [Lanckneus and De Moor, 1991] and [Allen, 1980]). It should be noted that inclusion of higher harmonic modes (M_4, M_6, etc.) will give contributions to Eq. (3.32) which are not taken into account here. However, for most locations the M_0 is assumed to give the largest contribution to the tidal asymmetry, so that it is likely to also play the most important role in sand wave migration. Further investigation, which incorporate higher harmonics, should test these expectations.

This model is likely to overestimate migration rates. The residual current is time-invariant, i.e. it always has the same strength and orientation. It is necessarily oriented perpendicular to the sand wave crests, due to the exclusion of the second horizontal dimension. If a different direction is incorporated, the net current responsible for migration, would have been the component perpendicular to the crests (Fig. 3.4). Furthermore, u_r has to be interpreted as a typical yearly averaged current[1]. In nature, this current will gradually change in magnitude and in orientation in time. The latter means that the tidal and the residual current will have different orientations, again. The effective residual current for sand wave migration will therefore be smaller than the magnitude of the residual current actually observe.

[1]According to Dronkers *et al.* [1990], the average subsurface residual current in the southern North Sea is directed northward and has a magnitude in the order of $0.05\,\mathrm{m\,s^{-1}}$ (see also Van der Molen [2000]).

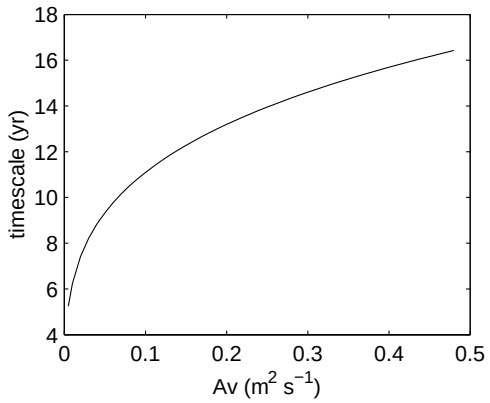

Figure 3.6: Timescale as a function of the eddy viscosity A_v. The timescale increases for larger values of the eddy viscosity.

3.5 Sensitivity analysis

Now we perform a sensitivity analysis for the resistance parameter (at the seabed), the viscosity and the slope parameter. For any combination of these parameters, the fastest growing mode can be determined. The analysis is performed for a depth-averaged residual current of $0.1\,\mathrm{m\,s^{-1}}$ (M_0), induced by a pressure gradient (case II), on top of tidal movement of $0.9\,\mathrm{m\,s^{-1}}$ (M_2) ($\beta = 0.1$).

Figs. 3.5 (a) and (b) show the wave number of the fastest growing modes and the corresponding growth rate, respectively, both as a function of the dimensionless resistance parameter divided by E_v. If the resistance at the seabed increases, the critical wave number and the growth rate increases (smaller wavelengths are found). The opposite holds for an increase in viscosity. The range on the horizontal axis between 0.03 and 0.08 coincides with wavelengths between 3000 and 500 m. We have to keep in mind that the dimensional wavelength for equal dimensionless wave numbers changes for different values of the viscosity. This is due to the use of the Stokes layer thickness instead of the water depth when scaling the spatial co-ordinates (Table 3.2). If the viscosity increases, the Stokes layer thickness increases also, thus changing the length scale. Furthermore, the timescale increases with the eddy viscosity (Eq. (3.15)). This means that the differences in the actual dimensional growth rates will be smaller, although still present (Fig. 3.6).

Fig. 3.5 (c) shows the angular frequency of the fastest growing mode. This quantity becomes smaller for longer wavelengths. If the value of the resistance parameter is increased, the angular frequency will increases too. For the smaller values of the viscosity, this relation is stronger. This is due to the fact that for these smaller values of the viscosity the wavelength of the fastest growing mode is much smaller.

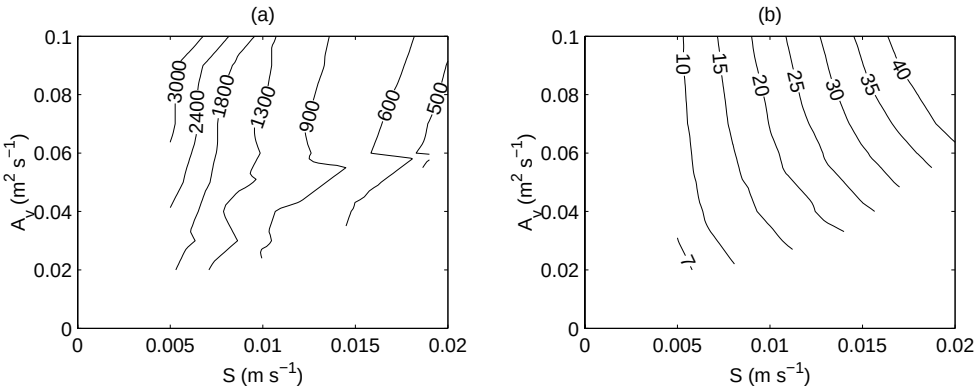

Figure 3.7: Properties of the fastest growing mode as a function of the slip parameter S for different values of the eddy viscosity A_v: (a) wavelength (m) and (b) migration rate ($\mathrm{m\ yr^{-1}}$).

If we plot the wavelength against A_v and S we see that if we increase the viscosity or decrease the resistance parameter, the wavelength of the fastest growing mode will increase (Fig. 3.7 (a)). If we look at the migration rates per year for the same range of A_v and S, we find a very strong dependency on the resistance parameter (Fig. 3.7 (b)).

The slope term does not have a direct effect on the rate of migration, but the slope term does play an important role in determining the fastest growing mode. The slope term dampens the smaller bed forms (Eq. (3.14)). Therefore, if we increase this term, the wave number of the fastest growing mode will become smaller. This corresponds with a larger wavelength having a smaller angular frequency. This means that the expected migration rate is indirectly decreased due to a different fastest growing mode.

In addition to the sensitivity analysis above, we have investigated the effect of varying the magnitude of the net current. It appeared that when β is varied, the default values of the resistance parameter and the slope parameter should be reconsidered. If the bed resistance is too small, very long bed forms will emerge if the ratio tidal movement/steady current decreases. If we increase the resistance by only a factor two, sand wave-like bed forms are found again. This can be see from Figs. 3.8 (a) and (b) showing the wave numbers and phase shifts for the fastest growing modes for different values of the resistance parameter which are unstable. A similar sensitivity was found for the slope parameter (λ).

Furthermore, the real part of omega is hardly influenced by the addition of the residual current. The wave number of the fastest growing mode is almost the same as in the case of only symmetrical tidal movement. Gerkema [2000] showed that value for the growth rate and for the wavelength can vary 28 and 13 percent respectively due to harmonic truncation. Due to the structure of the problem we expect similar deviations

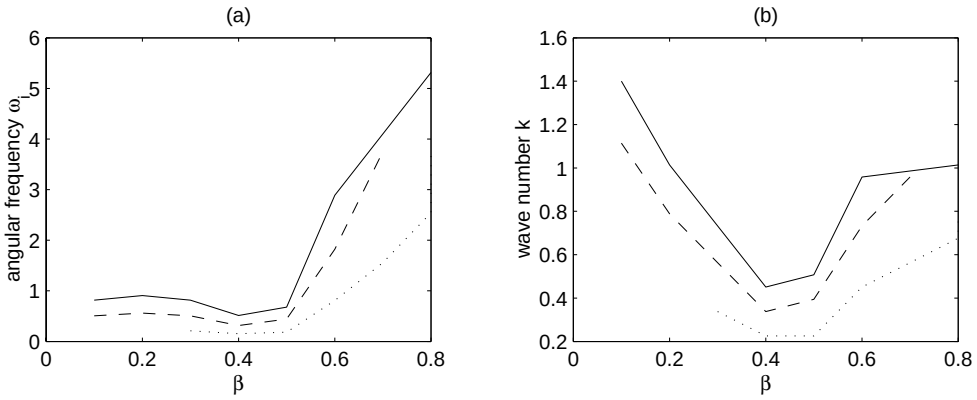

Figure 3.8: Properties of the fastest growing mode as a function of β for different values of the resistance parameter: $S = 0.01$ (solid), $S = 0.008$ (dashed) and $S = 0.005$ (dotted): (a) angular frequency ω_i and (b) wave number k.

for the model presented in this paper, which do not affect the main conclusions.

In the expression of the imaginary part of omega, the wave number can also be found. Since this wave number of the fastest growing does not vary a lot due to the inclusion of a residual current, we do not expect a large difference in the migration rate with respect to the dependency on the wave number.

3.6 Conclusions and Discussion

The foregoing analysis shows that a steady current inducing an asymmetry in the basic state can cause migration of sand waves. The order of magnitude for the migration rates and wavelengths found ($5 - 10\,\mathrm{m\,yr^{-1}}$ and 600 m, respectively) are in agreement with values reported in the literature. The wavelengths are only slightly influenced by the presence of a steady current superimposed on the M_2 tidal motion.

The steady current can be generated by (I) a wind stress and (II) a pressure gradient causing different magnitudes of the shear stress at the seabed, which in turn causes differences in the migration rate in the order of a factor 3. The predicted wavelength is about the same in either case.

Therefore, tidal currents are the main mechanism responsible for the formation of sand waves in this model. The inclusion of a steady current has only minor effects on the formation process. Furthermore, the steady current proved to cause sand wave migration.

Moreover, we found that the asymmetry in the basic bed shear stress is the most important factor in determining the migration of sand waves, the parameterisation of the velocity profile is of lesser importance. This implies that estimates for sand wave

migration rates can be obtained directly from their basic tidal bed shear stress (τ_{b0}) which probably also yields for tidal asymmetries caused by higher harmonics e.g. M_4 (see also Soulsby [1990]) which are not explicitly taken into account here.

We also found a strong dependency of the results, while varying the value of β in Eq. (3.20), on the value of the resistance and slope parameter (see also Hulscher [1996] and Gerkema [2000]).

3.7 Acknowledgements

We would like to thank R.M.J. van Damme (University of Twente) for his comments.

3.8 Appendix: Solution vertical flow structure

The solution of the linear stability problem describes the flow field as a function of the position in the vertical. The equations describing the perturbed tidal and steady current components are:

$$E_v a_0'' = -R\left(\frac{kL\sigma}{U}d_0 + \mathrm{i}ku_r a_0 + \frac{k}{2}u_c - \frac{1}{2}c_c u_c' + \frac{k}{2}a_s u_s - \frac{1}{2}c_s u_s' + \mathrm{i}c_0 u_r'\right) \quad (3.35)$$

$$E_v a_s'' = -a_c + R\left(k\frac{L\sigma}{U}d_s + c_0 u_s' - \mathrm{i}ka_s u_r + \mathrm{i}c_s u_r' + ka_0 u_s\right), \quad (3.36)$$

$$E_v a_c'' = a_s + R\left(k\frac{L\sigma}{U}d_c + c_0 u_c' - \mathrm{i}ka_c u_r + \mathrm{i}c_c u_r' + ka_0 u_c\right), \quad (3.37)$$

$$c_0' = -ka_0, \quad (3.38)$$

$$c_s' = ka_s, \quad (3.39)$$

$$c_c' = ka_c. \quad (3.40)$$

Furthermore, the following boundary conditions at the free surface are needed:

$$\frac{\partial a_0}{\partial z} = \frac{\partial a_s}{\partial z} = \frac{\partial a_c}{\partial z} = 0, \quad (3.41)$$

$$c_0 = c_s = c_c = 0. \quad (3.42)$$

And at the bed we find:

$$a_0' = \frac{\hat{S}}{E_v}a_0 - \mathrm{i}\frac{\hat{S}}{E_v}u_r'' + \mathrm{i}u_r', \quad (3.43)$$

$$a_s' = \frac{\hat{S}}{E_v}\{a_s + u_s'\} - u_s'', \quad (3.44)$$

$$a_c' = \frac{\hat{S}}{E_v}\{a_c + u_c'\} - u_c'', \quad (3.45)$$

$$c_0 = -\mathrm{i}ku_r, \quad (3.46)$$

$$c_s = -ku_s, \quad (3.47)$$

$$c_c = -ku_c. \quad (3.48)$$

3.9 Epilogue: Sand wave migration along a pipeline in the North Sea

This epilogue (not part of Németh *et al.* [2002]) discusses the application of the stability analysis on a field of sand waves located in the North Sea. Hereby, we will investigate if we can estimate the wavelength and migration rate of the sand waves in the data set, based on the parameters available of the environment[1].

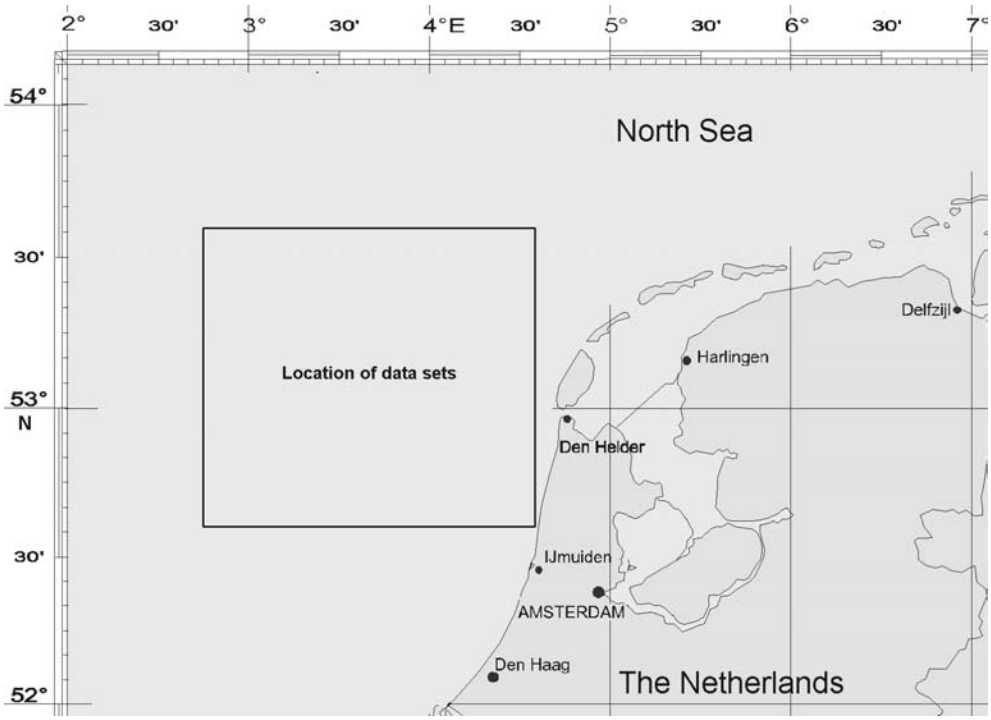

Figure 3.9: Location of the bathymetric data along a pipeline in the North Sea.

3.9.1 Bathymetric surveys along a North Sea pipeline

The bathymetric data used in this epilogue, have been digitised from pipeline alignment sheets. The data used here comes from one section of about 9 km of a pipeline in the southern Bight of the North Sea. Hereby, the crests of the sand waves lie almost

[1]Data analysis based on: Morelissen, R., Hulscher, S.J.M.H., Knaapen, M.A.F., Németh, A.A. and Bijker, R., 2003, Interacting sand waves and pipelines: a data-assimilation based mathematical model, *Coastal Engineering*, in press.

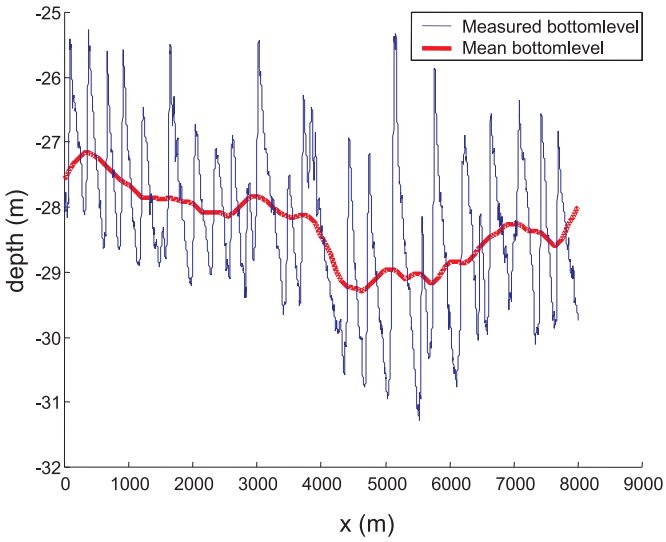

Figure 3.10: The original data (light solid line) and the mean bottom profile (dark dotted line) found using the low pass filter. The bed level on the vertical axis and the position along the pipeline on the horizontal axis are in metres. Short bed level undulations can be seen on the larger sand waves. These undulations are mega-ripples superimposed on the sand waves (Table 2.1). These mega-ripples fall outside the scope of this thesis. (Data courtesy of Clyde Petroleum Exploratie, Holland Offshore Consulting and the State Supervision of Mines.)

perpendicular to the pipeline and the principal direction of the current. Fig. 3.9 gives a rough indication of the position of this data set. Five surveys were available and carried out in 1995, 1996, 1998, 1999 and 2000, giving a total time span of 6 years.

The position of a pipeline is very stable in general. Therefore, it provides a reliable reference position for the bathymetric measurements on charts. This reference position is important to investigate sand wave migration. The position of the pipeline itself is given by only a couple of measurements. The total error of the horizontal positioning is less then $\pm$ 10 m. The total error of the vertical position of the seabed lies in the order of 0.2 m. Both the horizontal and vertical error are equally divided over measurement error and digitisation error.

3.9.2 Data pre-processing

To compare the measured data with results obtained with the sand wave model, the mean bed profile has been derived from the data set using a low-pass filter based on a Hanning window. Subsequently, this mean bottom profile was subtracted from the

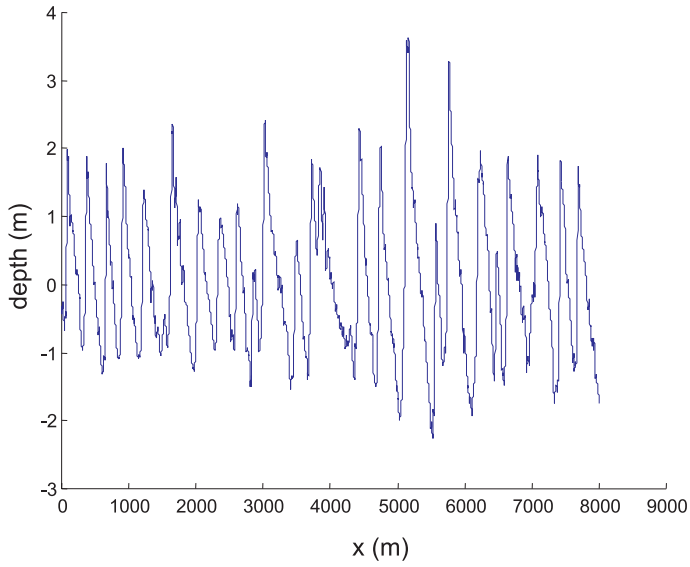

Figure 3.11: Resulting sand waves after subtraction of the mean bottom profile. The deviation from the mean depth on the vertical axis and the position along the pipeline on the horizontal axis are in metres.

original data to isolate the sand wave profile. Figs. 3.10 and 3.11 show the data before and after the filtering.

Looking at Fig. 3.11, the wavelengths of the sand waves found lie in the order of 400 m and their average height is about 3 m (10 % of the average water depth). However, in reality these are slightly smaller since the crests of the sand waves are not oriented perpendicular with respect to the pipeline, but at a small angle. The maximum sand wave height in the domain is 6 m (20 % of the average water depth). Furthermore, they are asymmetrical oriented to the North, coinciding with the residual current present in the Southern North Sea [Dronkers *et al.*, 1990] and with the general direction of movement of the sand waves according to Houbolt [1968]. This coincides further with the found migration of the sand waves in the northerly direction (to the left in Figs. 3.10 and 3.11). The migration rate of the sand waves was assessed by a comparison of successive data sets and varies over the domain. Between 0 & 1000 m and 7000 & 8000 m the migration rate is about 10 m yr^{-1}. Between 2000 and 3000 m, where the sand waves are less high compared to the rest of the data set, the migration rate found is about 20 m yr^{-1}. This is in agreement with other values reported in the literature ([Van Maren, 1998], [Lanckneus and De Moor, 1991] and [Allen, 1980b]).

3.9.3 Application stability analysis

We investigated with the model described in this chapter periodic water motion with a depth-averaged amplitude of 0.9 m s^{-1} together with a steady current of 0.1 m s^{-1}, based on a pressure gradient, as an estimate of the flow conditions present at the location of the data set (Fig. 3.9). Furthermore, the sediment diameter is about 2.4 10^{-4} m [Baptist *et al.*, 2001], giving us a value for λ (Eq. 4.3) following Komarova and Hulscher [2002] of about 0.00375, which is smaller than the value previously used. Hereby, the values of the other parameters needed to determine λ are kept the same. The average water depth is estimated to be about 28 m.

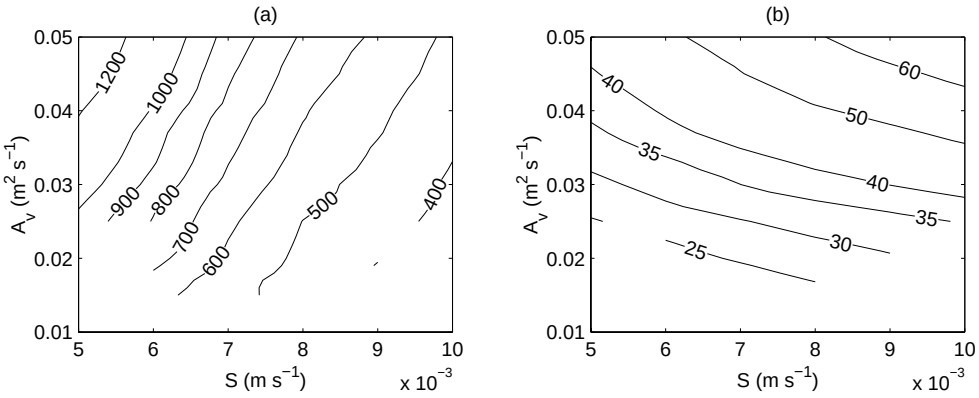

Figure 3.12: Properties of the fastest growing mode as a function of the slip parameter S (m s^{-1}) for different values of the eddy viscosity A_v (m^2 s^{-1}): (a) wavelength (m) and (b) migration rate (m yr^{-1}). A typical North Sea location has a value for the slip parameter S of about 0.008 m s^{-1} and an eddy viscosity A_v of 0.01 m^2 s^{-1}.

3.9.4 Results stability analysis

The properties of the FGM as a function of the slip parameter S for different values of the eddy viscosity A_v can be found in Fig. 3.12. These are the wavelength of the FGM and its coinciding migration rate. A typical North Sea location has a value of the slip parameter S of about 0.006-0.008 m s^{-1} and an eddy viscosity A_v of about 0.01 $m^2 s^{-1}$. This gives us according to the linear stability analysis a wavelength in the order of 400 m and a coinciding migration rate of about 20 m yr^{-1}.

In Chapter 5 of this thesis, while investigating the finite amplitude behaviour of sand waves, we will furthermore see that the migration rate diminishes only slightly during the evolution of sand waves. The migration rate of a fully-grown sand wave is about 20% less than that of an infinitely small sand wave. This gives us an estimate of the migration rate of about 16 m yr^{-1}.

3.9.5 Conclusions

The results from the stability analysis coincide very well with the observations made along the pipeline. Although the wavelengths are slightly too long. This deviation is allowed, considering the simplifications in the model, the errors in the estimated values of the different parameters and the errors in the data set.

To perform similar studies and further validate this and other models giving confidence in their predictions, we need more data. Like the data set used here, this data should span a couple of years with an interval of about a year. This to enable the identification of sand wave migration. The horizontal positioning error in the data should be less than the migration over the measurement period. Rigid structures like pipelines or other landmarks provide us with information to obtain the required accuracy of the horizontal position of the data.

This model forms a step in the direction of estimating sand wave migration when no time series of bathymetric data is available during the planning of a new pipeline, or the optimisation of the monitoring and dredging strategy of navigational routes (See also Le Bot *et al.* [2000] and Le Bot [2001]). However, we then need data on the seabed composition and velocity profiles in the water column to determine the roughness at the seabed (Eq. (3.11)), the magnitude of the slope effect and the other parameters in the sediment transport formulation (Eq. (3.13)). Furthermore, we need depth-averaged values of the (at least) yearly averaged current velocities (These depth-averaged values can come from large scale numerical models).

3.10 Acknowledgements

We thank Clyde Petroleum Exploratie, Holland Offshore Consulting and the State Supervision of Mines for providing the data.

Chapter 4

A sand wave simulation model

Abstract: Sand waves form a prominent regular pattern in the offshore seabeds of sandy shallow seas. A two-dimensional vertical (2DV) flow and morphological simulation model describing the behaviour of these sand waves has been developed. The simulation model contains the 2DV shallow water equations, with a free water surface and a general bed load formula. The water movement is coupled to the sediment transport equation with a seabed evolution equation. The domain is non-periodic in both directions. The spatial discretisation is performed by a spectral method based on Chebyshev polynomials. A fully implicit method is chosen for the discretisation in time. Firstly, we validate the simulation model mathematically by reproducing the results obtained using a linear stability analysis [Németh *et al.*, 2002] for infinitely small sand waves. Hereby, we investigate a steady current situation induced by a wind stress applied at the sea surface. The bed forms we find have wavelengths in the order of hundreds of metres when the resistance at the seabed is relatively large. The results show that it is possible to model the initial evolution of sand waves with a numerical simulation model. This chapter forms a part of a study to investigate the intermediate term behaviour of sand waves[1].

Keywords: stability analysis, numerical analysis, spectral method, sand waves, generation, shelf seas, 2DV.

4.1 Introduction

Large parts of shallow seas — such as the North Sea — are covered with bed features having a variety of spatial dimensions (Fig. 4.1). Sand waves form a prominent bed pattern with a crest to crest spacing of hundreds of metres. Sand waves are observed at water depths in the order of 30 m and their heights can reach up to several metres. The crests are often assumed oriented perpendicularly to the principal current ([Johnson

[1]Extended after: Németh, A.A., Hulscher, S.J.M.H. and Van Damme, R.M.J., 2001, Numerical simulation of sand wave evolution in shallow shelf seas, *Proceedings of the fourth conference on coastal dynamics*, Lund, Sweden, editors Hanson, H. & Larson, M., pp. 1048-1057.

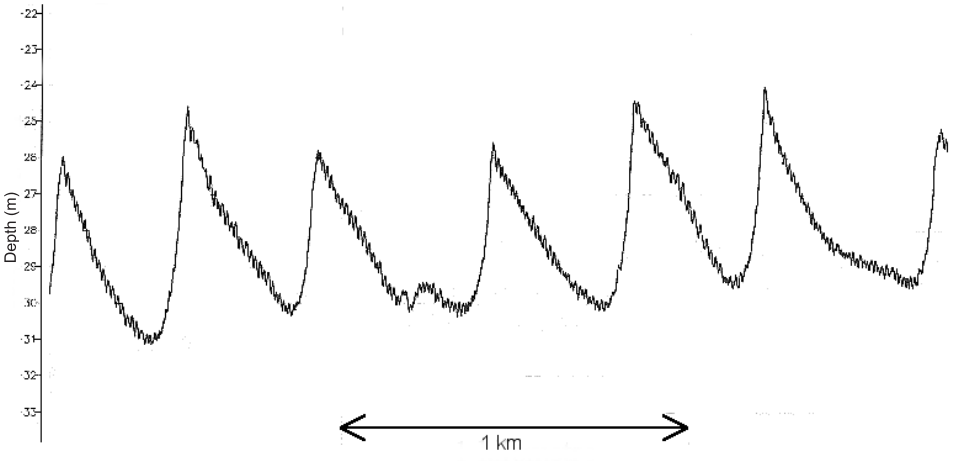

Figure 4.1: Cross-section of sand waves based on bathymetry measurements made in the North Sea (Courtesy Clyde Petroleum Exploratie; Holland Offshore Consulting; State Supervision of Mines, 2000).

et al., 1981] and [Langhorne, 1981]). Based on a theoretical analysis, Hulscher [1996] showed that sand wave crests may deviate up to 10^o anti-clockwise perpendicularly from the principal direction of the current.

An analysis of the sand market [Peters, 2000] showed that a shortage of sand is expected in the future in the Netherlands. The crests of sand waves are assumed to have the best composition for use in concrete. Knaapen and Hulscher [2002] showed that when a sand wave is dredged, it is able to recover in only a matter of years. Furthermore, the behaviour of sand waves plays an important role in the selection of areas for large-scale sand extraction pits and their design. The influence of a pit or artificial island on its surrounding bed topography (including sand waves) is still unclear. Besides, the presence of sand waves changes the hydrodynamics and therefore the recolonization possibilities of benthic fauna [Stolk, 2000]. Observations suggest that sand waves are dynamic ([Allen, 1980b] and [Lanckneus *et al.*, 1991]) and may migrate with speeds of up to several metres per year. Therefore, insight into the behaviour of these sand waves is crucial to enable cost-effective management practices.

Huthnance [1982] was the first to look at a system consisting of depth-averaged tidal flow and an erodible seabed. Within this framework, it is possible to investigate whether certain regular patterns develop as free instabilities of the system. Unstable modes comparable to tidal sandbanks were found, whereas smaller modes corresponding to sand waves were not initiated. This work was extended by Hulscher [1996] using a model allowing for vertical circulations and found formation of sand

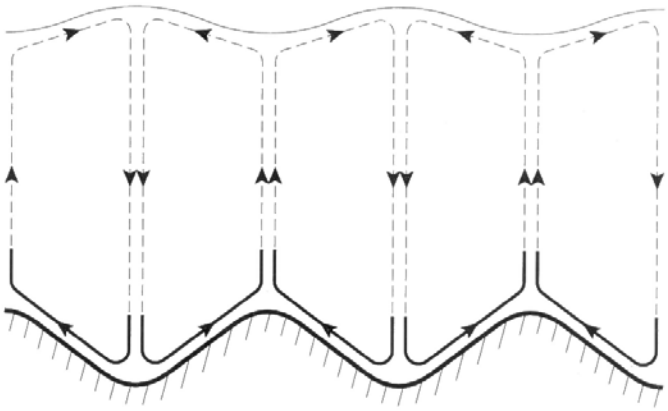

Figure 4.2: Residual current directed upwards towards the crest near the seabed over a tidal cycle [Hulscher, 1996].

waves based on a horizontally averaged symmetrical tidal motion. The work showed that net convergence of sand can occur at the top of the sand waves over an entire tidal cycle, as shown in Fig. 4.2 (see also Gerkema [2000] and Komarova and Hulscher [2000]). Németh *et al.* [2002] extended the previous work by including an asymmetric basic flow, inducing sand wave migration.

A consequence of linear stability analysis is that their validity is limited to small-amplitude sand waves. However, this is far from the final aim, which is understanding the entire evolutionary process of sand wave formation. Komarova and Newell [2000] have extended the linear analysis by Komarova and Hulscher [2000] into the weakly non-linear regime for investigation of the behaviour of finite-amplitude idealised sand waves. However, migration is not discussed. Fredsøe and Deigaard [1992] describe the behaviour of existing finite-amplitude dunes under a steady current. They assume the time-dependence of the flow to be negligible when modelling sand waves in a tidal environment. Johns *et al.* [1990] discuss the finite amplitude behaviour of bed forms similar to sand waves under a steady current.

Numerical methods are a tool to overcome the limitations of a linear analysis and enable the study of the non-linear behaviour of these bed sand waves. This possibly enables the description of the entire evolutionary process of sand waves and might give a clue to the most important mechanisms, determining the growth and stabilisation of sand waves. Furthermore, migration and irregular sand wave shapes can be investigated.

Within this chapter, we focus on the first step, which is to reproduce the results obtained using a linear stability analysis for small amplitude sand waves [Németh *et al.*, 2000] (from here on referred to as "stability analysis") with a new numerical simulation model (from here on referred to as "simulation model"). Hereby, we also

Parameters	Symbol	Default value	Dimension
Depth-averaged value velocity	U	1	$\mathrm{m\,s^{-1}}$
Average water depth	H	30	m
Kinematic eddy viscosity	A_v	$3 \cdot 10^{-2}$	$\mathrm{m^2 s^{-1}}$
Resistance parameter	S	$1 \cdot 10^{-2}$	$\mathrm{m\,s^{-1}}$
Gravitational acceleration	g	9.8	$\mathrm{m\,s^{-2}}$
Power of transport	b	$5 \cdot 10^{-1}$	–
Proportionality constant	α	$3 \cdot 10^{-1}$	$\mathrm{m^{-2}\,s}$
Bed slope factor	λ_1	$2 \cdot 10^{-3}$	$\mathrm{m^2\,s^{-2}}$
Bed slope factor	λ_2	3.33	–
Sand wave length	L_{sw}	600	m
Number of sand waves	N_{sw}	3	–

Table 4.1: Default values and dimensions of the parameters and variables existing in the system.

focus on sand waves in a unidirectional steady current only.

Firstly, we present the mathematical formulation of the sand wave simulation model. It is based on the two-dimensional vertical shallow water equations combined with a simple sediment transport equation, describing bed load transport. Next, the numerical set-up pursued in this work is discussed. We present the coordinate transformation method, the spatial and temporal discretisation. Subsequently, we validate the simulation model mathematically by comparing it with the linear stability analysis discussed in Chapter 3. In the final section, we present the discussion and conclusions.

4.2 2DV morphological model

4.2.1 Flow model

The simulation model presented in this chapter is based on Németh *et al.* [2002]. It is known that the Coriolis force only slightly affects sand waves [Hulscher, 1996]. Therefore, the behaviour of sand waves can be described with the help of the two-dimensional vertical (2DV) model. We start from the 2DV shallow water equations:

$$\frac{\partial u}{\partial t} + u\frac{\partial u}{\partial x} + w\frac{\partial u}{\partial z} = -g\frac{\partial \zeta}{\partial x} + \frac{\partial}{\partial z}\left(A_v \frac{\partial u}{\partial z}\right), \tag{4.1}$$

$$\frac{\partial u}{\partial x} + \frac{\partial w}{\partial z} = 0. \tag{4.2}$$

The symbols g and A_v indicate the acceleration due to gravity and the vertical eddy viscosity, respectively. Time is represented by t. The velocities in the x- and z-directions are u and w, respectively. The water level is denoted by ζ and H represents the mean water depth. The level of the seabed is represented by $-H+h$ (see Fig. 4.3).

4.2.2 Sediment transport and seabed behaviour

The sediment transport model in this chapter describes bed load transport. This mode of transport is assumed to be dominant in offshore tidal regimes. As the velocity distribution over the water column is calculated explicitly, bed load transport can be modelled as a function of the shear stress at the seabed. This is in contrast with depth-averaged models, which calculate the sediment transport as a function of the depth-averaged velocity. The following general volumetric bed load formula for S_b is used, following Komarova and Hulscher [2000]:

$$S_b = \alpha |\tau_b|^b \left[\tau_b - \lambda_1 \frac{\partial h}{\partial x} - \lambda_2 |\tau_b| \frac{\partial h}{\partial x} \right], \tag{4.3}$$

with τ_b the shear stress at the seabed:

$$\tau_b = A_v \left. \frac{\partial u}{\partial z} \right|_{z=-H+h}. \tag{4.4}$$

The power of transport, represented by b is set at $1/2$. The proportionality constant α is set at a value of 0.3 s m^{-2} following Van Rijn [1993] and incorporates the density difference between water and sediment. The first scale factor for the bed slope mechanism (λ_1) and the second scale factor λ_2 take directly into account that sand is transported more easily downhill than uphill. The default values of λ_1 and λ_2 are set at 0.002 and 3.33, respectively. In the stability analysis (Chapter 3), λ_1 and λ_2 were taken together (i.e. $\lambda = \lambda_1 + \lambda_2 |\tau_b|_{z=-H}$) since both terms in that case contribute in the same manner since $h \ll H$. A threshold of sediment motion is not taken into account explicitly at this point.

The sediment balance, which couples the flow model Eqns. (4.1) and (4.2) with the sediment transport model Eq. (4.3), calculates the position of the seabed based on the principle of conservation of mass as a function of time:

$$\frac{\partial h}{\partial t} = -\frac{\partial S_b}{\partial x}. \tag{4.5}$$

The bed level will hardly vary on a tidal timescale. The behaviour of the bed can therefore evaluated on a larger timescale if desired.

4.2.3 Boundary conditions and assumptions

The boundary conditions at the water surface ($z = \zeta$) are given as follows:

$$\frac{\partial \zeta}{\partial t} + u \frac{\partial \zeta}{\partial x} = w, \tag{4.6}$$

$$\frac{\partial u}{\partial z} = \frac{\tau_w}{A_v}. \tag{4.7}$$

in which τ_w describes the wind induced shear stress at the sea surface. The vertical velocity component at the seabed ($z = -H + h$) is described by the kinematic condition:

$$\frac{\partial h}{\partial t} + u\frac{\partial h}{\partial x} = w, \tag{4.8}$$

The horizontal flow components at the seabed are modelled with the help of a partial slip condition (S is the resistance parameter controlling the resistance at the seabed). The boundary condition couples the resistance at the seabed with the water movement across the seabed:

$$A_v\frac{\partial u}{\partial z} = Su. \tag{4.9}$$

Furthermore, we use non-periodic boundary conditions in the horizontal and vertical direction. This set up also gives more freedom to the system with respect to the selection of the fastest growing mode. In a periodic set up, the amount of modes which can be unstable is limited by the horizontal length of the grid, since we pose a limitation on the wavelength the simulation model is allowed to select. Since we are also interested in the behaviour of the wavelength of a sand wave during its evolution, we keep the simulation model set up as generic as possible.

At the inflow boundary, a discharge is prescribed, with a certain velocity profile in the vertical plane. In case of a steady flow, two possible origins can be investigated. These are (I) a wind driven current (τ_w) and (II) a current induced by a pressure gradient. The vertical structure for each of these cases is:

$$\text{I}: \quad u_r = \frac{\tau_w}{A_v}\left(H + \frac{A_v}{S} + z\right), \tag{4.10}$$

$$\text{II}: \quad u_r = P\left(\frac{1}{2}z^2 - \frac{A_v}{S}H - \frac{1}{2}\right), \tag{4.11}$$

with P a parameter determining the magnitude of the pressure gradient and thereby the depth averaged velocity. These profiles are equivalent to the analytical expressions of the basic state situation over a flat seabed used in the stability analysis with the seabed positioned at $z = -H + h$.

The outflow boundary is physically an open boundary. However, the simulation model requires a prescribed boundary condition. Therefore, an estimate of the water level is supplied to the simulation model at the outflow boundary. Furthermore, the derivatives in the horizontal direction for the horizontal and vertical velocities are set to zero at the outflow boundary.

4.2.4 Discussion boundary conditions

Even though we are setting up the simulation model in a non periodic way, we investigate the possibility of applying periodic conditions. This we wish to do since these

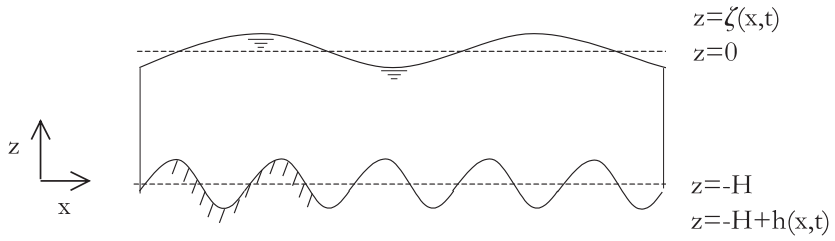

Figure 4.3: Definition sketch of the non-periodic dimensional model geometry of the physical domain. The horizontal and vertical direction are denoted by x and z. The water surface is defined by ζ relative the $z = 0$. The seabed is defined as h and is relative to the average seabed position, $-H$.

boundary conditions provide the main benefit of simplifying the system, decreasing calculation time. Since the outflow and inflow boundary are then the same, no extra physical space needs to be reserved near the boundaries, avoiding the problem of physical disturbances reaching the boundaries and reflecting.

A wind stress applied at the sea surface (Eq. (4.10) and (4.7)) is balancing the resistance in the system equally over the entire domain. This forcing mechanism induces water movement without a gradient in the water level for a flat seabed. The water level and velocity profile at the outflow boundary are therefore the same as the inflow boundary (when the position and gradient of the seabed are the same at both boundaries). Therefore, it is also possible to use periodic boundary conditions in the horizontal direction. Obviously, the vertical direction always has to remain non-periodic.

When we apply a pressure gradient at the inflow boundary Eq. (4.11), the water level decreases moving away from the inflow boundary, due to resistance in the domain. Due to continuity Eq. (4.2), the depth-averaged velocity increases along the reducing water level. Therefore, the velocity profiles, water and seabed levels at the in- and outflow boundary can never coincide. Tidal motion can be seen as a time-dependent pressure gradient at the inflow boundary. Therefore, in the set up of applying periodic boundary conditions, the entire tidal wave needs to be described. This is practically not feasible, since we require accuracy on a relative small length scale (sand waves with a wavelength of hundreds of metres compared to the wavelength of a tidal wave of hundreds of kilometres). However, periodic boundary conditions are also here possible in the case of a (time-dependent or not) pressure gradient if we incorporate the pressure gradient directly in the momentum equation Eq. (4.1). The simulation model still contains a free surface, which responds to variations in the seabed. However, no gradient is present in the case of a flat seabed, making periodic boundary conditions possible.

4.3 Numerical approximation

4.3.1 Spatial discretisation

A spectral collocation method is used to obtain a discrete approximation of the equations of the solution, on a set of discrete grid points [Canuto *et al.*, 1988] and Fornberg [1996]). This method is applied in both coordinate directions. The discrete grid points are specified by collocation points. The grid points are given by the most commonly used Chebyshev Gauss-Lobatto points:

$$\xi^k = \cos(\frac{\pi j}{N}), \quad \text{with} \quad j = 0, 1, ..., N^k \quad \text{and} \quad k = 1, 3. \tag{4.12}$$

The collocation method implies that the residual function is forced to zero at these points. N^k defines the number of intervals in the ξ^k-direction. The solution is represented at each grid point using one-dimensional basis functions. The basis functions consist of the Chebyshev polynomials defined by:

$$T_p(Z) = \cos(p \cos^{-1}(Z)), \quad \text{with} \qquad p = 1, 2, ... \tag{4.13}$$

For the grid points, the Chebyshev collocation derivative can be obtained in two different ways. The first method is to calculate the derivatives in spectral space (transform method). This method involves three steps. Firstly, a Discrete Chebyshev Transform has to be applied, after which differentiation can take place in spectral space. The solution than has to be transformed back to physical space using the Inverse Discrete Chebyshev Transform.

The second method — differentiation in physical space — combines the three steps of the transform method. This results in a matrix D given by [Canuto *et al.*, 1988], which can be used to calculate the first derivative at the grid points:

$$D_{ij} = \begin{cases} \frac{c_\mathrm{i}^{i+j}}{c_\mathrm{j} x_\mathrm{i} - x_\mathrm{j}}, & i \neq j \\ \frac{-x_\mathrm{j}}{2(1-x_\mathrm{j}^2)}, & 0 < i = j < N \\ -\frac{2N^2+1}{6}, & i = j = 0 \\ \frac{2N^2+1}{6}, & i = j = N. \end{cases} \tag{4.14}$$

where

$$c_\mathrm{j} = \begin{cases} 2, & j = 0 \; or \; j = N \\ 1, & 1 \leq j \leq N-1. \end{cases} \tag{4.15}$$

The matrix necessary to calculate a second derivative at the grid points can be calculated by taking the square of matrix D given in Eq. (4.14). The vector containing the function values U at the collocation points is multiplied with this first or second derivative matrix to obtain a vector containing the values for the first or second derivative values at the collocation points, respectively. The two-dimensional version of Eq. (4.14) in the horizontal and vertical direction can be found in the appendix in Eqns. (4.44) and (4.45).

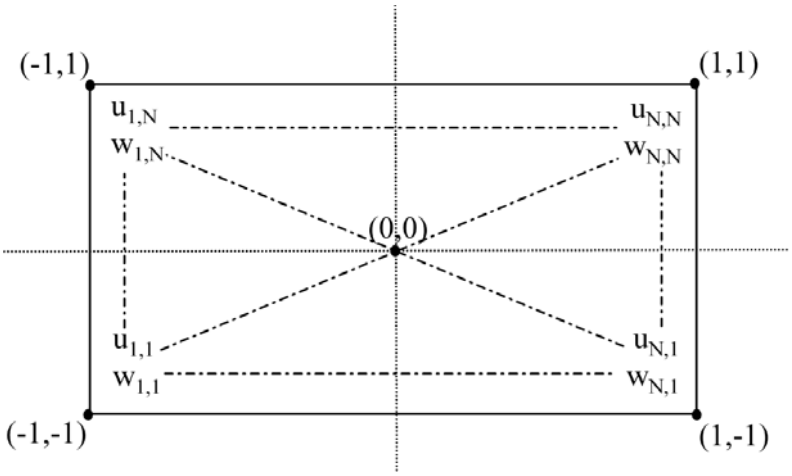

Figure 4.4: Computational grid and indices used in the code.

4.3.2 Coordinate transformation

The coordinate system used for the computational space is represented by ξ^1 for the horizontal direction and ξ^3 for the vertical direction (see also Fig. 4.4). Both directions of the computational coordinate system have a domain of [-1,1] to coincide with the Gauss-Lobatto grid. This system is obtained by mapping the physical space, represented by the Cartesian coordinates x and z, with the following analytical transformations:

$$\xi^1 = 1 - \frac{2x}{N_{sw} L_{sw}}, \tag{4.16}$$

$$\xi^3 = 1 - \frac{2(z-\zeta)}{\zeta + H - h}, \tag{4.17}$$

with L_{sw} the initial wavelength of the sand wave chosen to be investigated with the simulation model and N_{sw} the number of sand waves in the domain. The total length of the domain is therefore N_{sw} times the wavelength L_{sw}.

Following this transformation, the total number of collocation points remains the same irrespective of the local water depth. This representation allows for a smooth description of the seabed topography together with a varying water surface on a rectangular grid.

4.3.3 Partial derivatives

Next, we compute the necessary partial derivatives for (ζ, h, u, w), to compensate for the changes in physical space projected on the fixed computational grid:

$$\frac{\partial u}{\partial x} = \frac{\partial u}{\partial \xi^1}\frac{2}{N_{sw}L_{sw}} + 2\frac{\partial u}{\partial \xi^3}\frac{\zeta_x - \frac{1}{2}(\xi^3 - 1)(\zeta_x - h_x)}{\zeta + H - h}, \tag{4.18}$$

$$\frac{\partial u}{\partial z} = \frac{\partial u}{\partial \xi^3}\frac{2}{\zeta + H - h}, \tag{4.19}$$

$$\frac{\partial^2 u}{\partial z^2} = \frac{\partial^2 u}{\partial {\xi^3}^2}\{\frac{2}{\zeta + H - h}\}^2, \tag{4.20}$$

$$\frac{\partial u}{\partial t} = 2\frac{\partial u}{\partial \xi^3}\frac{\partial \zeta}{\partial t}\frac{1 - \frac{1}{2}(\xi^3 - 1)}{\zeta + H - h} + \frac{\partial u}{\partial \eta}. \tag{4.21}$$

The necessary partial derivatives for the other variables w, h and ζ can be derived in a similar manner.

4.3.4 Temporal discretisation flow model and grid

The spatial approximation using a Chebyshev grid is the best in the interior of the domain. Therefore an increased density of grid points is required near the boundaries. The numerical convergence rate of the method decreases significantly if this is not the case. This aspect has an effect on the choice of the time scheme. An explicit scheme is desirable, with respect to the computational effort necessary per time step. However, the size of the time step, is determined by the smallest distance between grid points in the domain. Therefore, a higher density of grid points near the boundaries — as with the Gauss-Lobatto grid — poses a problem. If we increase the total number of grid points, the smallest distance between grid points will decrease more than the relative increase in points. The time step will become too small to be efficient.

The most practical approach is therefore to use a fully implicit formulation. In this case the time step does not depend anymore on the spatial discretisation for stability reasons. All the properties of u, w, ζ and h are calculated simultaneously at each time step. The calculation cost per time step is higher than for an explicit formulation. However, the time steps that can be taken are much larger.

The system is solved with the routine D02NGF from the Nag library. It is a general-purpose routine which can integrate initial value problems, for a stiff system of ordinary differential equations, with coupled algebraic equations. The system is written in the form:

$$A(t, Y)\frac{dY}{dt} = r(t, Y), \tag{4.22}$$

with $Y = (u, w, \zeta, h)$ the solution vector. On the left hand side, we find the derivatives of the solution vector Y. Matrix A can be found in the Appendix Eq. (4.46).

On the right hand side, their dependency on time can be found. Here, the differential equations, which do not have a time-dependent term, appear as the residuals of the continuity equation (4.2) and most of the boundary conditions. When the right hand side is zero, we are looking at a steady state solution. If it is non-zero, the solution is changing in time.

The momentum balance Eq. (4.1) containing the temporal discretisation in the form of Eq. (4.22) can be written as follows:

$$\begin{aligned}\frac{du}{dt} = -2\frac{\partial\zeta}{\partial t}\frac{1-\frac{1}{2}(\xi^3-1)}{\zeta+H-h}D_1^3u - \frac{2}{N_{sw}L_{sw}}uD_1^1u \\ - 2\frac{\zeta_x-\frac{1}{2}(\xi^3-1)(\zeta_x-h_x)}{\zeta+H-h}uD_1^3u + \frac{2}{\zeta+H-h}wD_1^3u \\ - g\frac{2}{N_{sw}L_{sw}}D_1^1\zeta + A_{\mathrm{v}}\{\frac{2}{\zeta+H-h}\}^2D_2^3u. \quad (4.23)\end{aligned}$$

Here D_i^k is the k-th derivative in the i-th direction. The partial derivatives h_x and ζ_x are of the form of Eq. (4.18).

The continuity equation Eq. (4.2) is an instantaneous constraint that applies at each time level and can be found on the right hand side of Eq. (4.22) as a time independent equation:

$$\frac{2}{N_{sw}L_{sw}}D_1^1u + 2\frac{\zeta_x-\frac{1}{2}(\xi^3-1)(\zeta_x-h_x)}{\zeta+H-h}D_1^3u - \frac{2}{\zeta+H-h}D_1^3w = 0. \quad (4.24)$$

At the inflow boundary Eq. (4.10) and Eq. (4.11) we find:

$$u = \text{prescribed}|_{x=-1} \quad \text{and} \quad w = 0|_{x=-1}\,. \quad (4.25)$$

At the outflow boundary, we find the horizontal derivatives of u and w set to zero, resulting in:

$$\frac{2}{N_{sw}L_{sw}}D_1^1u + 2\frac{\zeta_x-\frac{1}{2}(\xi^3-1)(\zeta_x-h_x)}{\zeta+H-h}D_1^3u = 0\Big|_{x=1}, \quad (4.26)$$

$$\frac{2}{N_{sw}L_{sw}}D_1^1w + 2\frac{\zeta_x-\frac{1}{2}(\xi^3-1)(\zeta_x-h_x)}{\zeta+H-h}D_1^3w = 0\Big|_{x=1}. \quad (4.27)$$

Furthermore, the water level is fixed at the downstream boundary. The boundary condition at the free surface can now be written as a kinematic condition Eq. (4.6) together with a shear stress at the surface equal to the wind stress Eq. (4.7) (if present):

$$\frac{\partial \zeta}{\partial \eta} + u \frac{2}{N_{sw} L_{sw}} D_1^3 \zeta = w \Big|_{z=\zeta}, \tag{4.28}$$

$$-\frac{2}{\zeta + H - h} D_1^3 = \tau_{\mathrm{w}} \Big|_{z=\zeta}. \tag{4.29}$$

At the seabed we find another kinematic condition Eq. (4.8) and the partial slip condition Eq. (4.9):

$$w - u \frac{2}{N_{sw} L_{sw}} D_1^1 h = 0 \Big|_{z=-H+h}, \tag{4.30}$$

$$u - \frac{2}{\zeta + H - h} \frac{A_{\mathrm{v}}}{S} D_1^3 u = 0 \Big|_{z=-H+h}. \tag{4.31}$$

The sediment transport model Eq. (4.3) in discretised form can be written as:

$$S_b = \alpha |(\frac{2}{\zeta + H - h})^2 D_1^3 u|^b \left[D_1^1 u - (\lambda_1 + \lambda_2 |\tau_b|) \frac{\zeta + H - h}{N_{sw} L_{sw}} D_1^1 h \right], \tag{4.32}$$

with τ_b the shear stress at the seabed defined by Eq. (4.4). The net inflow of sediment is assumed to be zero. The seabed evolution Eq. (4.5) can now be described on the computational grid by:

$$\frac{\partial h}{\partial t} = \frac{2}{N_{sw} L_{sw}} D_1^1 S_b. \tag{4.33}$$

For completeness, we have to specify a boundary condition at a boundary coinciding with the horizontal position of the flow boundaries for the bottom evolution equation. This is equivalent to the boundary condition necessary for the water level. This can also be done by taking the derivative of the sediment transport equal to zero coinciding with a fixed seabed. At this point, only the initial response is needed here for comparison with the results from the stability analysis.

4.3.5 Initial values and time stepping

For a flat seabed, the initial conditions can be derived analytically. In case the seabed is not flat, but contains for example a sinusoidal feature, we can use this solution for a flat seabed — which is equivalent to a basic state solution in a stability analysis — as an estimate for the initial condition. Secondly, a better initial condition can be given by the solution of the stability analysis (especially for small amplitudes ($h \ll H$)) in Chapter 3 [Németh *et al.*, 2002].

However, the estimate of the initial solution prescribed with these two approaches for a sinusoidal sand wave are still not the exact solutions of the system. This difference in applied solution and the actual solution can be seen as an initial disturbance in the system. The order of magnitude of the error/disturbance depends on the ratio of h/H, the spatial discretisation and the requested accuracy from the time integrator. The propagation velocity c of a wave in shallow water is calculated with:

$$c = \sqrt{gH} \tag{4.34}$$

A steady state solution, which we in general require to start a simulation, can be achieved by letting the disturbances travel through the domain a couple of times. For a typical water depth of 30 m, the propagation velocity is about 17 m s^{-1} according to Eq. (4.34). For a domain with a length of 2 km, this would mean that a disturbance in the water motion due to the incorrect initial solution takes about 120 s to travel from one end of the domain to the other. After about 600 s we can expect a virtually steady state solution. This solution can then form the starting point for a simulation.

In the limit ($t \to \infty$) the changes in time for a steady state solution should be equal to zero. Therefore the residuals of Eq. (4.22) are practically zero which is discussed below. Furthermore, this aspect can be seen by looking at the magnitude of the time step of the time integrator. This time step is small initially due to the calculation of all the dependencies of the system and possible initial changes in the physical system. Large time steps can be taken when the steady state situation has been attained, as long as the seabed does not change.

When the seabed is allowed to change, the magnitude of the time step becomes a function of this seabed change. The time steps are then still large due to the slow evolution of the seabed compared to the water movement, in case of a steady state current. This is due to the difference in timescale for the water motion and seabed change. This only holds for the case of a steady current or a block current. In the case of pure tidal motion, the time step size is again determined by the timescale of the water motion. Therefore, if we wish to avoid long computation times during long-term morphological simulations including tidal motion, we need to incorporate a different time stepping mechanism for seabed change.

4.4 Results

We start with the investigation of a steady flow. First, we discuss in short this steady flow and its effects on the behaviour of the seabed with the help of a stability analysis. The steady flow is assumed to be induced by a wind stress applied at the sea surface. Next, we show that the results from the simulation model coincide with the stability analysis.

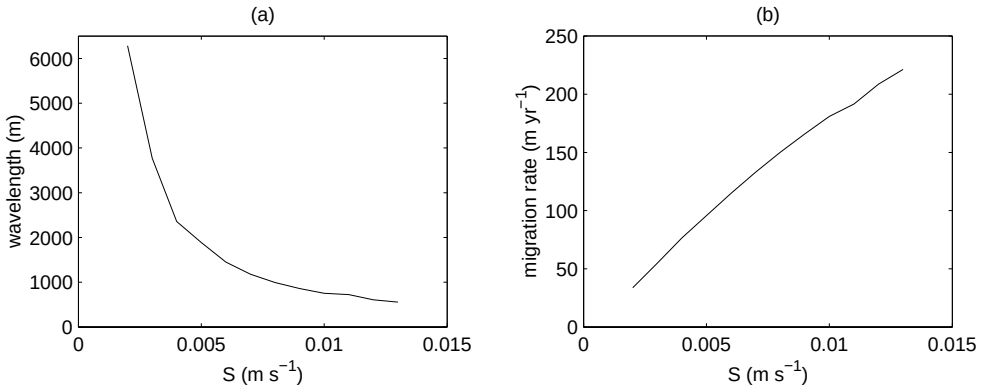

Figure 4.5: Wavelength and migration rate in a unidirectional steady current induced by a wind stress applied at the sea surface. Fig. (a) shows the wavelength (m) of the fastest growing mode (FGM) as a function of the value of the slip parameter S ($\mathrm{m\,s^{-1}}$). Fig. (b) shows the migration rate in metres of the FGM shown in (a). If we increase the value of the resistance parameter S we obtain sand waves with dimensions in the order of hundreds of metres.

4.4.1 Steady flow and sand waves in stability analysis

We start by focussing on a unidirectional steady current inducing the initial evolution of bed forms. The bed forms we find in this case can also be referred to as dunes [Fredsøe and Deigaard, 1992], since a unidirectional steady current is similar to river flow. For typical values of the slip parameter S in the North Sea (see Table 4.1), we find long wavelengths (see Fig. 4.5). Hereby, we used in the stability analysis a combined non-dimensional value for λ_1 and λ_2:

$$S_b = \alpha|\tau_b|^b \left[\tau_b - \lambda\frac{\partial h}{\partial x}\right] \quad \text{with } \lambda = \lambda_1 - \lambda_2|\tau_b|, \tag{4.35}$$

with λ equal to 0.0085. However, if we increase the value of the slip parameter, we find shorter bed forms [Németh *et al.*, 2001] (See Fig. 4.5 and Fig. 4.7. The latter figure is discussed later in more detail.), with wavelengths of a couple of hundreds of metres. This coincides with the result found in [Németh *et al.*, 2002]. In a tidal environment with a small asymmetry in the water motion, the tidal motion is the main factor determining the choice of sand wave length. The residual currents due to tidal motion (see Fig. 4.2) induce a wider range of modes which can become unstable than the unidirectional steady current. An increase in resistance can increase this range of modes, for which the wavelength of the fastest growing mode (FGM) is smaller (larger wave number). Here, the FGM is the mode which has the largest growth rate from linear theory, and is expected to dominate over the rest.

4.4.2 Mathematical validation simulation model

Flat bed

We start with a steady current over a flat bed, which is equivalent to the basic state used in the stability analysis. We apply a wind stress at the sea surface (see Eq. (4.10) and Fig. 4.6) together with a coinciding inflow boundary across a flat seabed. This analytically obtained profile is the same over the entire domain. This investigation of a flat seabed shows the functionality of the continuity equation Eq. (4.2), the boundary conditions Eqns. (4.6)- (4.11) and the viscosity term in the momentum equation Eq. (4.1).

We investigate the magnitude of the residuals on the right hand side of Eq. (4.22), whether the solution coincides with the solution of the physical system. Since the solution provided is a steady state solution and the velocity in the vertical is zero (there is no slope in the seabed or water level), all the residuals on the right hand side of Eq. (4.22) should be zero within machine accuracy limits. The profile in the vertical can be found in Fig. 4.6.

If we would apply a pressure gradient at the inflow boundary, a gradient is present in the water surface due to the friction in the system. This is in contrast to the stability analysis, where the velocity profile is the same over the entire domain. This makes a direct comparison more difficult. However, this can also be seen as a good test for the simulation model and the usage of the basic state in the stability analysis.

We can take an initial condition for a flat seabed and an equal velocity profile over the entire domain equal to inflow boundary for a pressure gradient Eq. (4.11). If we fix the water level downstream ($z = 0$) and fix the depth-averaged velocity at the inflow boundary, we obtain a steady state solution with a slope in the water level. The continuity equation enforces the depth-averaged velocity to increase along this decreasing slope. This slope decreases $8.45 \cdot 10^{-3}$ m per 10 km for a standard value of the resistance parameter S of $1 \cdot 10^{-3}$ m s^{-1} (see Table 4.1). In case we are looking at bed forms in a unidirectional steady current, the typical value for S is $1 \cdot 10^{-2}$ m s^{-1} and gives a slightly larger slope of $1.46 \cdot 10^{-2}$ m per 10 km. This slope is so small compared to the length scale under investigation, that we can assume the validity as expected of the basic state used in the stability analysis.

Residuals small sand waves

The question to be answered is whether the formation process of small amplitude sand waves can be reproduced and verified with a simulation model. To check this we use the results obtained with the stability analysis. The vertical velocity is zero for a flat bed situation. The vertical velocity to be imported in the simulation model is equal to the calculated vertical velocity in the perturbed state in the stability analysis. The sum of the residual horizontal velocity and the basic state forms the actual horizontal velocity with sand waves applied on the seabed. These results, produced on an equidistant grid,

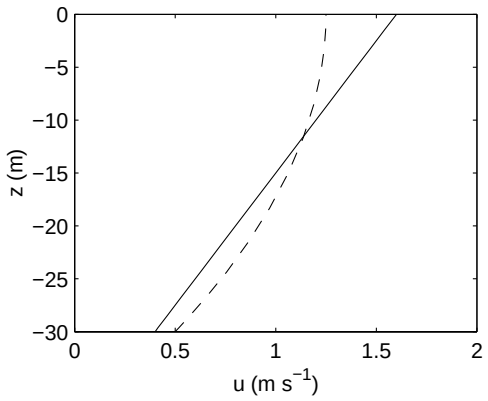

Figure 4.6: Analytical solution of the horizontal velocity profile over a flat bed in case of a wind stress applied at the sea surface (straight solid line) Eq. (4.10) and a pressure gradient (curved dotted line) Eq. (4.11). The linearity of the velocity profile in case of a wind stress is due to the choice of a constant viscosity. The free surface coincides with $z = 0$ m and the seabed with $z = -30$ m. The vertical velocity is equal to zero. This profile is applied at the inflow boundary for all times (with a fixed or time-dependent discharge) and as initial condition over the entire domain.

$$x_l, \quad l = 0, 1, .., N, \tag{4.36}$$

are interpolated on the Gauss-Lobatto grid, using cardinal polynomials:

$$K_j(x) = \frac{\omega(x)}{(x - x_j)\omega'_j}, \quad \omega'_j = \omega'(x_j), \tag{4.37}$$

and

$$\omega(x) = \prod_{k=0}^{N} (x - x_l). \tag{4.38}$$

These cardinal polynomials can be used to represent a polynomial ($I_N f$) which interpolates a general function, in this case the solution of the stability analysis, at the Gauss-Lobatto points:

$$(I_N f)(x) = \sum_{j=0}^{N} K_j(x) f_j. \tag{4.39}$$

The time derivative is equivalent to the residuals in Eq. (4.22). For the other equations, the magnitude of the residuals, is a measure for the error. To check the validity of the spatial discretisation, we therefore do not need to use the time integrator. The results for a wavelength of 600 metres are imported in the simulation model. The

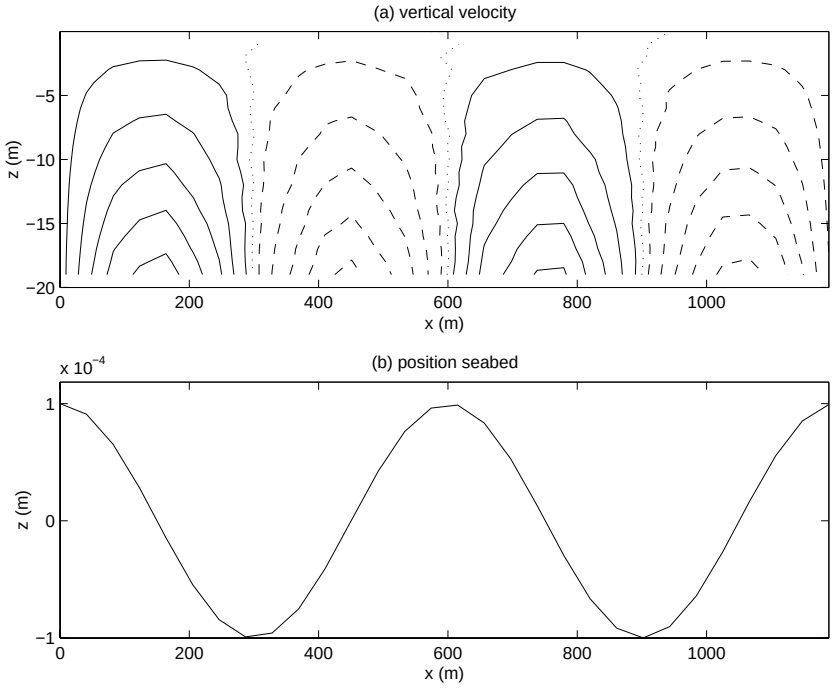

Figure 4.7: Solution of the stability analysis giving residuals equal to zero in the simulation model. In the upper figure (a), the vertical velocity is shown with the solid line showing negative, the dashed line positive and the dotted line velocities equal to zero. The magnitude of the velocities depends on the ratio of the sand wave amplitude over the water depth ($\epsilon = h/H$). The vertical velocity looks different from previous work discussing sand waves in a tidal environment (see Fig. 4.2). The main difference is that we are looking here at a steady current and not at the residuals over a tidal cycle. This means looking at the boundary condition for the horizontal flow Eq. (4.8), that the vertical velocity needs to follow the profile of the seabed. This is due to the occurrence of a horizontal velocity $\neq 0$, due to the horizontal viscosity model enabling long bed waves to be excited (there is evolution due to water movement, and the slope effect is very small for long bed forms). The figure below (b) shows the two sand waves with a typical wavelength of 600 metres over which the water is flowing.

solution of the stability analysis is multiplied by $\epsilon = h/H$. For a small enough ϵ, the solution from the simulation model is equal to the solution from the stability analysis (residuals equal zero within numerical accuracy, with a difference of the order (ϵ^2).

Growth and migration

As a final check, we turned on the simulation model and let the simulation model calculate a seabed change over a period of 7000 s. This is a small time interval, insignificant from a morphological perspective. However, from a mathematical point of view sufficient, since the aim is here to check the validity of the simulation model. We applied again a steady flow induced by a wind stress. With the system set up following the values in Table 4.1, except for the value of the slip parameter which is set to 0.01 m s^{-1} and the slope factor. For comparison, we used the same combined bed slope factor used above (Eq. (4.3)). Furthermore, we took $N^1 = 30$ and $N^3 = 15$, which are the number of grid points in the horizontal and vertical direction (Eq. (4.12)), respectively. The amplitude h is set at 0.01 m, which is small compared to the water depth H of 30 m. Hereby, we investigated a pattern of three sand waves in a non-periodic domain.

We calculated the growth and migration rates, for a whole range of wavelengths. We use a least squares method, to estimate the growth and migration rates based on the initial and calculated seabed obtained with the simulation model. This curve fitting process is used to fit a sinus with a minimal deviation to the position of the seabed, with sinusoidal sand waves imprinted on it, in the grid points. Here we investigate the initial response. Therefore, we are allowed to assume the wavelength does not change, and only the amplitude and position in the horizontal (phase/migration) changes. This approach gives an estimate of the amplitude and phase of a sinusoidal signal, in this case the sand wave. This coincides with the properties the stability analysis gives insight into (growth and migration of a sinusoidal sand wave), which we are comparing the results with. These properties of the imposed sand waves and calculated initially changed sand wave can now be determined as follows:

$$h(x) = A_{ls}\cos(kx) + B_{ls}\sin(kx), \tag{4.40}$$

with $h(x)$ the position of the seabed as a function of the horizontal coordinate and φ the phase shift defined by:

$$\varphi = \text{atan}(\frac{B_{ls}}{A_{ls}}), \tag{4.41}$$

and A and B based on the depths at the grid points:

$$A_{ls} = \frac{\sum h(x)\ \cos(kx)}{\sum \cos^2(kx)}, \tag{4.42}$$

$$B_{ls} = \frac{\sum h(x)\ \sin(kx)}{\sum \sin^2(kx)}. \tag{4.43}$$

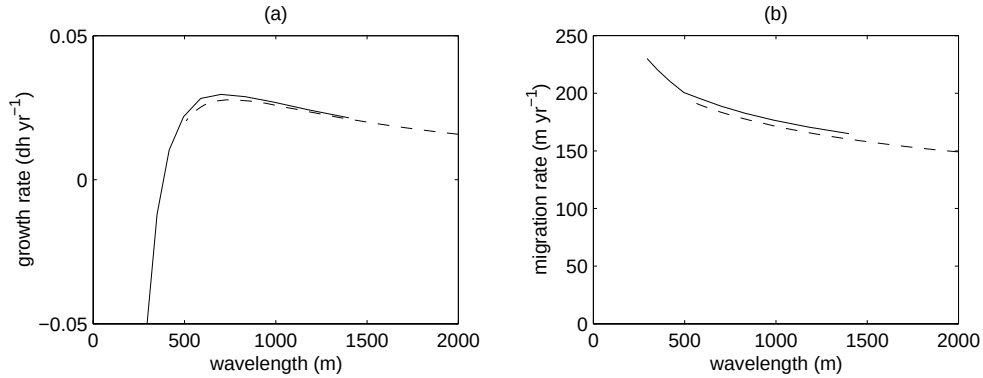

Figure 4.8: Comparison growth and migration rates of the stability analysis and simulation model. Fig. (a) shows the initial growth rate presented in the change of amplitude per year (m yr^{-1}). Here we have to keep in mind that the growth rate is, according to the stability analysis, an exponential function of the amplitude. This means that the growth rate will increase during the initial evolution of a sand wave. The solid line depicts the results from the simulation model. The dotted line corresponds to the results from the stability analysis. Fig. (b) shows the migration rate (initial response calculated in m yr^{-1}).

Fig. 4.8 shows the characteristics of the initial response for a range of wavelengths. Fig. 4.8 (a) depicts the growth rates, whereby we find a range of wavelengths for which these growth rates are positive. For this range, sand waves are initially unstable. Furthermore, we find for all long bed waves positive growth rates. This is due to the usage of a constant viscosity. It can be explained by looking at the boundary conditions showing that the vertical velocity at the seabed is a function of the horizontal velocity at the seabed (Eq. (4.8) and Eq. (4.9)). Both the horizontal and vertical velocity are therefore not equal to zero. This is due to the usage of a slip parameter to obtain a more realistic shear stress with this simplified viscosity model. Smaller wavelengths than about 400 m show negative growth rates. These bed forms are dampened by the simulation model, as coincides with the results for this case with the stability analysis. Here, the FGM has a wavelength of about 750 m. Also this coincides with the results from the stability analysis.

The migration rate of the sand waves is shown in Fig. 4.8 (b). Typical rates for various wavelengths are about 200 m yr^{-1}. These migration rates are due to the asymmetry in the water motion since we are looking at a unidirectional steady current. Compared to observations these migration rates are much higher than those observed for sand waves. However, observations generally discuss sand waves in a tidal environment with only a small non-periodic part in the water motion (usually in the range of 0.1 m s^{-1} inducing migration rates in the order of 10 m yr^{-1} ([Allen, 1980], [Lanckneus and De Moor, 1991], [Van Maren, 1998] and [Németh *et al.*, 2002]).

Therefore these larger migration rates can be explained and give further confidence in the simulation model set up. As was found in the stability analysis, the phase speeds are a linear function of the wave number ($k = 2\pi/L_{sw}$). This means that a larger wave number or smaller wavelength implies a larger phase speed. This results in a larger migration rate for smaller bed forms. The magnitude of this migration rate for a certain wavelength depends largely on the magnitude of the steady current and on the value of the slip parameter S.

The results seem to coincide very good. Hereby, we have to acknowledge a couple of sources of error in the analysis:

- The results from the stability analysis have an inaccuracy;
- We are looking at a non-periodic domain in the simulation model and in the stability analysis we have a periodic domain;
- An error is made translating the result from the simulation model with the least square method, to enable a comparison with the stability analysis.

Therefore, it is not our goal to reproduce the results exactly. However, it is possible to obtain a result with the simulation model which converges asymptotically to the result of the stability analysis if we increase the accuracy of the time integrator, the number of nodes in the system (N^k in Eq. (4.12)) and the number of sand waves in the domain. To obtain Fig. 4.8, we already needed to increase the time integrators accuracy for smaller wavelengths, whereby the solution converged to the analytical solution. Furthermore, we found that if we increase the number of wavelengths in the domain from two to three, we decrease the difference from the stability analysis from $5 \cdot 10^{-2}$ to $2 \cdot 10^{-2}$. The latter results (determined with a domain with three sand waves) are shown in Fig. 4.8.

4.5 Discussion

We developed a simulation model, aimed at describing the behaviour of sand waves, present in shallow shelf seas. We started with validating the simulation model mathematically by comparing an analytical solution for a flat seabed with the results from the simulation model. Next, we investigated the residuals of the time integrator after importing the analytical solution from the stability analysis for a steady state situation. Subsequently, we simulated a small amount of time with the simulation model to compare the results directly with the results from the linear stability analysis. Hereby, remains the difference that the simulation model is discrete and that the domain is non-periodic in the horizontal in the simulation model and periodic in the stability analysis. Furthermore, the analysis method to compare the results introduces an error. However, the analysis showed that if we take enough grid points (equivalent to the number of modes in the approximation), enough sand waves, and request a high enough accuracy from the time integrator we can obtain a solution close to the solution of the stability analysis.

4.6 Conclusions

In this chapter we developed a numerical simulation model able to describe sand wave excitation and select the initially most unstable mode assuming sand waves are free instabilities of the water-seabed system.

In the stability analysis the sand waves predicted did not allow for interference of modes due to the linear assumption. This interference encompasses energy being transferred from one component or wave number of the bed pattern to another. Therefore, this stability analysis does not say anything about the final pattern, since only one component can be investigated at a time. The simulation model developed and validated mathematically here, can be used to investigate the non-linear behaviour of sand waves.

Furthermore, we investigated the results for small amplitude sand waves under a steady flow with the help of the stability analysis. It has been shown that with a set up describing sand waves in a tidal environment, we find bed features existing in a unidirectional steady current similar to *dunes*. These dune-like bed forms are found when the roughness of the seabed, compared to a typical North Sea situation, is large. For smaller values of the resistance of the seabed, taken into account by the slip parameter S, the instability mechanism is very weak, resulting in a FGM with very long wavelengths.

Lastly, the numerical approach presented here enables us to incorporate more realistic aspects into the modelling framework. It is clear that the simulation model presented here can straightforwardly be extended to include other aspects such as a critical shear stress, suspended sediment transport or a non-erodible layer in the seabed.

4.7 Acknowledgements

We thank Clyde Petroleum Exploratie, Holland Offshore Consulting and the State Supervision of Mines for providing the data for Fig. 4.1.

4.8 Appendix

The two-dimensional version of the derivative matrix D in Eq. (4.14) in the horizontal direction can be written with the derivative matrix D of the size $N^1 \times N^1$ as N^3 blocks on the diagonal of the following square matrix with $N^1 \times N^3$ columns:

$$D^1 = \begin{pmatrix} D^1_{11} & \dots & D^1_{1N} & & & & & & \\ \vdots & \ddots & \vdots & & & & & 0 & \\ D^1_{N1} & \dots & D^1_{NN} & & & & & & \\ & & & D^1_{11} & \dots & D^1_{1N} & & & \\ & & & \vdots & \ddots & \vdots & & & \\ & & & D^1_{N1} & \dots & D^1_{NN} & & & \\ & & & & & & D^1_{11} & \dots & D^1_{1N} \\ & 0 & & & & & \vdots & \ddots & \vdots \\ & & & & & & D^1_{N1} & \dots & D^1_{NN} \end{pmatrix} \tag{4.44}$$

The rest of the elements are zero. The two-dimensional version of the derivative matrix D in Eq. (4.14) with size $N^3 \times N^3$ to determine derivatives in the vertical direction can be written as the elements of D^3 in a diagonal pattern with a spacing of N^1 elements as follows:

$$D^3 = \begin{pmatrix} D^3_{11} & & 0 & D^3_{12} & & 0 & D^3_{1N} & & 0 \\ & \ddots & & & \ddots & & & \ddots & \\ 0 & & D^3_{11} & 0 & & D^3_{1j} & 0 & & D^3_{1N} \\ D^3_{i1} & & 0 & D^3_{ij} & & 0 & D^3_{iN} & & 0 \\ & \ddots & & & \ddots & & & \ddots & \\ 0 & & D^3_{i1} & 0 & & D^3_{ij} & 0 & & D^3_{iN} \\ D^3_{N1} & & 0 & D^3_{Nj} & & 0 & D^3_{NN} & & 0 \\ & \ddots & & & \ddots & & & \ddots & \\ 0 & & D^3_{N1} & 0 & & D^3_{Nj} & 0 & & D^3_{NN}, \end{pmatrix} \tag{4.45}$$

The rest of the elements are zero.

The matrix below with a total size of $N^1 \times N^3 \times 2 + N^1 \times 2$ can be found in Eq. (4.22) and consist of the variables depending on time in the momentum equation Eq. (4.1) (the first $N^1 \times N^3$ rows), the continuity equation Eq. (4.2) giving elements equal to zero (the next $N^1 \times N^3$ rows), and the equation for the water level Eq. (4.6) and the bed evolution Eq. (4.8) ($2 \times N^1$ rows). For the water level, we use the kinematic boundary condition at the free surface. This is equivalent to using a depth-averaged formulation based on the continuity equation and this kinematic boundary condition

often used to describe a free surface:

$$A = \begin{pmatrix} \frac{\partial u}{\partial t} & 0 & f(\frac{\partial \zeta}{\partial t}) & f(\frac{\partial h}{\partial t}) \\ 0 & 0 & 0 & 0 \\ 0 & 0 & \frac{\partial \zeta}{\partial t} & 0 \\ 0 & 0 & 0 & \frac{\partial h}{\partial t} \end{pmatrix} \tag{4.46}$$

See Eq. (4.23) for the numerical notation.

Chapter 5

Finite amplitude sand waves

Abstract: A two-dimensional vertical (2DV) flow and morphological numerical model describing the behaviour of offshore sand waves has been developed. The model contains the 2DV shallow water equations, with a free water surface and a general bed load formula. The water movement is coupled to the sediment transport equation by a seabed evolution equation. Using this model, we investigate the properties of the system for finite values of the amplitude of sand waves for a unidirectional steady current and unidirectional block current simulating tidal motion. As a result, we find sand wave saturation for heights of 10-30% of the average water depth with a timescale of decades. The stabilisation mechanism found here causing sand waves to saturate is based on the balance between the shear stress at the seabed and the fact that sediment is transported easier downhill than uphill. The migration rate of the sand waves decreases slightly during their evolution. For a unidirectional steady flow the sand waves become asymmetrical in the horizontal direction and for a unidirectional block current asymmetrical in the vertical. A sensitivity analysis showed the slope effect of the sediment transport plays an important role herein. Furthermore, the magnitude of the resistance at the seabed and the eddy viscosity influence both the timescale and the height of the fully-developed sand wave. The order of magnitudes found of the time and spatial scales coincide with observations made in the southern bight of the North Sea, Japan and Spain. Finally, the recovery of dredged sand waves is investigated[1].

Keywords: sand waves, finite amplitude, migration, evolution, saturation, dredging, shelf seas, 2DV.

[1] A shortened version of this chapter has been submitted to the 3rd IAHR Symposium on River, Coastal and Estuarine Morphodynamics by A.A. Németh and S.J.M.H. Hulscher entitled "Finite amplitude sand waves in shallow seas".

5.1 Introduction

Offshore sand waves have typical wavelengths of several hundreds of metres and can be found in shallow seas such as the North Sea. Their crests are oriented more or less perpendicularly to the principal direction of the current [Hulscher, 1996]. The heights of sand waves can grow to as much as 30% of the average water depth. Therefore, the relative sand wave height can be considered as significant. According to Johnson *et al.* [1981], the sand wave heights diminish from the south to the north of the North Sea due to a diminishing tidal amplitude, the lower availability of sediment needed for the formation of sand waves and the increase in the ratio of suspended load to bed load transport.

The sand waves are found to be almost symmetrical near the top of the sandbanks (e.g. [Lanckneus *et al.*, 1995]), whereas their amplitude diminishes near the top of these sandbanks [Langhorne, 1982]. This corresponds with the observations that the sand wave height is often smaller at smaller depths. Furthermore, several authors have determined the lee side of sand waves, on sandbanks, is often oriented towards the crest of the sandbank and towards the residual current. Belderson and Stride [1969] found a correlation between the direction of sand wave asymmetry and the tidal current asymmetry (see also Fig. 5.1). However, the problem is more complicated. In the Taiwan Strait, uniform asymmetrical, symmetrical as well as irregular sand waves are found. These differences in sand wave shapes, all found in the same region, are believed to be caused by residual currents induced by tidal movement, seasonal fluctuation of the flow and disturbances in these flow patterns caused by different topographical features [Boggs, 1974]. Harris [1989] found that over a period of five months, the asymmetry of the sand waves reversed due to wind-driven currents during the Monsoon season in the Adolphus Channel of Australia. This indicates that asymmetry can change over a short period of time relative to the timescale of sand waves. If the timescale of the variations in sediment flux are smaller than the response time of the bed form, the shape will not change significantly [Bokuniewicz *et al.*, 1977]. The response time depends on the volume of the sand wave. The difference in response time can be the cause of opposite asymmetrical orientations found within one study area.

Insight into the behaviour of these sand waves is crucial to enable cost-effective management practices. Due to the large height of sand waves compared to the water depth in combination with the timescale of years on which they are assumed to be active, they play an important role with respect to for example navigation in coastal seas (see also Chapter 2).

Knaapen and Hulscher [2002] developed an evolution model based on data assimilation, and investigated data sets of a field of sand waves near Japan. This analysis showed that when a sand wave is dredged, it is able to recover with a timescale of eight years. Morelissen *et al.* [2002] extended this model by allowing sand waves to migrate using a modified Landau equation. Despite the success of this empirical method, it does not include the full knowledge of sand wave physics. Therefore, it

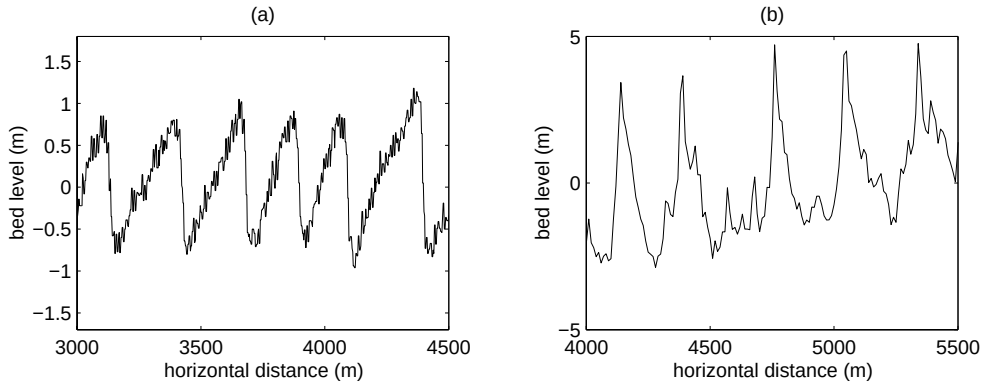

Figure 5.1: Sand waves in the North Sea. Fig. (a) shows sand waves of the coast near IJmuiden in the Netherlands. The sand waves are asymmetrical and have a wavelength of about 250 m and a height of maximum 2 m. Fig. (b) shows sand waves at Noord-Hinder in the North Sea, located near the Eurogeul at an average water depth of about 38 m. Their wavelengths are 300 m and their height is typically 6 m. The sand waves are more symmetrical in the horizontal direction and asymmetrical in the vertical with their sharp crests and elongated troughs.

cannot facilitate the investigation of the mechanisms leading to sand wave behaviour.

Based on Huthnance [1982a and 1982b], Hulscher [1996], Gerkema [2000] and Komarova and Hulscher [2000]), Németh *et al.* [2002] (see Chapter 3) developed a model describing the formation and migration of infinitely small sand waves based on a stability analysis. This for periodic water motion in combination with a steady part based on either a wind stress at the sea surface or a pressure gradient. The model gives insight into the initial evolution and migration of sand waves assuming they are free instabilities of the seabed water system.

Komarova and Newell [2000] investigated the model by Hulscher [1996] combined with the time-dependent viscosity parameterisation from Komarova and Hulscher [2000] with a weakly non-linear analysis. This analysis led to coupled spatial variations of sand waves and the average bed level, of which the latter shows similarities with tidal sandbanks. However, sand wave migration cannot be investigated with this analysis.

Johns *et al.* [1990] and Stansby [1998] discussed unidirectional steady water movement over dune-like features with steep slopes. Due to the steep slopes, the focus is on flow separation, which we do not expect for offshore sand waves with a smaller steepness than dunes found in rivers. Fredsøe and Deigaard [1992] discuss the behaviour of sand waves based on a model describing fully-developed sand dunes in rivers (see also a.o. Hansen [1989]). Sand waves under the influence of oscillatory water movement are schematised as bed forms formed under the influence of a unidirectional steady current, with a modification for the reversing current. This is based on the assumption made by Stride (1982). Therefore, periodic water motion is not taken

directly into account. Furthermore, the model does not describe bed form evolution. Richards and Taylor [1980] discussed flow and sediment transport characteristics for more sandwave-like bed forms in a unidirectional steady flow, with milder slopes than river dunes. In addition, they discuss the response of the seabed for various shapes of the sand wave. Idier [2003] investigated sinusoidal sand waves for various amplitudes with a numerical model for unidirectional steady flow conditions.

Assuming sand waves to be free instabilities of the seabed-water system, we more or less understand the initial instability mechanism. However, the behaviour of finite-amplitude offshore sand waves (especially for periodic water motion) is still not fully understood. Here, we are interested in the evolution of the finite amplitude sand waves and their stabilisation processes, together with their maximum height.

In Chapter 4, a numerical model has been developed and validated mathematically with the help of the linear stability analysis discussed in Chapter 3. This model enables the description of the entire evolutionary process of sand waves. Within this chapter, we will investigate the behaviour of finite amplitude sand waves. It can give a clue to the most important mechanisms, determining the stabilisation of the evolution of sand waves and their saturation height for unidirectional steady flow and periodic water motion. Furthermore, we consider what happens to the shape and migration rates of sand waves when we allow them to become finite. Lastly, can we use this information to simplify models describing sand waves?

First, the physics forming the basis of the used simulation model is discussed briefly. For a detailed description of the model, we refer to Chapter 4. Next, the processes for sand waves of finite extent are discussed for sinusoidal modes having different amplitudes. Subsequently, we investigate the evolution of sand waves using a fully coupled model for a unidirectional steady current based on data from the Gulf of Cadiz, and for periodic water motion, aimed at describing North Sea conditions. In the unidirectional steady flow case, we investigate the change in migration rate during the evolution of a sand wave. Next, we investigate the effect of the different parameters on the results. Subsequently, the impact of dredging a field of sand waves is investigated. In the final section, we present the conclusions.

5.2 Description of the model set up

5.2.1 2DV Flow model

The model used in this chapter is the two-dimensional vertical (2DV) numerical simulation model developed in Chapter 4. For completeness, we present the basic equations forming the basis of the model.

Since the Coriolis force only slightly affects sand waves, we are allowed to omit for simplicity the second horizontal direction. After making the shallow water approxi-

Parameters	Symbol	Default value	Dimension
Depth-averaged value velocity	U	1	$\mathrm{m\,s^{-1}}$
Average water depth	H	30	m
Kinematic eddy viscosity	A_v	$1 \cdot 10^{-2}$	$\mathrm{m^2 s^{-1}}$
Slip parameter	S	$8 \cdot 10^{-3}$	$\mathrm{m\ s^{-1}}$
Gravitational acceleration	g	9.8	$\mathrm{m\,s^{-2}}$
Power of transport	b	$5 \cdot 10^{-1}$	–
Proportionality constant	α	$3 \cdot 10^{-1}$	$\mathrm{m^{-2}\,s}$
Bed slope factor	λ_1	$6 \cdot 10^{-3}$	$\mathrm{m^2\,s^{-2}}$
Bed slope factor	λ_2	3.33	–

Table 5.1: Typical values and dimensions of the parameters and variables used in the simulation model.

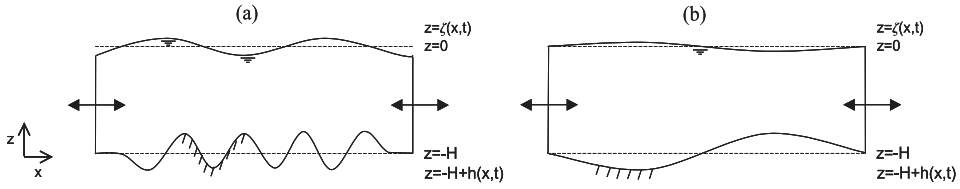

Figure 5.2: Definition sketch of the model geometry. Fig. (a) shows the non-periodic set up. Fig. (b) shows the usage of periodic boundary conditions. Here, the properties of the variables at the inflow boundary are the same as at the outflow boundary.

mation, we obtain the 2DV shallow water equations:

$$\frac{\partial u}{\partial t} + u\frac{\partial u}{\partial x} + w\frac{\partial u}{\partial z} = -g\frac{\partial \zeta}{\partial x} + \frac{\partial}{\partial z}\left(A_v \frac{\partial u}{\partial z}\right), \tag{5.1}$$

$$\frac{\partial u}{\partial x} + \frac{\partial w}{\partial z} = 0. \tag{5.2}$$

The velocities in the x- and z- directions are u and w, respectively. The water level is denoted by ζ and H represents the mean water depth. The level of the seabed is represented by $z = -H + h$ (see Fig. 5.2). Time is represented by t. The symbols g and A_v indicate the acceleration due to gravity and the vertical eddy viscosity, respectively.

5.2.2 Sediment transport and seabed behaviour

Bed load transport is the mode of transport presumed dominant in offshore tidal regimes. The following general bed load formula is used following Komarova and

Hulscher [2000], modelling bed load transport as a function of the shear stress at the seabed:

$$S_b = \alpha|\tau_b|^b \left[\tau_b - \lambda_1 \frac{\partial h}{\partial x} - \lambda_2|\tau_b|\frac{\partial h}{\partial x}\right], \tag{5.3}$$

with the volumetric bed load transport described by S_b and τ_b the shear stress at the seabed by:

$$\tau_b = A_v \left.\frac{\partial u}{\partial z}\right|_{z=-H+h}, \tag{5.4}$$

and with:

$$\alpha = \frac{8\gamma}{(s-1)g}, \quad \lambda_1 = \frac{3\Theta g(s-1)d}{2\gamma \tan\phi_s}, \quad \lambda_2 = \frac{1}{\tan\phi_s}. \tag{5.5}$$

Hereby, Θ is the critical Shields parameter modelled by a constant of 0.047, s is the relative density of sediment equal to 1.65 and γ takes into account that during a tidal cycle sediment is not transported when the critical shear stress is too low. For unidirectional steady flow, this parameter is equal to 1, otherwise estimated at 0.5. The grain diameter is denoted by b and ϕ_s is the internal friction angle of the bed with $\tan\phi_s = 0.3$. The power of transport, represented by b, is set at 0.5 and the proportionality constant, denoted as α, is about 0.3 s m^{-2}. The scale factors for the bed slope mechanism are λ_1 and λ_2, taking directly into account that sand is transported more easily downhill than uphill. A threshold of sediment motion is not explicitly taken into account at this point (Table 5.1).

The sediment balance, which couples the flow model (Eqns. (5.1) and (5.2)) with the sediment transport model Eq. (5.3), calculates the position of the seabed h based on the principle of conservation of mass as a function of time t:

$$\frac{\partial h}{\partial t} = -\frac{\partial S_b}{\partial x}. \tag{5.6}$$

5.2.3 Boundary conditions at the free surface and seabed

The boundary conditions at the water surface ($z = \zeta$)(see Fig. 5.2) are defined as follows:

$$\frac{\partial \zeta}{\partial t} + u\frac{\partial \zeta}{\partial x} = w, \tag{5.7}$$

$$\frac{\partial u}{\partial z} = \frac{\tau_w}{A_v}. \tag{5.8}$$

in which τ_w describes the wind induced shear stress at the sea surface. The vertical velocity component at the bed ($z = -H + h$) is described by the kinematic condition:

$$\frac{\partial h}{\partial t} + u\frac{\partial h}{\partial x} = w. \tag{5.9}$$

The horizontal flow components at the seabed are modelled with the help of a partial slip condition (S is the slip parameter controlling the resistance at the seabed). The boundary condition couples the resistance at the seabed with the water movement across the seabed:

$$A_v\frac{\partial u}{\partial z} = Su. \tag{5.10}$$

5.2.4 Inflow and outflow boundary conditions

In this chapter, we investigate the non-linear behaviour of sand waves with periodic and non-periodic boundary conditions in the horizontal direction.

For the non-periodic approach (see Fig. 5.2 (a)), an estimate of the water level is supplied to the model at the outflow boundary. Furthermore, the derivatives in the horizontal direction for the horizontal and vertical velocities are set to zero at the outflow boundary.

A constant discharge together with a velocity profile in the vertical plane is prescribed at the inflow boundary. Two possible origins of steady flow can be investigated. These are (I) a wind driven current and (II) a current induced by a pressure gradient. The vertical structure for each of these cases is:

$$\text{I}: \quad u_r = \frac{\tau_w}{A_v}\left(H + \frac{A_v}{S} + z\right), \tag{5.11}$$

$$\text{II}: \quad u_r = P\left(\frac{1}{2}z^2 - \frac{A_v}{S}H - \frac{1}{2}\right). \tag{5.12}$$

With P a parameter determining the magnitude of the pressure gradient. Furthermore, we are able to impose a time-dependent signal at the inflow boundary to simulate tidal motion. However, if we provide an incorrect estimate of the water level downstream, we supply false information to the system. This is no problem from a physical point of view, since we do not expect that a small discrepancy in the water level will affect the position of the seabed. However, numerically this can pose difficulties. To overcome this problem, we can prescribe the pressure gradient ($\frac{\delta\zeta}{\delta x}$) directly in the momentum equation (Eq. (5.1)). In this case, no slope will develop in case of a flat bed, since the pressure gradient is present throughout the domain (not only at the inflow boundary). Note, that we still have a free surface. For a flat seabed, the velocity profile in the vertical is then equal to Eq. (5.12) throughout the domain. Prescribing the pressure gradient in this way is equivalent to the basic state in the linear stability analysis (Chapter 3), where the basic state is valid throughout

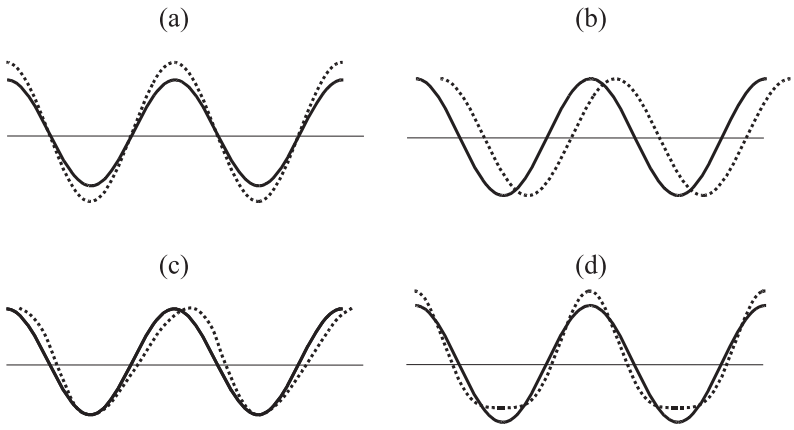

Figure 5.3: Changes sand wave profile. The following aspects are shown: (a) growth, (b) migration, (c) change in horizontal asymmetry and (d) change in vertical asymmetry.

the horizontal domain. At the outflow boundary, we can then prescribe a water level equal to zero, being an accurate estimate of the analytical solution. If we now impose a bed form on the seabed, we need to keep the sand wave far enough from the outflow boundary, to minimize the interaction between the boundary and the sand waves under investigation.

When using periodic boundary conditions (see Fig. 5.2 (b)) the values of the variables at the inflow boundary are equal to the values of the variables at the outflow boundary. We can choose between either a wind stress, a pressure gradient or a combination as the forcing mechanism in the water motion. The pressure gradient is again imposed directly in the momentum equation as described above. The existence of a net slope in the domain in the water level would be in contradiction to the usage of periodic boundary conditions.

The physical interpretation of periodic boundary conditions is that we have a train of identical sand waves next to each other. The limitation of this approach is that we introduce a length scale in the physical system due to the selection of the length of the domain. Therefore, the wavelengths selected on the intermediate term are limited (only the wavelength of the fastest growing mode and its higher harmonics).

While investigating sand waves in the non-linear regime due to a unidirectional steady current we will have to deal with sand wave evolution, change in shape and migration. Hereby, we expect the sand wave to become asymmetric. However, if we look at periodic water motion — more typical for offshore locations — the bed forms will not migrate and remain symmetrical in the horizontal. This simplifies the analysis, since the only response of the system remaining to observe are the evolution of the sand wave and the change in shape (see Fig 5.3).

We simulate unidirectional tidal motion with a unidirectional block current. It

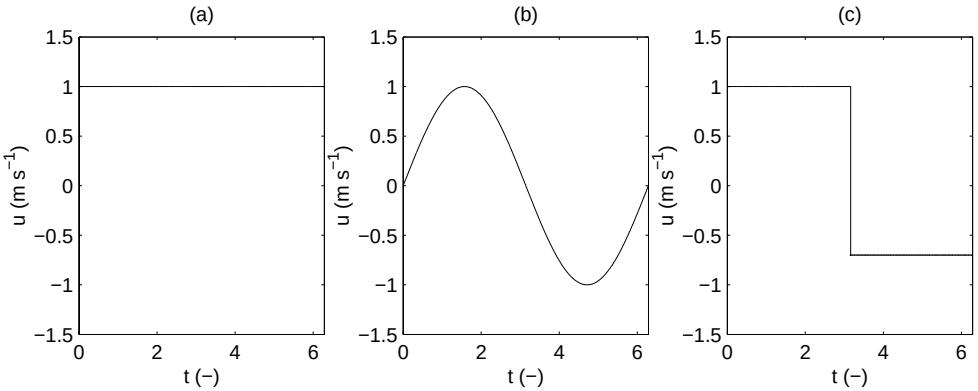

Figure 5.4: Water motion optional in the simulation model. Fig. (a) shows a unidirectional steady current. Fig. (b) shows time-dependent water motion, in this case sinusoidal tidal motion. In Fig. (c) a block current can be found simulating periodic tidal motion by looking at two steady currents (a) in opposite direction.

is based on two unidirectional steady currents in opposite direction (see Fig. 5.4 (a): unidirectional steady flow and Fig. 5.4 (c): unidirectional block current). The growth rates for a range of wavelengths for a block current can be found in Fig. 5.5, indicating the wavelength of the fastest growing mode (about 500 m) lies in the same order of magnitude of that of sinusoidal tidal motion (see Chapter 4). Furthermore, the numerical effort of investigating tidal motion with a block current is much smaller than for sinusoidal tidal motion (see Fig. 5.4 (b)). This is especially true when doing long-term morphological calculations.

We will investigate two cases:

- a unidirectional steady current with a depth-averaged velocity of 1 m s^{-1} induced by a pressure gradient;
- and a unidirectional block current with a depth-averaged velocity of 1 m s^{-1} based on a pressure gradient, from here on referred to as block current.

5.3 Sand waves of finite extent, a morphostatic approach

We will start by imposing a sinusoidal sand wave for a range of amplitudes on the seabed and investigate the properties of the seabed-water system. Hereby, we do not close the morphodynamic loop, which would allow the seabed changes to influence the water motion (morphostatic) (see Fig. 5.6). This is the first step to understand the non-linear behaviour before we start with calculations with a fully coupled model (morphodynamic) in paragraph 5.4.

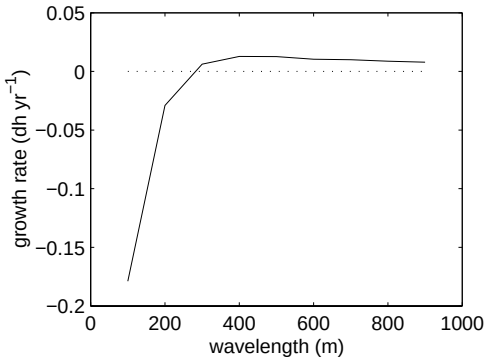

Figure 5.5: Growth rate for small amplitude sand waves in a unidirectional block current based on a pressure gradient with a depth-averaged velocity of 1 m s^{-1} for a range of wavelengths.

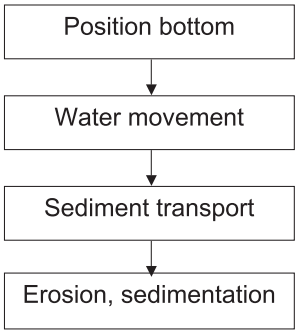

Figure 5.6: Not closed morphological loop.

5.3.1 Unidirectional steady current

First, we investigate the behaviour of sinusoidal sand waves with different amplitudes for a unidirectional steady current in an average water depth of 30 m. The value of the slip parameter S is set at 0.01 m s^{-1} and the eddy viscosity A_v at 0.03 m^2 s^{-1}, based on the calculations in Chapter 4 for dune-like bed forms.

We see in Fig. 5.7 (a) and (b) that the maximum shear stress, located at the top of the sand wave, increases for larger amplitudes. The shear stress on the stoss side of the sand wave, where the slope is maximal, at $z = -H$ (see also Fig. 5.2), increases initially for larger amplitudes. This increment can be seen until an amplitude of about 4 m. For larger amplitudes, this shear stress starts to decrease, indicating that less sand can be transported upwards towards the crest of the sand wave (see also Richards and Taylor [1980]). At the same time, we find a sharper gradient in the shear stress. This is possibly the result of the sheltering effect of one sand wave behind another.

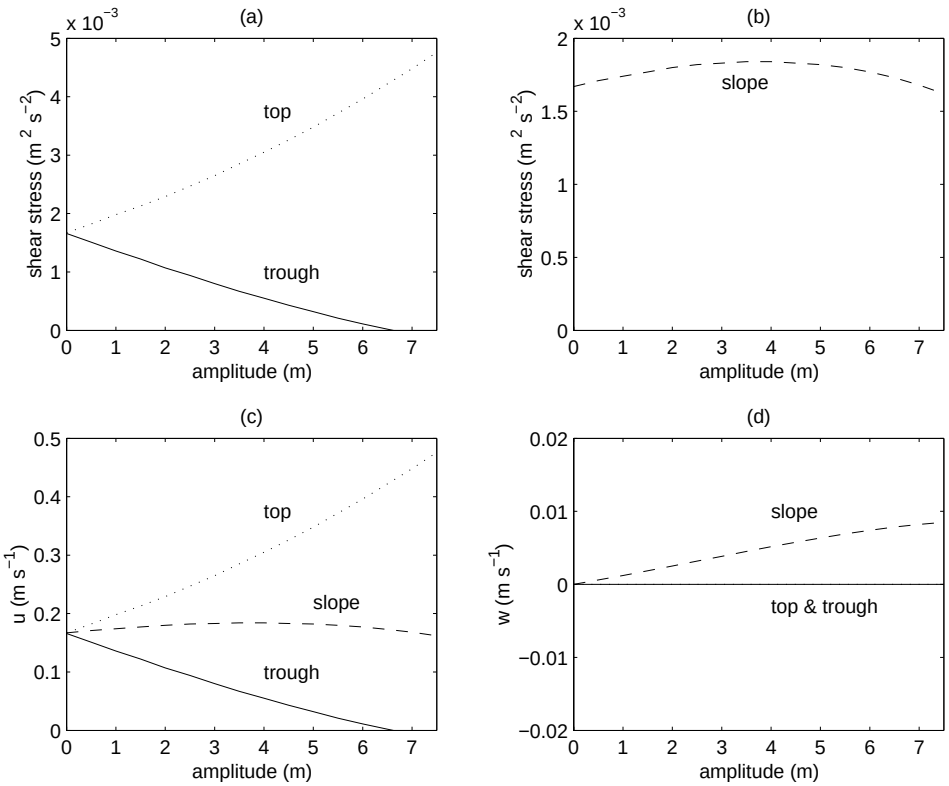

Figure 5.7: Shear stresses and velocities at the seabed as a function of the amplitude of a sinusoidal sand wave for a unidirectional steady current of 1 $\mathrm{m\ s^{-1}}$. Fig. (a) and (b) show the shear stress, Fig. (c) the horizontal velocity u and Fig. (d) the vertical velocity w at the top (dotted line), in the trough (solid line) and on the stoss side of the sand wave at $z = -H$, where the slope is maximal (dashed line). An amplitude of zero corresponds with a flat bed.

The fact the shear stress at at the stoss side at $z = -H$ increases initially, supporting the evolution of sand waves, and decreases for larger amplitudes is an indication of a mechanism supporting sand wave saturation for steady flow situations. The minimum shear stress located in the trough becomes negative for these very large amplitudes, indicating flow separation.

The current set up of the simulation model is not able to describe flow separation due to the usage of the shallow water approximation. Therefore, for very large amplitudes the model is not valid. To describe flow separation the pressure in the domain needs to be taken explicitly into account (see a.o. [Johns *et al.*, 1990], [Fredsøe and Deigaard, 1992] and [Stansby, 1998]). However, sand waves in this context are not expected to attain these heights. We are investigating sand waves in an offshore

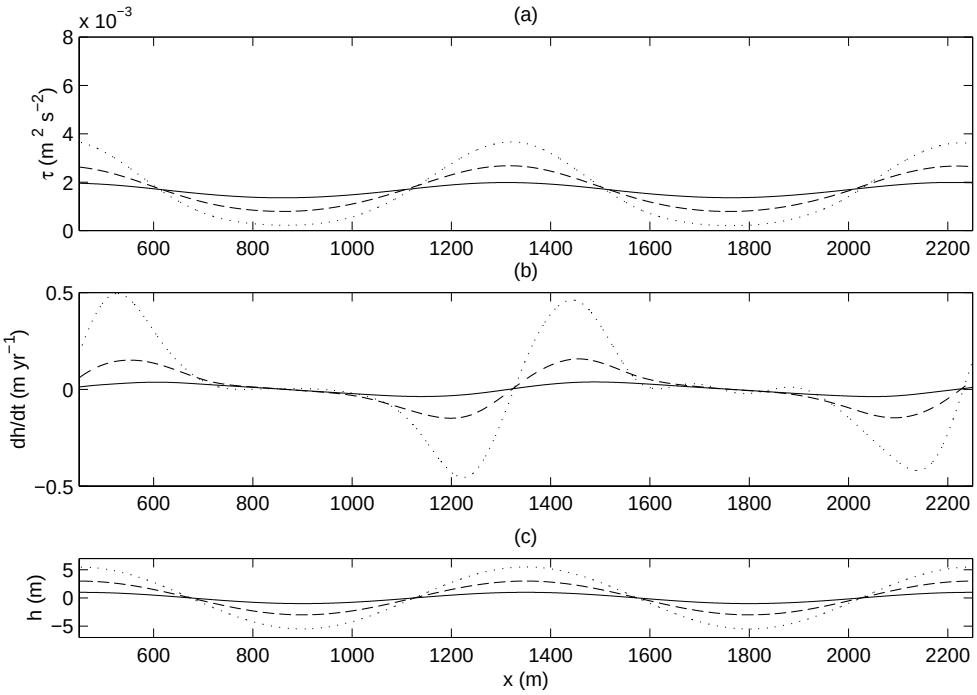

Figure 5.8: Shear stress (τ) and change in bed level for a sinusoidal sand wave pattern with an amplitude of 1 m (solid line), 3 m (dashed line) and 5.5 m (dotted line) shown in Fig. (c). A unidirectional steady current is investigated with a depth-averaged magnitude of 1 $\mathrm{m\ s^{-1}}$. Fig. (a) shows the shear stress at the seabed. Fig. (b) shows the seabed change, which is more non-linear than the pattern of the shear stress due to the non-linear nature of the bottom evolution equation.

environment and these bed forms in general are not very high and steep (vertical change of metres along a horizontal domain of hundreds of metres). We believe that the latter is due to the more symmetrical water motion instead of the unidirectional *steady* flow found in rivers.

For the horizontal velocity u and vertical velocity w, we find similar trends (see Fig. 5.7 (c) and (d)). The minimal horizontal velocity in the trough also becomes negative for large amplitudes indicating flow separation as well. However, the vertical velocity at the stoss side of the sand wave at $z = -H$ keeps on increasing for larger amplitudes (Eq. (5.9)).

In a unidirectional steady current we expect the sand wave to be asymmetrical. Therefore, the system is not in equilibrium since it requires a more asymmetrical bed form. This can be seen from the sedimentation downstream and erosion upstream shown in Fig. 5.8 (b). We find for the small amplitude smooth functions of the shear

stress and bed level change (see Fig. 5.8 for unidirectional steady flow and Fig. 5.10 for a block current). However, for larger amplitudes we find higher harmonics in the shear stress at the seabed attempting to make the pattern more capricious. The effect on the smoothness of the seabed change (see Fig. 5.8 (b)) compared to the shear stress at the seabed (see Fig. 5.8 (a)) is large since the bottom evolution equation (Eq. (5.6)) is stronger non-linear than the water motion. Therefore, the seabed change shown here should not be attributed entirely to the sand wave evolution and migration (especially for the sand waves with large amplitudes).

5.3.2 Block current

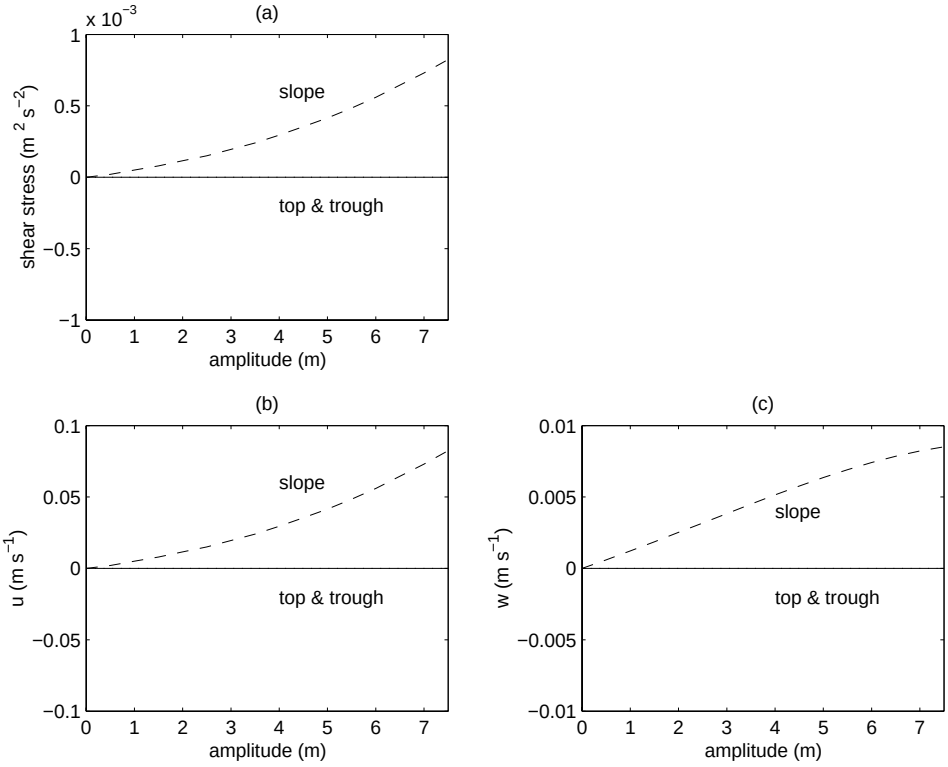

Figure 5.9: Net shear stresses and velocities at the seabed as a function of the amplitude of a sinusoidal sand wave for a block current with an amplitude of 1 $\mathrm{m\ s^{-1}}$. Fig. (a) shows the shear stress, Fig. (b) the horizontal velocity u and Fig. (c) the vertical velocity w at the top (dotted line), in the trough (solid line) and where the slope of the sand wave is maximal at $z = -H$ (dashed line) (coinciding with the solid line). An amplitude of zero corresponds with a flat bed.

Fig. 5.9 shows the net values of the shear stress and flow velocities at the seabed,

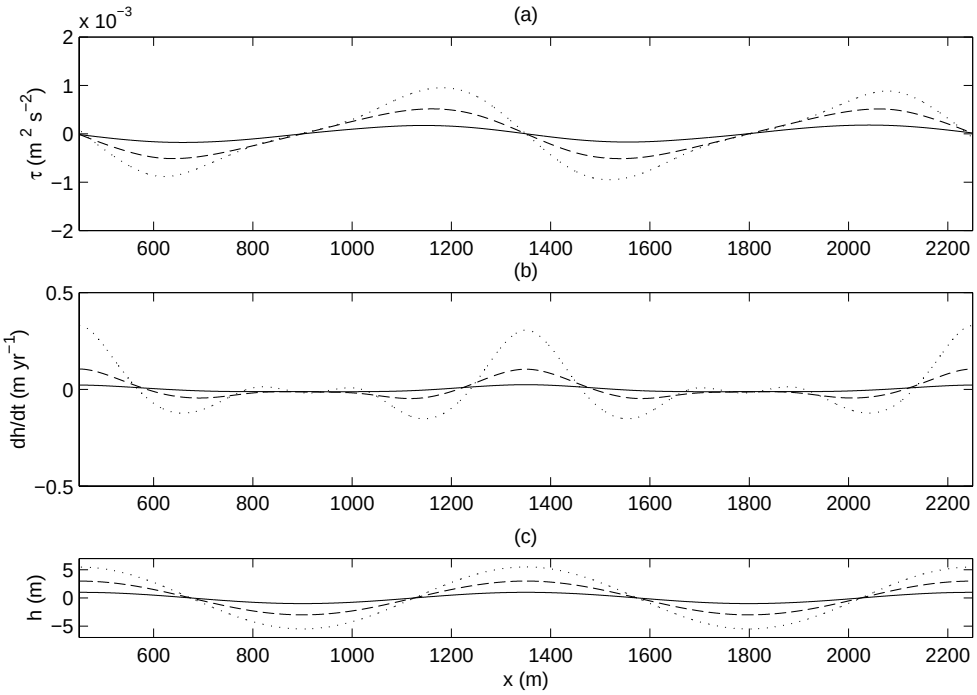

Figure 5.10: Shear stress (τ) and change in bed level for a sinusoidal sand wave pattern with an amplitude of 1 m (solid line), 3 m (dashed line) and 5.5 m (dotted line) shown in Fig. (c). Here a block current is investigated with a depth-averaged magnitude of 1 $\mathrm{m\ s^{-1}}$. Fig. (a) shows the shear stress at the seabed. Fig. (b) shows the seabed change, which is more non-linear than the pattern of the shear stress due to the non-linear nature of the bottom evolution equation.

over one period for a block current The principal difference with Fig. 5.7, besides the fact that these are net values, is that the net shear stress at $z = -H$, where the slope is maximal, does not show a decrease for larger sand wave amplitudes. Furthermore, the vertical and horizontal velocities, u and w, show a net flux of water oriented towards the top of the sand wave for all amplitudes.

For a block current, the sinusoidal shape of the investigated sand waves forms a better first approximation, since we expect a symmetrical bed form in the horizontal direction. Looking at Fig. 5.10 (b) we can see the sand wave shows a tendency to become more sharp-crested than the sinusoidal shape. The top of the sand wave intends to keep growing, whereby the area near the top wants to erode for large amplitudes. The troughs show little change in time. Based on this analysis, we expect for this case sand waves with elongated troughs and relatively sharp crests (see also Fig 5.1 (b)).

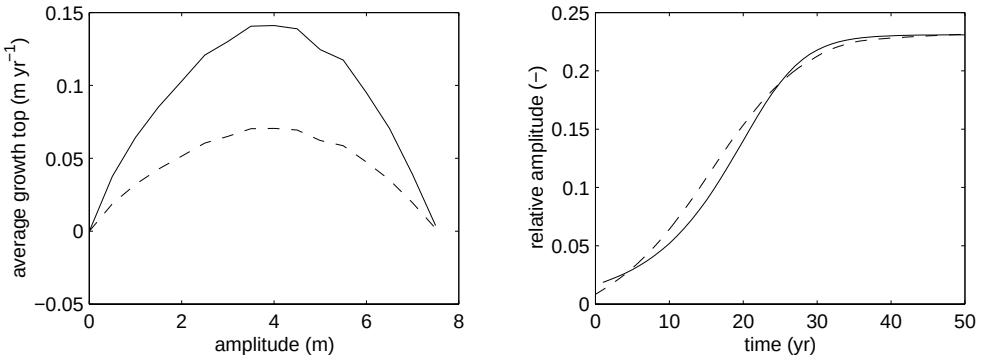

Figure 5.11: Growth rate sand wave evolution. Fig. (a) shows the average growth of the top of a sand wave as a function of amplitude based on a domain consisting of 3 sand waves with a block current (solid line) and a unidirectional steady current (dashed line). Fig. (b) shows the amplitude evolution of a sand wave based on the Landau equation (solid line) (see also Schielen [1995], Knaapen and Hulscher [2002] and Morelissen *et al.* [2002]) and the evolution based on the determined growth rates for the steady current (dashed line). The vertical scale denotes the relative amplitude (amplitude/average water depth). The horizontal axis encompasses the time in years.

5.3.3 Discussion

In Fig. 5.11 (a) an estimate of the growth rate for a range of amplitudes is shown, based on the imposed sinusoidal sand waves in a unidirectional steady current and block current. It is an estimate since the sinusoidal shape is not the natural shape, and the difference with the actual shape becomes more clear for larger amplitudes, as can be seen by the asymmetry in the vertical and horizontal of the different properties in the system (see Fig. 5.8 and Fig. 5.10). For large amplitudes we see the top of the sand wave intending to grow, while the rest of the area surrounding the top shows a tendency to erode. This poses a problem to define the actual growth rate, since we do not want that the desire of the imposed bed form to change its shape is confused with the actual evolution.

We chose to take the average seabed change of the top half of the sand wave as a measure for its evolution. Hereby, the position of the trough changes less than the position of the crest for larger amplitudes. This gives us the values of the growth rate in Fig. 5.11 (a), which can be rewritten as the amplitude as a function of time resembling the amplitude evolution based on the Landau equation (see also Schielen [1995], Knaapen and Hulscher [2002] and Morelissen *et al.* [2002]) (see Fig. 5.11 (b)).

The growth rate appears to decrease for large amplitudes. The slope term in Eq. (5.3) is assumed to play the most important role here. The magnitude of the slope increases for larger values of the amplitude. The slope term balances with the shear stress in the sediment transport equation. An increasing slope term will

decrease the amount of sediment transported uphill. Furthermore, the shear stress at the seabed in the case of unidirectional steady flow increases if the amplitude increases slightly. However, from a certain amplitude on, the shear stress at the stoss side (at $z = -H$) starts to decrease, aiding the slope term to decrease the growth rate. This process was not found for periodic water motion. In fact, for the block current, the change in the gradient of the sediment transport Eq. (5.3) is due to the slope term, which appears to be able to counteract the increasing shear stress at the seabed for larger amplitudes, such that it reduces the growth rate of the sand wave.

5.4 Sand wave evolution, a morphodynamic approach

In this section we will investigate the evolution of sand waves with a fully coupled model. This means that the seabed is allowed to change during the long-term morphological calculations (see Fig. 5.12). This will omit the restriction of the sinusoidal shape discussed above.

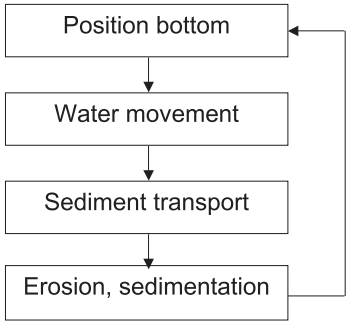

Figure 5.12: Closed morphological loop.

Hereby, we will use periodic boundary conditions. Using this approach, we choose the length of the domain to be equal to the initially preferred wavelength based on linear theory. During the morphological calculations this wavelength is fixed. Therefore, the model is not allowed to alter the wavelength of the sand wave during its evolution. However, this is a common approach. Other related studies into the dynamics of bars in rivers (see Schielen *et al.* [1993]) and shoreface-connected sand ridges (see Calvete *et al.* [2002]) have shown that the initially most preferred mode can play a dominating role in the non-linear regime. Furthermore, this assumption is supported by bathymetric data containing offshore sand waves. The data shows that the ratio of the height of the sand waves compared to the average water depth is relatively small (see Terwindt [1971], Van Alphen and Damoiseaux [1989], Van Maren [1998], Knaapen *et al.* [2002] and Morelissen *et al.* [2002]). This indicates the system

Parameters	Symbol	A	B	C	Dimension
Mean grain size diameter	d	4.15	5.37	0.58	10^{-4} m
Steady current velocity	U	1.5	0.8	0.2	m s^{-1}
Average water depth	H	19	21	22	m
Range sand wave length	L_{sw}	100/850	50/4000	50/350	m
Mean sand wave length	L_{sw}	275	190	145	m
Range sand wave height	h_{sw}	1/11	1/6	1/5	m
Mean sand wave height	h_{sw}	3.75	2	1.9	m
Asymmetry ratio	-	1/5.6	1/7.5	1/6	-

Table 5.2: Values for the different areas under investigation of the Gulf of Cadiz.

is not strongly non-linear, but weakly non-linear. Therefore, we expect a maximal difference in wavelength within the same order of magnitude as the non-linearity, which is about 10-20%.

We will start by investigating unidirectional steady flow, with the Gulf of Cadiz as a case study, and then investigate periodic water motion focussing on North Sea conditions.

In the previous section we were looking at sinusoidal sand waves, whereby it is common to refer to the magnitude in the vertical using the term amplitude. However, in this section the bed forms are not sinusoidal anymore. Therefore, we will use the term sand wave height, defined as the distance from the trough to the top. In the previous section the height is equal to two times the amplitude.

5.4.1 Unidirectional steady flow - The Gulf of Cadiz

Sand waves in the Gulf of Cadiz

In Spain in the Gulf of Cadiz sand wave like bed forms in a predominantly unidirectional steady flow are found in average water depths of 20 metres on a continental shelf of about 30 km wide (see Fig. 5.13). Due to the nature of the tidal motion in combination with the shape of the coastal environment, the ebb and flood parts of the tidal motion pass over different areas in the Gulf. The wavelengths and heights of the sand waves are typically 150-300 m and 2-4 m, respectively. Symmetrical and asymmetrical sand waves are found. In Table 5.2 the characteristics can be found based on one measurement of the bathymetry. Therefore, no information concerning their migration rates is available. Rommel *et al.* [2003] showed that it is possible to predict sand wave migration with the help of the model presented in Chapter 3. Here, we will use this data to investigate sand wave evolution and saturation.

Three zones have been differentiated according to the assumed migration direction of the sand waves based on their asymmetry, which is in the direction of the water motion. Zone A is located south of Barbate High. Zone B is situated at Barbate High and zone C can be found in the Northern part of the shelf (see Fig. 5.13).

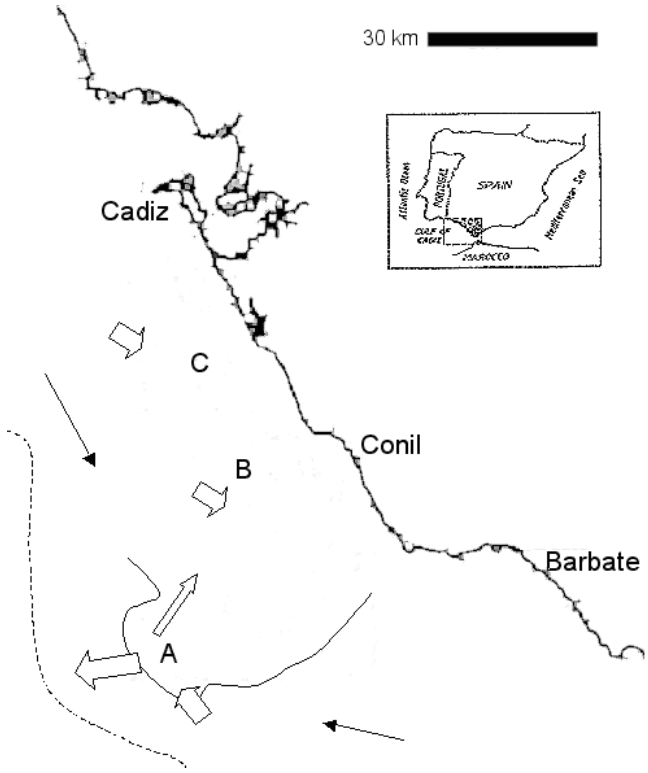

Figure 5.13: Enlargement of study area consisting of four zones A, B and C located at 36 degrees latitude and -6 degrees longitude. The arrows denote the current and presumed migration direction of the sand waves. The figure is adapted after Lobo *et al.* [1999] and Munoz-Perez *et al.* [2001].

In zone A the largest sand waves have average wavelengths of about 275 m and average heights of 3.75 m (see Table 5.2). In zone B we find the most asymmetrical sand waves in the Gulf. Hereby, the asymmetry is defined as the horizontal length of the lee side divided by the horizontal length of the stoss side. Between these two zones we can distinguish a transitional zone where sand waves are symmetrical. Zone C contains relatively small sand waves, with wavelengths of about 145 m and heights with a maximum of 2 m, with rounded and eroded crests.

Water motion in the Gulf of Cadiz

The current patterns found in the Gulf of Cadiz are complex. Two main current patterns can be identified. The first is an inflow south eastward of the North Atlantic water in the direction of the Mediterranean Sea over the shelf domain [Lobo *et al.*,

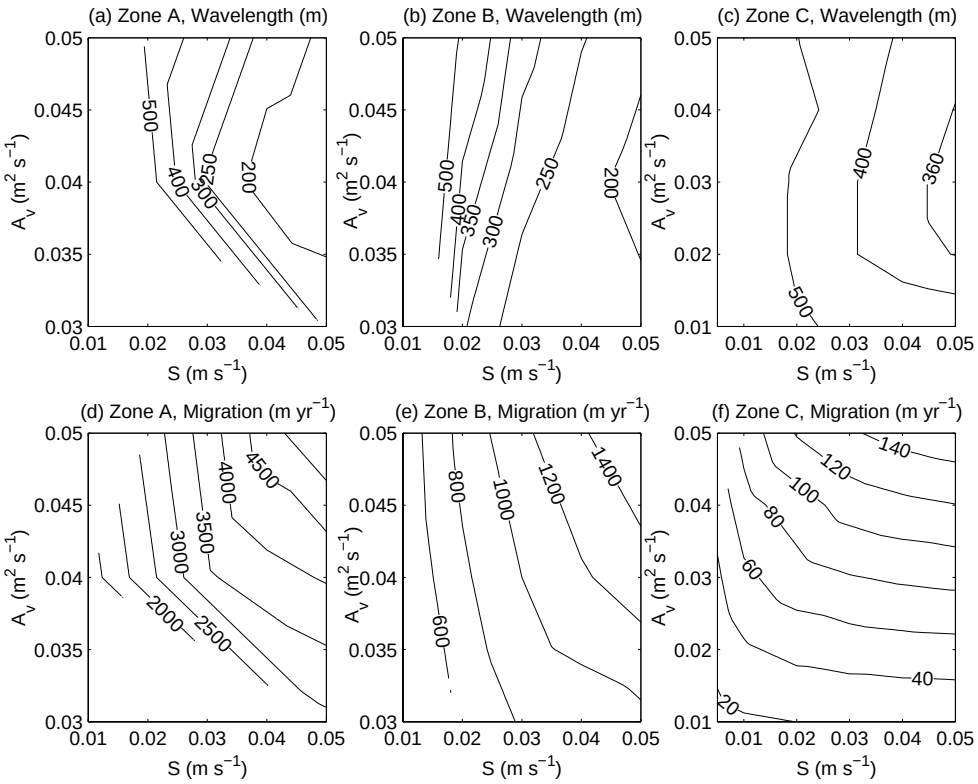

Figure 5.14: Estimated wavelengths and coinciding migration rates for three zones in the Gulf of Cadiz. The three figures above show the wavelengths of the fastest growing modes according to the linear analysis for zones (a), (b) and (c). The flow conditions go from highly energetic in zone A to low energy conditions in zone C. The figures below show the corresponding migration rates in the different zones.

1995] (Zones B and C). The second is a north eastward outflow from the Mediterranean sea [Nelson *et al.*, 1999] due to the density contrast between this water and the fresh water coming from the Atlantic. This density contrast enforces a reverse estuarine circulation, in which the Mediterranean water flows westward along the seabed under the eastward flowing Atlantic water (Zone A).

This distinguishes the area from the North Sea where periodic water motion is dominant, which is sometimes modified by a steady component. Therefore, in the Gulf of Cadiz we find offshore sand waves existing in unidirectional more or less steady flows.

Figs. 5.14 (a), (b) and (c) show the wavelengths of the fastest growing modes according to the linear stability analysis for zones A, B and C. This for a range

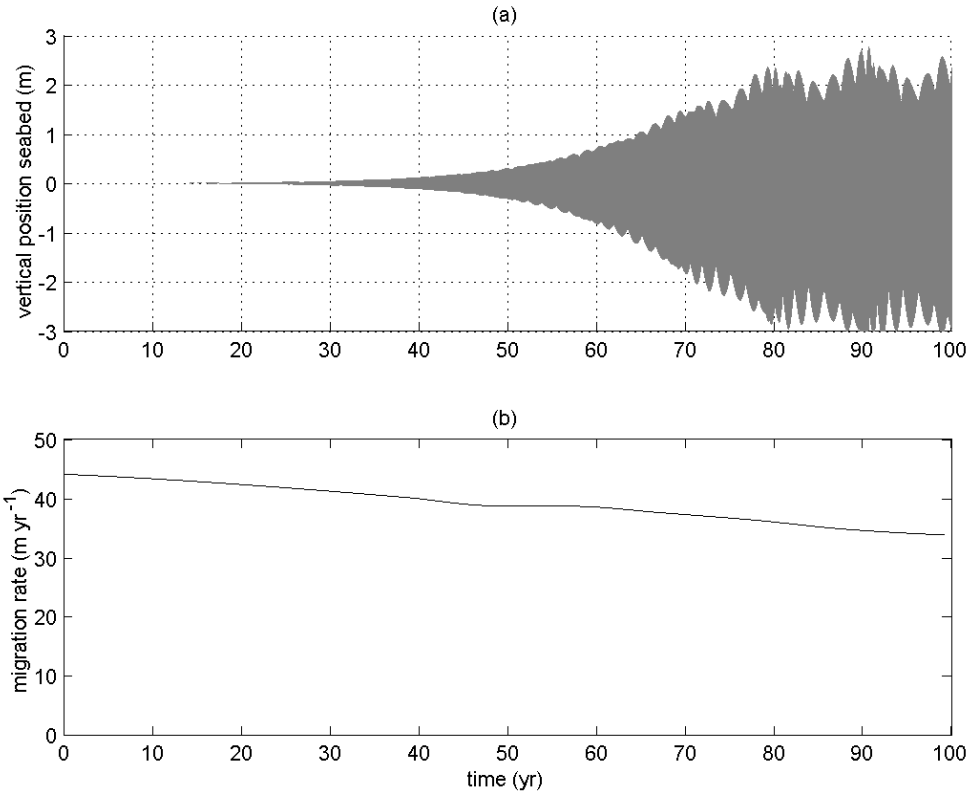

Figure 5.15: Evolution and migration of a sand wave in zone C of the Gulf of Cadiz. Fig (a) shows sand wave evolution in a unidirectional steady current using periodic boundary conditions. We see the development of the seabed (on the vertical axis in metres) as a function of time (yr). The total period calculated is about 100 years. Hereby, we show the values only in the grid points, giving the appearance of modulations due to the higher density of the grid points near the boundaries. Therefore, this is not a physical process. The initial amplitude of the imposed perturbation is 1 mm. It takes about 30 years to evolve from 10% to 90% of the saturation height. This slow evolution coincides with the moderate flow conditions. Fig. (b) shows the corresponding migration rate during the evolution of the sand wave.

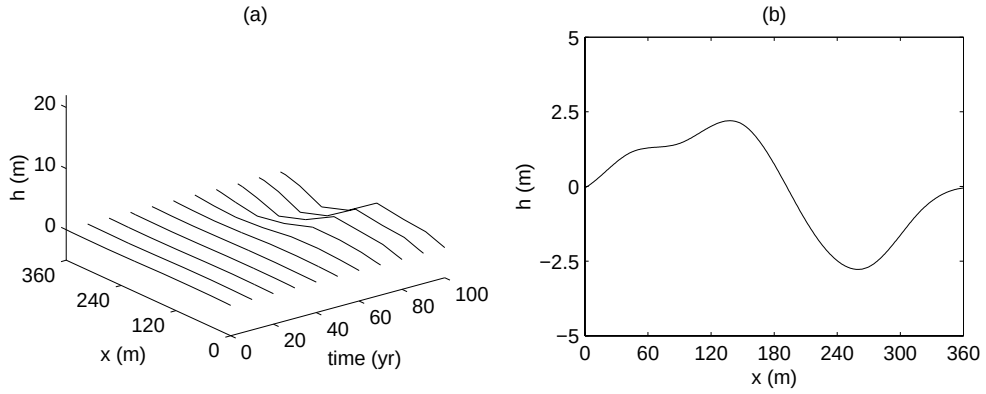

Figure 5.16: Cross section of a sand wave during its evolution in zone C of the Gulf of Cadiz. Fig. (a) shows the evolution in time of the seabed for a unidirectional steady current in zone C of the Gulf. We start the figure when the disturbance has an amplitude of 0.1 m, which then saturates in about 60 years at a total wave height of about 5 m, which is 22% of the average water depth. Fig. (b) shows the position of the seabed for the fully-developed sand wave (see also Fig. 5.1 (a) and Fig. 5.3 (c)).

of values of the slip parameter S and the eddy viscosity A_v. These two variables are considered to be the most difficult to estimate. The rest of the values of the parameters can be found in Table 5.2. The wavelengths calculated are slightly longer than the actual wavelengths found. Since the order of magnitude is correct and the available data is limited we can conclude that the approach is successful, indicating the bed forms found in the Gulf of Cadiz can be free instabilities of the system.

There was no data available whether or not the sand waves migrate. Based on the results described here, we can expect that the sand waves are migrating (see Fig. 5.14 (d), (e) and (f)). In zone A the sand waves are in fact expected to migrate very fast due to the large current velocities. Zone C has migration rates which correspond more to North Sea conditions. Here, the magnitude of the depth-averaged current is also of about the same order of magnitude as the steady part found in the North Sea.

Sand wave evolution

In Fig. 5.15 and Fig. 5.16 (a) the development of the seabed in zone C as a function of time is presented. We started with the fastest growing mode determined with the linear stability analysis (Chapter 3) for a steady current induced by a pressure gradient and a value of the slip parameter S of 0.04 m s^{-1} and the eddy viscosity A_v of 0.02 m^2 s^{-1} (see also Table (5.1) for the rest of the values of the parameters and Fig. 5.14).

We can identify the evolution of the sand wave pattern. In Fig. 5.15 (a) the positions of the seabed in all the grid points are plotted as a function of time. The

distortion apparent is not a numerical error or higher harmonic in the seabed topography. This is due to the narrowing grid density near the boundary of the computational domain, where the sand waves passes through while migrating. The evolution of the height of the sand wave according to the current model is therefore a smooth line as Fig. 5.11 (b).

The bed form initially develops slowly, after which the amplitude increases quicker, equivalent to the exponential solution of the linear stability analysis. Next, the growth rate diminishes (due to the change in balance between the shear stress at the seabed, transporting sediment upward and the slope term in the sediment transport formula (Eq. (5.3)) and saturation is found. It takes about 30 years to develop from 10% to 90% of the saturation height of about 5 m, which is 22% of the average water depth. The found height and wavelength of the sand waves lie within the range of the observations. However, they are above average. Hereby, we should note the slope effect becomes more important for sand waves with smaller wavelengths. Therefore, a smaller wavelength of the fastest growing mode should result into a smaller sand wave height.

The slopes found are still small (the maximum is about 4%). Therefore, no flow separation occurs. This coincides with the observation that the bed forms in this zone C are more symmetrical than in the other zones A and B. The fully-developed bed pattern is migrating with a migration rate of about 36 m yr^{-1}. The cross section shown in Fig. 5.16 (b) is the one after the sand wave has fully developed. However, the asymmetric shape is not yet in equilibrium, and changes further. See below for a more detailed discussion on sand wave migration.

Similar calculations have been performed for zones A and B for different values of the slip parameter S and the eddy viscosity A_v. However, for all cases the asymmetries of the bed forms become so large during their evolution, that we were not able to describe their entire evolution without flow separation. This is due to the larger shear stresses (due to the higher current velocities). To enable the description of these bed forms, the model needs to be modified as discussed above. The strong asymmetry (in the horizontal) the simulation model predicts coincides with the asymmetry of the sand waves found in zones A and B.

5.4.2 Periodic water motion - The North Sea

Fig. 5.17 and Fig. 5.18 (a) show the evolution of a sand wave for a typical North Sea location. This for a value of the slip parameter S of 0.008 m s^{-1}, an eddy viscosity A_v of 0.005 m^2 s^{-1} and a average water depth of 30 m. The value of λ_1 is set at 0.006 and we investigated a block current based on a pressure gradient inducing a depth-averaged velocity of 1 m s^{-1}. For the rest of the values of the parameters see Table 5.1.

We started calculations with a sinusoidal sand wave with a wavelength coinciding with the fastest growing mode, determined with the simulation model. The initial amplitude of the bed form is 0.025 m. The seabed develops initially slowly. However,

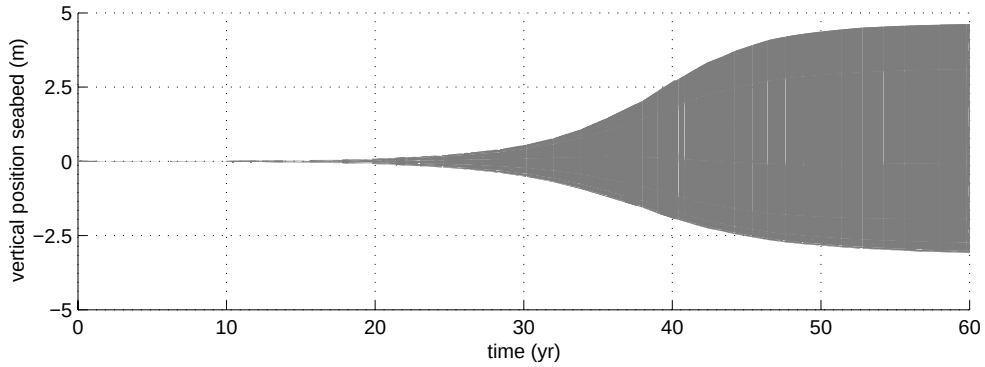

Figure 5.17: Sand wave evolution in a block current using periodic boundary conditions. We see the development of the seabed (on the vertical axis in metres) as a function of time (yr). We start the simulation with the fastest growing mode for a slip parameter of 0.008 m s^{-1} and an eddy viscosity of 0.005 m^2 s^{-1}. The initial amplitude of the imposed sand wave is 0.025 m. It takes about 20 years to evolve from 10% to 90% of the saturation height.

it takes only 20 years to develop from 10% to 90% of the saturation height. Next, the growth rate of the sand wave diminishes again, due to the increased importance of the slope effect with respect to the uphill directed shear stress for larger heights. The height of the fully-developed sand wave is about 7.8 m, which is 26% of the average water depth. This height lies within the range seen in the North Sea (see also paragraph 3.9). The water motion still has residual circulation cells oriented towards the crest (see Fig. 5.19). Furthermore, the sand wave does not migrate and shows no asymmetry in the horizontal. It resembles a sinusoidal pattern with a slightly elongated trough.

5.5 Sand wave migration

Fig. 5.15 shows the evolution of a sand wave in zone C of the Gulf of Cadiz as a function of time (see also Table 5.1). Hereby, we are interested in the migration rate obtained with the linear stability analysis (Chapter 3) compared to the migration rates for finite amplitudes.

The migration rate is defined as the time it takes for the lee side of the sand wave at $z = -H$ to migrate one wavelength. This definition is chosen since we are looking at a unidirectional steady current, inducing an asymmetric shape not equal to the sinusoidal sand waves investigated with the linear stability analysis. The migration rate decreases slightly, from 44 m yr^{-1} for an amplitude of 1 mm to 36 m yr^{-1} for the fully-developed sand wave. This means an 18% difference between the result from the linear stability analysis and the fully-grown sand wave.

Therefore, the linear stability analysis provides a good estimate of the migration

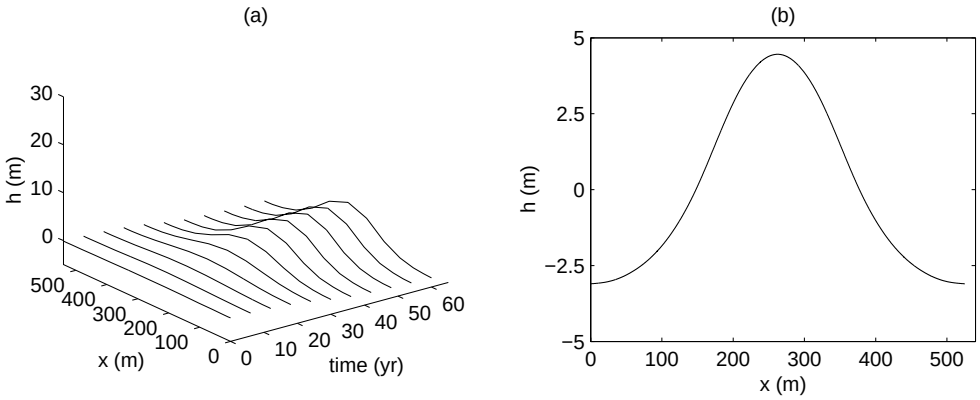

Figure 5.18: Cross section of a sand wave during its evolution and its final shape in the North Sea. Fig. (a) shows the evolution in time of the seabed for a block current representing a typical North Sea location. We start with a disturbance with an amplitude of 0.025 m, which saturates in about 60 years at a total wave height of about 7.8 m, which is 26% of the water column. Fig. (b) shows the position of the seabed for the fully-developed sand wave.

rate, even though the analysis is based on infinitely small sinusoidal sand waves. Furthermore, this is as can be expected from a weakly non-linear problem where we expect the change in sand wave migration to be of the order of the relative sand wave height.

5.6 Sensitivity analysis

5.6.1 Slope term

In Eq. (5.3) we can see the slope effect is modelled by two separate terms with the parameters λ_1 and λ_2. In the linear analysis, only the sum of the two terms is important, since the amplitude of the sand waves is very small. However, for larger sand wave heights the effect of the different terms are different, since the shear stress on the seabed changes during the evolution of the sand wave.

In Fig. 5.20 (a) the profile of a fully-grown sand wave for the typical case calculated for a block current (see Table 5.1 and Figs. 5.17 and 5.18) can be seen. Fig. 5.20 (b) shows the profile using the same value of the slope term for the small amplitude sand wave case, giving the same wavelength for the fastest growing mode, but based on λ_1 ($\lambda_1 = 0.00896$ and $\lambda_2 = 0$). This gives a more peaked profile of the sand wave resembling the pattern found in the North Sea in Fig. 5.1 (b), with more elongated troughs and sharp crests. The height is about the same as in Fig. 5.20 (a). If we set λ_1 to zero and base the slope term for the instability mechanism on λ_2 ($\lambda_1 = 0$ and $\lambda_2 = 10.1$) we obtain Fig. 5.20 (c). Hereby, we have to mention that just before

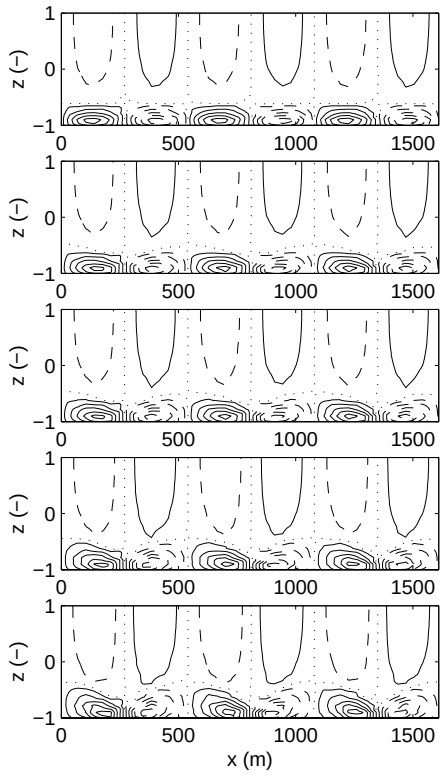

Figure 5.19: Contour plot of the horizontal residual current for a block period during the evolution of a sand wave. The sand wave height during its evolution from top to bottom is 0.05 m, 2 m, 4 m, 6 m, and 7.8m. The solid lines depict the positive, the dashed lines the negative and the dotted lines a residual flow equal to zero. The position of the water surface and seabed are $z = 1$ and $z = -1$, respectively.

reaching its maximum height, flow separation occurred. This is due to the larger attained height of 10 m. For illustrational purposes we plotted this profile to show the more smooth shape compared with Fig. 5.20 (a) and Fig. 5.20 (b) due to the different more diffusive character of the slope term containing λ_2, which can already be identified during the evolution.

Which of the two terms dominate depends on the magnitude of the shear stress and on the magnitude of the slope parameters. We expect for relatively higher shear stresses more peaked sand waves, and for more moderate conditions smooth sand waves.

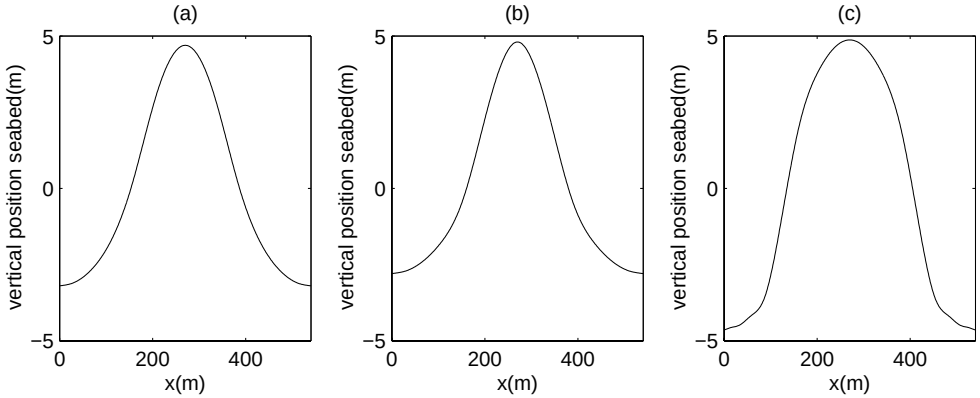

Figure 5.20: Fig. (a) shows the shape of the fully-developed sand wave induced by a block current for a typical North Sea location with a λ_1 of 0.006 and λ_2 of 3.33. Fig. (b) and (c) show fully-developed sand waves for the same conditions except for a λ_1 of 0.00896 and λ_2 of 0 in (b) and λ_1 of 0 and λ_2 of 10.1 in (c). See also Figs. 5.3 (a) and (d).

5.6.2 Viscosity and resistance at the seabed

We can test the effect of the magnitude of the eddy viscosity A_v and slip parameter S on the behaviour of finite amplitude sand waves, by varying their values. Hereby, we need to calculate, for each combination of S and A_v, the wavelength of the fastest growing mode.

For larger roughness of the seabed, we find shorter wavelengths of the sand waves due to the increased shear stress at the seabed. The growth rate of the sand waves for these larger values of the slip parameter is larger (see Figs. 5.21 (a), (c) and (e)) due to the combination of the higher shear stress and the shorter wavelengths (smaller volume). The maximum height increases as well (see Figs. 5.21 (b) and (d)). Therefore, the increase in shear stress dominates the increase in slope effect due to the shorter wavelengths. The large resistance at the seabed in Figs. 5.21 (e) and (f)) caused the flow to separate from the sand wave crest. This effect was enhanced by the sharper gradient in the velocity profile.

Longer fastest growing modes are found for larger values of the eddy viscosity (Chapter 3) (see Fig. 5.22). The rate of the evolution increases as well (see Figs. 5.22 (a), (c) and (e)). Starting for the same amplitude of 0.025 m, we find fully-developed sand waves after about 90, 60 and 40 years for values of the eddy viscosity A_v of 0.05, 0.01 and 0.015 $\mathrm{m}^2\ \mathrm{s}^{-1}$, respectively. Furthermore, the maximum height of the sand waves increases almost linear as a function of the eddy viscosity (see Figs. 5.22 (b), (d) and (f)). This increase in wave height is partly due to the longer fastest growing modes, which have relatively less inhibitions by the slope effect during their evolution.

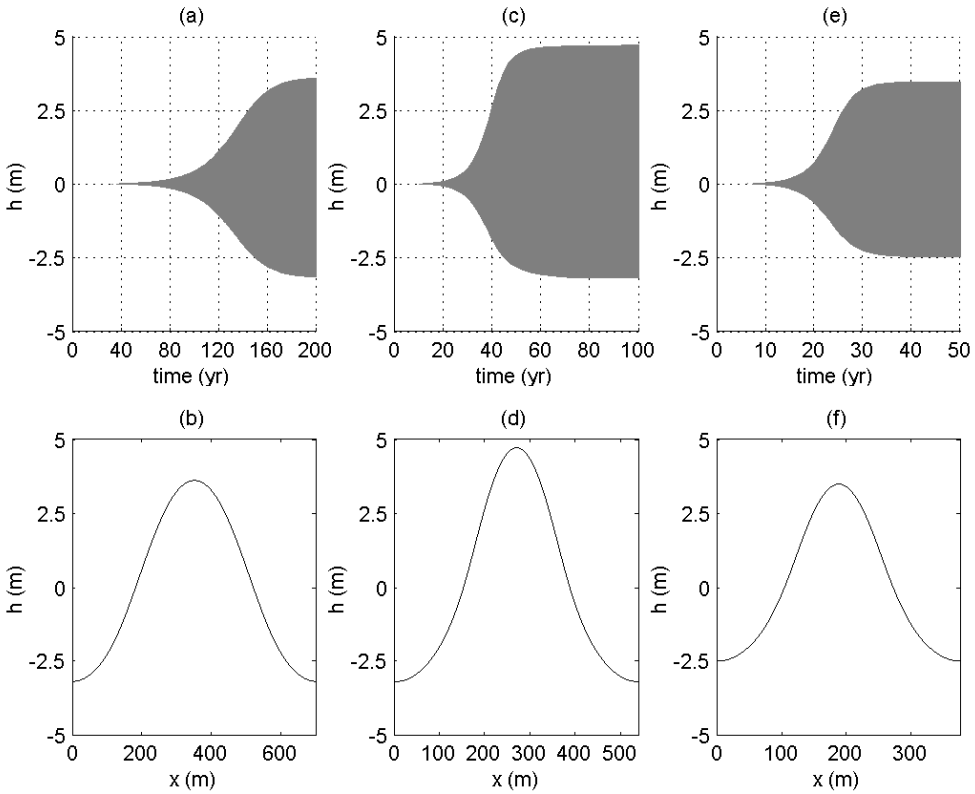

Figure 5.21: The three columns show the evolution of the sand wave in time (above) and the cross section of the fully-grown sand wave (below) for three values of the slip parameter S: 0.005, 0.008 and 0.011 m s^{-1}.

5.6.3 Sand wave height and average water depth

Wilkens [1997] investigated with the help of a GIS several characteristics of sand waves and found an almost linear relationship between sand wave height and the average water depth (see Fig. 5.23). This linear relationship holds for the range of average water depths in which sand waves are believed to exist [Hulscher and Van den Brink, 2001].

We investigated the effect of the water depth by considering a range of depths. Hereby, we investigated for each water depth the same magnitude of the pressure gradient. Therefore, the magnitude of the depth-averaged velocity decreases for larger water depths. For each case we needed to calculate the wavelength of the fastest growing mode, which was longer for larger water depths (see Fig. 5.24 (a)).

The range of water depths investigated starts at 10 m, where we expect other

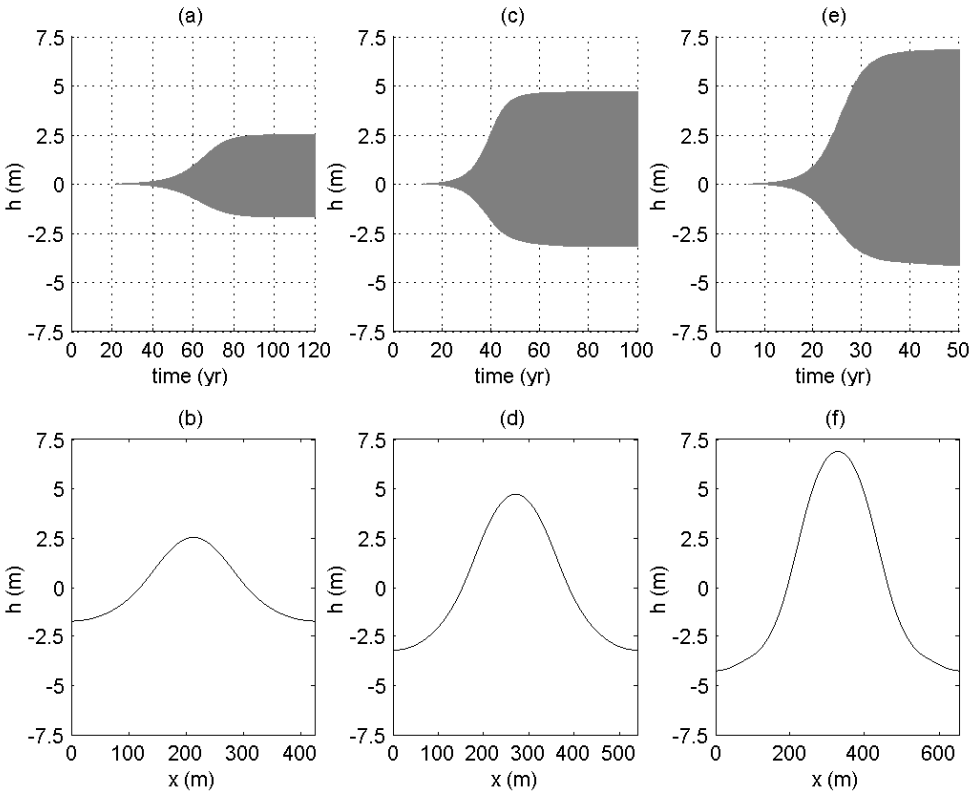

Figure 5.22: The three columns show the evolution of the sand wave in time (above) and the cross section of the fully-grown sand wave (below) for three values of the eddy viscosity A_v: 0.05, 0.01 and 0.015 $m^2\ s^{-1}$.

processes such as suspended sediment and wind waves to play an important role. It ends at 55 m, where according to Fig. 5.23 the sand waves are very small.

With the current parameter settings, flow separation occurs for average water depths less then 25 m. Therefore, the heights shown in Fig. 5.24 are only indications of the maximum profile of the sand wave in these shallower waters. However, we do not find sand waves of these magnitudes in nature at these water depths. It is possible the parameter settings for this region should be different. Furthermore, aspects such as suspended sediment and wind waves influencing sediment transport are assumed to play an important role in the saturation mechanism under these conditions. These aspects have not yet been incorporated in the model.

At larger water depths, we see that the maximum height for a fixed pressure gradient remains about the same. The wavelengths become longer, and the slope term only starts playing a role in the saturation when the heights are large. The

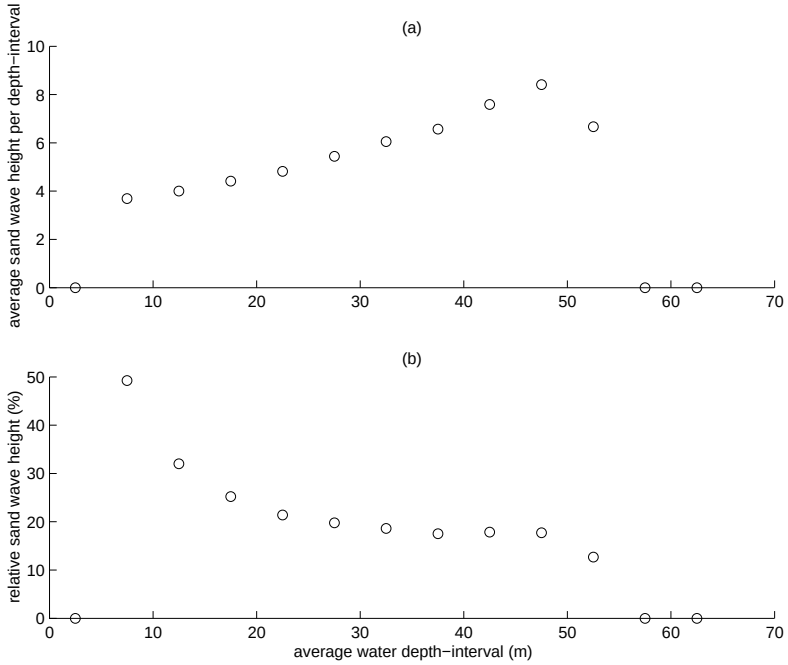

Figure 5.23: (a) shows the sand wave height (m) distribution over the average water depth (m) as a function of the average sand wave height over a depth-interval [Wilkens, 1997]. For small water depths, no sand waves occur since other processes are assumed to become relevant. For large water depths, also no sand waves occur. Possibly, due to the low shear stresses, initiation of motion is not achieved. (b) shows the relative sand wave height (m) over the average water depth (m) (height/average water depth) as a function of the average sand wave height over a depth-interval.

relative sand wave height shown in Fig. 5.24 (c) coincides very well with Fig. 5.23 (b). However, the absolute heights remain large for larger average water depths. The position of the water surface appears not to encompass the mechanism to explain the absence of sand waves for larger water depths (see Fig. 5.23). However, Fig. 5.24 coincides better with the idea that the role of the position of the free surface is of lesser importance when the average water depth is of the same order or larger compared to the Stokes layer thickness (the boundary layer).

5.7 Dredging

In Fig. 5.25 we investigated the response of dredging the seabed containing fully-developed sand waves for the typical North Sea location (see Fig. 5.17). We will dredge the top 5 m of an infinitely wide field of sand waves (fully developed sand

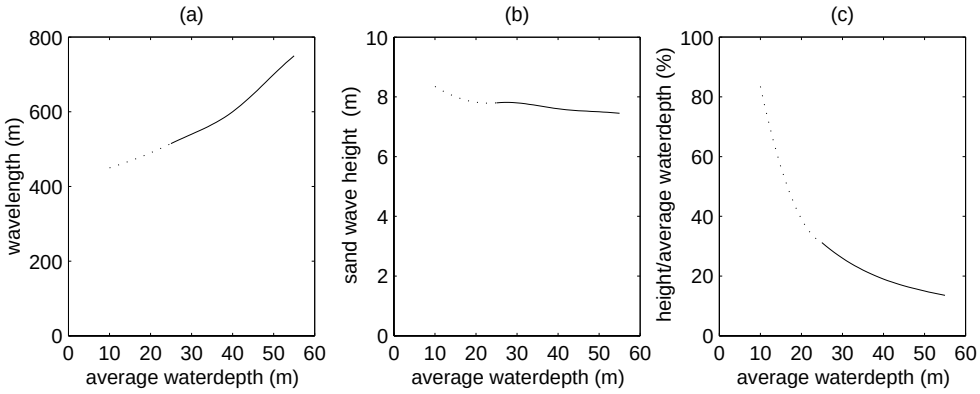

Figure 5.24: Fig. (a) wavelength (m) of the fastest growing mode for a range of water depths, based on a block current. Fig. (b) shows the maximum sand wave height calculated Fig. (c) shows the relative sand wave height ($\frac{height}{average\ water\ depth} * 100\%$). For average water depths smaller than 25 m, we encountered flow separation for this parameter setting (dotted part).

wave to be dredged can be found in Fig. 5.25 (a) (solid line)), resulting in a bed form after dredging (dotted line). Furthermore, after dredging, the average seabed is 1.5 m lower.

The initial profile of the seabed to start calculations after dredging is smooth, since we expect that the rough edges and other disturbances in the profile, can be seen as features having small wavelengths. These small scale features are dampened on a very short time-scale compared to the timescale of sand waves (according to linear theory (see Chapter 3)).

The development of the trough and top of the dredged sand wave can be seen in Fig. 5.25 (b). The dredged sand wave recovers in a matter of a decade. The top of the fully-developed sand wave is about 1.5 m lower than of the original profile (solid line Fig. 5.25 (a)).

Here, we made the assumption that the wavelength of the sand wave remains the same after dredging. Based on the linear theory, we expect that the wavelength of the fastest growing mode is longer than for the dredged sand waves. This is due tot the larger average water depth, since sand was extracted from the system. However, since a bed pattern with a relatively large height remains, we assume that the initial response of the recovering sand wave based on the wavelength coinciding with this bed form, is a good approximation of reality on the intermediate term (decades).

Since sand was extracted from the system, the crests of the fully-developed sand waves after a decade will be 1.5 m lower than the original ones. On a longer time-scale, it is possible the system will reorganise itself. Firstly, due to the fact that the fastest growing mode of the system changes due to the changed average water depth. Hansen *et al.* [2001] investigated experimentally the response of fully grown ripples,

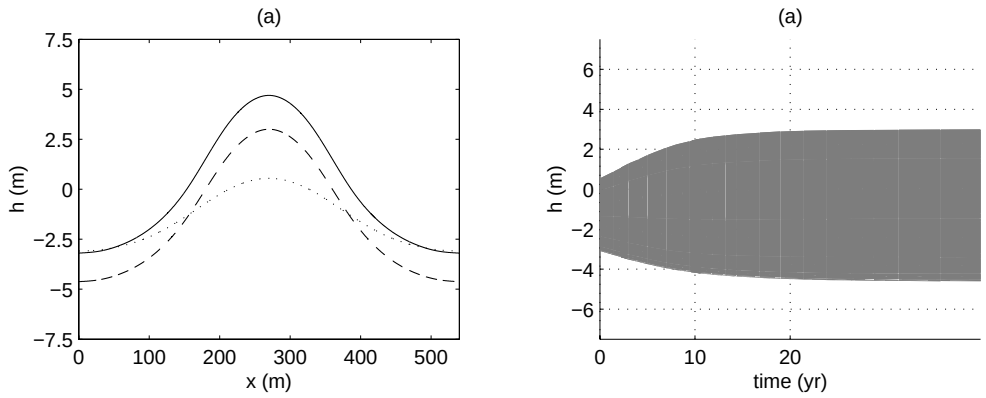

Figure 5.25: Dredging of sand waves and their recovery. Fig. (a) shows the original sand wave (solid line), sand wave after dredging (dotted line) and recovered sand wave (dashed line). Fig. (b) shows the recovery of the dredged sand wave in time.

on changes in forcing. The pattern and wavelength of the already existing ripples almost did not change on the short term for changes in the forcing. This suggested that reorganization of the patterns seems to take place on a longer timescale than the formation of the ripples starting from a flat seabed. This process is different from dredging and ripples are formed by a different mechanism than sand waves. However, this work still forms an interesting analogy, indicating that the reorganisation of the sand wave pattern after dredging will take place on a longer time scale than the recovery of the sand wave.

Furthermore, here we are dredging an area which is infinitely wide. However, in reality, this area will be more likely in the order of kilometres (at most). If the average seabed is lowered over an area of kilometres, we are introducing a length scale in the order of kilometres. Roos and Hulscher [2002] showed that this can cause patterns similar to sandbanks on a longer timescale of centuries.

If the dredged sand obtained from the top of the sand wave is dumped in the troughs, to increase the least depths, the average water depth does not change. The evolution of the bed form can then be estimated with Fig. 5.17, assuming the dredged sand wave is a free instability of the system. The time it takes for the sand wave to become fully developed again, depends on the height of the remaining bed form. For each metre dredged, a rough estimate of the resulting lowering of the height is two meters. The time-scale for its recovery is then a matter of decades or less (See Table 5.3), after which the sand wave has regained its original height again.

Dredging the top (m)	Regeneration 90% (yr)
0.5	1
1	5.5
1.5	8
2	10
2.5	13
3	15

Table 5.3: Regeneration of sand waves after dredging. The material obtained by dredging the top of the sand wave is deposited in the trough of the sand wave. Therefore, for each metre the top of a sand wave is lowered (left column), the total remaining height decreases with two metres. The right column shows the time it takes for the sand wave to regain 90% of its original height for a typical North Sea situation (See paragraph 5.4.2). Note, that for this dredging strategy, the average water depth does not change.

5.8 Conclusions

With the numerical model developed herein, we are able to allow a sand wave to evolve and become saturated. They reach heights of 10-30% of the average water depth. It takes about 20 years to evolve from 10% to 90% of the saturation height. This coincides with values reported in the literature ([Knaapen and Hulscher, 2002] ,Idier [2003]).

The stabilisation mechanism found here causing sand waves to saturate is based on the balance between the shear stress at the seabed and the fact that sediment is transported easier downhill than uphill. Hereby, the shear stress is a function of the resistance at the seabed and the eddy viscosity. The water motion has residual circulation cells oriented towards the crest for periodic water motion for infinitely small as well as fully-developed sand waves. At larger heights, the slope term reduces the net amount of sediment transported upwards towards the crest, which causes the sand wave to saturate.

The steepness found for fully-developed sand waves is less for periodic water motion than for sand waves in unidirectional steady flow. In the latter case, sand waves can evolve without flow separation when flow conditions are moderate. For less moderate flow conditions, the sand waves become too asymmetrical and require the description of flow separation processes.

The migration rate becomes only slightly smaller during the evolution from an infinitely small to a fully-grown sand wave. This allows us to use the linear stability analysis to estimate the migration rate.

An isolated hump at the scale of a sand wave is different from a field of sand waves. For larger heights, the different sand waves seem to interact more, as can be seen from the shear stress at the stoss side of the sand wave for unidirectional steady flow.

The resistance at the seabed and the viscosity are important factors determining the value of the shear stress at the seabed. Therefore, they play an important part in the balance between the shear stress and the slope term in the sediment transport formula. Larger resistance at the seabed and larger values of the eddy viscosity decrease the timescales and increase the saturation height.

For periodic water motion, the balance between the shear stress at the seabed and the slope term determines not only the height but also the shape of the sand wave. When the λ_1 component of the slope term is larger than the λ_2 component, the sand wave also tends to be more sharp-crested. In the opposite case, the sand wave will have a smoother shape.

The water depth plays an important role determining the wavelength of the fastest growing mode. Therefore, the saturation height is correlated to the average water depth, since it indirectly effects the influence of the slope effect on the sand wave saturation. However, when the ratio of the average water depth divided by the Stokes layer is larger, the relative effect becomes smaller.

Sand waves are able to recover in a matter of decades after they have been dredged. The resulting saturation height depends on the amount of sand extracted and on the location where the sand is dumped. When the sand is extracted from the system, the resulting saturation sand wave height will be lower than when the dredged sand is dumped in the troughs.

5.9 Appendix

5.9.1 Numerical considerations

If we decrease the number of grid points used in the domain, we obtain numerical oscillations near the boundaries. This is a known property of Chebyshev polynomials approximating a solution. The accuracy in the interior is larger than near the boundaries of the domain.

If we investigate a steady current over a group of sand waves, and we increase manually the amplitude of the perturbation, the disturbance in the water movement becomes larger with respect to a flat bed situation. The inflow boundary is related directly to a flat bed situation with a gradient of zero in the seabed topography (Eq. (5.10)). At the outflow boundary, (physically an open boundary) we find boundary conditions stating that the derivatives in the horizontal are zero in the non-periodic case. This is correct for a flat bed situation, but not if gradients in the flow, seabed or water surface are present. Therefore, if we allow the height of a bed form in the model to increase, it is possible the disturbance in the water movement starts to conflict with the boundaries.

If we preserve a certain flat bed area adjacent to the boundaries, we can overcome the physical part of this problem. One would expect that at least half a wavelength is needed, since this is the minimum length scale of the residual cells responsible of the formation of sand waves. If this approach is followed, the problem becomes more local. We therefore need to increase the number of modes/grid points to maintain the required maximum numerical error of the approximation. We find for a non-local smooth problem, the accuracy increases significantly when increasing the number of modes/grid points. However, if the problem becomes more local, we require a larger number of grid points increasing the calculation time. The inclusion of splines should improve the efficiency of the approximation method near the boundaries.

Chapter 6

Conclusions

"What are the key practical problems concerning sand waves and their coinciding time and length scales?"

Sand waves pose a threat to a range of offshore activities. The combination of their timescale (years), length scales (hundreds of metres) and height (metres) make sand waves bed features to be reckoned with for activities having similar temporal and spatial scales. Firstly, sand waves decrease the least navigable depths and pose a threat to navigation routes and access channels. Furthermore, due to sand wave migration, pipelines and cables may become exposed, which can result in free spans. These free spans may cause the pipeline to buckle or break. Moreover, the exposed pipelines and cables can be damaged by anchors and fishing nets. In addition, exposed objects may be covered by a sand wave, making it difficult to locate them. Lastly, continuous monitoring and, if necessary interventions such as dredging or rock dumping are required to avoid unsafe situations, which are costly operations.

"What processes can cause sand waves to migrate?"

A steady current (here investigated by a pressure gradient and/or a wind stress at the sea surface) inducing an asymmetry in the basic state can cause migration of sand waves. The orders of magnitude for the migration rates and wavelengths found with the models developed here, are in agreement with values reported in the literature and an investigated data set along a pipeline in the North Sea.

"Can the processes determining the initial sand wave formation be simulated by a numerical model?"

The numerical simulation model developed in this thesis is able to simulate the processes which are assumed to be responsible for the initial formation of offshore sand waves. It was validated mathematically against the results of a stability analysis.

"What processes are responsible for the stabilisation of sand wave evolution?"

The offshore sand waves investigated here saturate at a height of 10-30% of the water depth. They form over decades, starting from a perturbation which is small compared to the water depth. The stabilising mechanism that leads to saturation is the principle that sediment is transported more easily downhill than uphill. For the saturated sand wave, we still see a net flux of water oriented upwards towards the crest in case of periodic water motion, as we do for an infinitely small sand wave.

The sediment characteristics partly determine the shape of the sand waves. We find sand waves with a smooth almost sinusoidal shape, or a sharp crest together with an elongated trough.

For unidirectional flows, asymmetric bed forms are found of which the entire evolutionary process for moderate flow conditions can be described with the developed simulation model. For more energetic flow conditions, this is not possible, since the sand waves become too asymmetric and give rise to flow separation downstream of the crest.

"How do the migration rates and shape of a sand wave change in the intermediate term?"

The migration rate of a sand wave decreases slightly during its evolution. The migration rate of a fully-grown sand wave is about 18% less than of an infinitely small sand wave. This allows us to use the results from the stability analysis in Chapter 3 as an estimate of the migration rate of a fully-developed sand wave.

Furthermore, sand waves are able to recover after they have been dredged. The timescale and resulting maximum height depend on how much sand is dredged and where it is dumped.

"What data do we need to validate and apply the developed models in reality?"

Information is required on the sediment characteristics to determine the values of the input parameters for the sediment transport formulation. Furthermore, a depth-averaged estimate of the non-periodic component of the water motion is necessary to estimate sand wave migration rates. Moreover, to describe the finite amplitude behaviour of sand waves using the present model, we need actual velocity profiles to determine the input values for the resistance at the seabed and the eddy viscosity. This will enable us to describe the shear stresses at the seabed as accurately as possible.

Chapter 7

Recommendations

Future research on the following subject matters is recommended.

7.1 Data and validation

7.1.1 Migrating sand waves

We are interested in bathymetric data sets with a total span of several years and intervals of about one year, to validate the models with respect to sand wave migration. These data sets should contain sand waves which are modified as little as possible by human intervention. Furthermore, the horizontal accuracy should be larger than the assumed migrated distance of the sand waves over the time span of the data set.

These data sets can be used to perform case studies with the developed models, giving insight in what knowledge is missing further. An example of such a case study is Morelissen *et al.* [2002]. Here, we applied a data assimilation technique, combined with a Landau equation, on a pipeline study. This work can now be extended by using the stability analysis and simulation model (see also paragraph 3.9).

7.1.2 Sand wave evolution

To validate sand wave evolution as calculated by the numerical simulation model, we need morphological data over several years, after a sand wave or a field of sand waves has been dredged. Together with information on the water motion in the area under investigation, this will enable use to validate the evolutionary processes found with the simulation model. This information is not available at this moment. Here, the vertical accuracy of the position of the seabed is important.

Further morphological data surrounding offshore interventions, changing the sediment supply in an area containing fully-developed sand waves, is interesting. This data can be used to investigate the influence of sediment availability and changes in water motion on the behaviour of fully-developed sand waves and validate the existing models further. An example of such an intervention is an offshore island or a large-scale sand extraction pit.

7.2 Calculation time and use

Numerical codes are more useful when the necessary calculation time is shorter. They then allow a wider range of parameters to be explored, increasing the confidence and helping the interpretation of the results. This can be achieved by omitting the free surface, which increases the numerical efficiency, since only one time-varying wall (the seabed) remains. Furthermore, the efficiency of the spatial approximation method can be increased by incorporating splines. These should increase the accuracy near the boundaries of the domain, thus requiring less grid points (resulting in less calculation time) for equal numerical accuracy.

Moreover, the results from the models can be translated to models like the Landau equation (See [Schielen *et al.*, 1993], [Knaapen and Hulscher, 2002] and [Morelissen *et al.*, 2002]), which are from a computational point of view less requiring. The coefficients of the Landau equation, which now need to be calibrated based on data sets gathered over several years, can after validation of the current models be determined with other models. Solving this Landau equation is relatively fast, which increases the possibilities of using the information while developing management strategies.

7.3 Stochastic variations and reality

The present deterministic model approach means that we have to drastically schematise the environment. The actual natural variations in water motion and seabed composition are only taken into account to a certain extent. Therefore, the representativeness of the results for real life situations is not straightforward [De Vriend, 1987]. Furthermore, legislation and management strategies are more easily formulated based on stochastic terms. Therefore, it is necessary to implement stochastic variations in the model. These variations can be caused by, for example, random variations in the tidal movement or water motion in general due to e.g. storms and variations in sediment characteristics. Furthermore, on top of sand waves smaller bed forms are assumed to be the cause of the differential movement of the sand waves along the crests. The implementation of stochastic variations will increase the usability of the model and give new insight into the natural variations of the seabed position.

7.4 Sediment grain size

In general, the sediment found in the troughs is slightly finer than that found on the crests of sand waves. This is attributed to the reduction of flow velocity in the troughs and increase near the crests. Both wind waves (in shallower parts) and the larger current velocities will wash away the finer sediments from the top, leaving the coarser sediment behind. Insight into the impact of the sediment characteristics on the value of the slope term will add to the understanding of the stabilising mechanism.

Moreover, insight into this sorting process enables a more efficient mining strategy, when requirements to the type of sediment to be mined exist.

7.5 Additional processes

Lastly, several physical processes can be implemented or refined in the simulation model. They can increase the insight into the behaviour of sand waves and increase the predictive capabilities of the model. Furthermore, it is possible they are necessary to investigate a practical problem having special characteristics with respect to the environment containing the sand waves. An interesting example is the inclusion of a rocky layer. During the evolution of a sand wave in a sandy bed, it can cut into different bed layers, encountering rocky layers. Incorporation of this rocky bed can give insight in how this rocky bed influences the morphology on top of it, given the sediment available (see Aliotta and Perillo [1987]). Other examples of processes are suspended sediment transport, the critical shear stress to bring sediment in motion, the effect of wind waves on the sediment transport and the effect of ripples and mega-ripples on top of sand waves.

Bibliography

Aliotta, S. and Perillo, G.M.E., 1987, A sand wave field in the entrance to Bahia Blanca estuary, Argentina, *Marine Geology*, Vol. **76**, pp. 1-14.

Allen, J.R.L., 1980a, Sand waves: A model of origin and internal structure, *Sediment Geology*, Vol. **26**, pp. 281-328.

Allen, J.R.L., 1980b, Sand wave immobility and the internal master bedding of sand wave deposits, *Geological Magazine*, Vol. **117** (5), pp. 347-446.

Ashley, G.M., 1990, Classification of large-scale subaqueous bedforms: a new look at an old problem, *Journal of Sedimentology Petrology*, Vol. **60** (1), pp. 160-172.

Baptist, M.J., Van Bergen, C.N., Boers, M., Van Heteren, S., Hoogewoning, S., Hulscher, S.J.M.H., Jacobse, J.J., Knaapen, M.A.F., Mulder, J.P.M., Passchier, S., Van der Spek, A.J.F. and Storbeck, F., 2001, Theme 3: Coast and river, Ecomorphodynamics of the seafloor, Progress report 2000, Laban, C., Delft Cluster, The Netherlands.

Belderson, R.H. and Stride, A.H., 1969, Tidal currents and sand wave profiles in the north-eastern Irish Sea, *Nature*, London, Vol. **222**, pp. 74-75.

Bisquay, H. and Ledu, P., 1999, Banc de la Schôle Levé hydrographique: Mission Hydrographique de l'Atlantique, *Marine Sandwave Dynamics*, International Workshop, March 23-24 2000, University of Lille 1, France. Proceedings. Trentesaux A. and Garlan T. Ed, cover.

Blondeaux, P., Brocchini, M., Drago, M., Iovenitti, L., Vittori, G., 1999. Sand waves formation: Preliminary comparison between theoretical predictions and field data, *IAHR symposium on River Coastal and Estuarine Morphodynamics*, Genova, Italy, Proceedings, Vol. **1**, pp. 197-206.

Boggs, S., 1974, Sand wave fields in Taiwan Strait, *Geology*, Vol. **2**, pp. 251-253.

Bokuniewicz, H.J., Gordon, R.B. and Karstens, K.A., 1997, Form and migration of sand waves in a large estuary, Long Island Sound, *Marine Geology*, Vol. **24**, pp. 185-199.

Bos, K.J., Chen, Z. and Bijker, R., 1996, Interactie tussen zandgolven en pijpleidingen, WL—Delft Hydraulics, prepared for the North Sea Directorate, Directorate General for Public Works and Water Management, Report H3016, the Netherlands.

Calkoen, C.J., Hesselmans, G.H.F.M, Wensink, G.J., Vogelzang, J., 2001, The Bathymetry Assessment System, Efficient depth mapping in shallow seas using radar images, *International Journal of Remote Sensing*, Vol. **22**, Nr. 15, pp. 2973-2998.

Canuto, C., Quarteroni, A. and Yousuff Hussaini, M., 1988, Spectral methods in fluid dynamics, ISBN 0-387-17371-4.

Coleman, S.E. and Melville, B.W., 1994, Bed-Form Development, *Journal of Hydraulic Engineering*, Vol. **120**, pp. 544-560.

De Vriend, H.J., 1987, 2DH Mathematical modelling of morphological evolutions in shallow water, *Coastal Engineering*, Vol. **11**, pp. 1-27.

De Vriend, H.J., 1991, Offshore sand banks and sandwaves. MAST-G6M Workshop, Edinburgh, UK.

Dronkers, J., Van Alphen, J.S.L.J. and Borst, J.C., 1990, Suspended sediment transport processes in the Southern North Sea, *Coastal and Estuarine studies*, Vol. **38**, pp. 302-320.

Fenster, M.S., Fitzgerald, D.M., Bohlen, W.F., Lewis, R.S. and Baldwin, C.T., 1990, Stability of giant sand waves in eastern Long Island Sound, U.S.A., *Marine Geology*, Vol. **91**, pp. 207-225.

Fornberg, B., 1996, A Practical Guide to Pseudospectral Methods, Cambridge Monographs on Applied and Computational Mathematics, Vol. 1, University of Colorado, Cambridge University Press.

Fredsøe, J. and Deigaard, R., 1992, Mechanics of coastal sediment transport, Institute of Hydrodynamics and Hydraulic Engineering, Technical University of Denmark, pp. 260-289.

Gerkema, T., 1998, A note on the effect of finite Stokes-layer thickness in a morphodynamic stability problem, In: *Proceedings 8th International Biennial Conference On Physics of Estuaries and Coastal Seas*, Balkema, pp. 387-395.

Gerkema, T., 2000, A linear stability analysis of tidally generated sand waves, *Journal of Fluid Mechanics*, Vol. **417**, pp. 303-322.

Hansen, E.A., 1989, Migration rate minimum and equilibrium heigth of moving sand dunes, *Institute of Hydrodynamics and Hydraulic Engineering*, Progress Report **69**, Technical University of Denmark, pp. 39-46.

Hansen, J.L., Van Hecke, M., Haaning, A., Ellegaard, C., Andersen, K.H., Bogr, T and Sams, T., 2001, Pattern formation: Instabilities in sand ripples, *Nature*, Vol. **410**, pp. 324-325, doi:10.1038/35066631.

Harris, P.T., 1989, Sand wave movement under tidal and wind-driven currents in a shallow marine environment: Adoplhus Channel, north-eastern Australia, *Continental Shelf Research*, Vol. **9**, No. 11, pp. 981-1002.

Hoogewoning, S., 1997, Effecten van grootschalige zandwinning, Verkennend advies ten dienste van globale richtlijnen voor grootschalige zandwinning, Ministerie van Verkeer en Waterstaat, Directoraat-Generaal Rijkswaterstaat, Rijksinstituut voor Kust en Zee/RIKZ, Rapport RIKZ-97.033, Netherlands.

Houbolt, J.J.H.C., 1968, Recent sediments in the Southern Bight of the north Sea, *Geology en Mijnbouw*, Vol. **47** (4), pp. 245-273.

Hulscher, S.J.M.H., 1996. Tidal induced large-scale regular bed form patterns in a three dimensional shallow water model, *Journal of Geophysical Research*, Vol. **101** (C9), pp. 20727-20744.

Hulscher, S.J.M.H. and Van den Brink, G.M., 2001, Comparison between predicted and observed sand waves and sandbanks in the North Sea, *Journal of Geophysical Research*, Vol. **106** (C5), pp. 9327-9338.

Hulscher, S.J.M.H., De Swart, H.E. and De Vriend, H.J., 1993, The generation of offshore tidal sand banks and sand waves, Institute for Marine and Atmospheric Research Utrecht and Delft Hydraulics, *Continental Shelf Research*, Vol. **13**, No. 11. pp. 1183-1204.

Huntley, D.A., Huthnance, J.M., Collins, M.B., Liu, C.L., Nicholls, R.J. and Hewitson, C., 1993, Hydrodynamics and sediment dynamics of North Sea sand waves and sandbanks, *Philosophical Transactions of the Royal Society of London*, Vol. **343**, pp. 461-474.

Huthnance, J., 1982a, On one mechanism forming linear sandbanks, *Estuarine, Coastal and Shelf Science*, Vol. **14**, pp. 79-99.

Huthnance, J., 1982b, On the formation of sand banks of finite extent, *Estuarine, Coastal and Shelf Science*, Vol. **15**, pp. 277-299.

Idier D. and Astruc D., 2001, Numerical modelling of large scale rhythmic bedforms in shallow water, River, Coastal and Estuarine Morphodynamics, IAHR, Obihiro, Japan, pp. 565-574.

Idier D., 2003, Dynamique des bancs et des dunes de sable du plateau continental, Observations in-situ et modélisation numérique, Phd-thesis, L'institut national polytechnique de Toulouse, France.

Johns, B., Soulsby, R.L. and Chesher, T.J., 1990, The modelling of sand wave evolution resulting from suspended and bed load transport of sediment, *Journal of Hydraulic Research*, Vol. **28**, No.: 3 pp. 355-374.

Johnson, M.A., Stride, A.H., Belderson, R.H. and Kenyon, N.H., 1981, Predicted sand-wave formation and decay on a large offshore tidal-current sand-sheet; in: *Special Publications International Association of Sedimentologists*, Vol. **5**, pp. 247-256.

Knaapen, M.A.F. and Hulscher, S.J.M.H., 2002, Regeneration of dredged sand waves, *Coastal Engineering*, Vol. **46** (4), pp. 277-289.

Knaapen, M.A.F., Hulscher, S.J.M.H., De Vriend, H.J., and Stolk, A., 2002, A new type of bedwaves, *Geophysical Research Letters*, Vol. **28**, No 7, pp. 1323-1326, 2001.

Komarova, N.L. and Hulscher, S.J.M.H., 2000, Linear instability mechanisms for sand wave formation, *Journal of Fluid Mechanics*, Vol. **413**, pp. 219-246.

Komarova, N.L. and Newell, A.C., 2000, Non-linear dynamics of sandbanks and sand waves, *Journal of Fluid Mechanics*, Vol. **415**, pp. 285-321.

Lanckneus, J. and De Moor, G., 1991, Present-day evolution of sand waves on a sandy shelf bank, Oceanologica Acta, *Proceedings of the international Colloquium on the environment of epicontinental seas*, Lille, sp. No. 11, pp. 123-127.

Langhorne, D.N., 1981, An evaluation of Bagnolds dimensionless coefficient of proportionality using measurements of sand wave movements, *Marine Geology*, Vol. **43**, pp. 49-64.

Le Bot, S., 2001, Morphodynamique de dunes sous-marines sous influence des marées et des tempêtes. Processus hydro-sédimentaires et enregistrement. Example du Pas-de-Calais, Ph.D. Thesis, Université des Sciences et Technologies de Lille, U.F.R. des Sciences de la Terre, France.

Le Bot, S., Idier, D., Garlan, T., Trentesaux, A., and Astruc, D., 2000, Dune dynamics: from field measurements to numerical modelling. Application to the bathymetric survey frequency in the Calais-Dover Strait, *Marine Sandwave Dynamics*, International Workshop, March 23-24 2000, University of Lille 1, France. Proceedings. Trentesaux A. and Garlan T. Ed, pp. 101-108.

Li, F. and Cheng, L., 1999, Numerical model for local scour under offshore pipelines, *Journal of Hydraulic Engineering*, Vol. **125**, No. 4, pp. 400-406.

Lobo, F.J., Hernandez-Molina, F.J., Somoza, L., Rodero, J., Maldonado, A. and Barnolas, A., 1999, Patterns of bottom current flow deduced from dune asymmetries over the Gulf of Cadiz shelf (southwest Spain), *Marine Geology*, Vol. **164** (2000), pp. 91-117.

Middelkoop, I., 1998, Large scale bed pattern recognition by means of remote sensing, ARGOSS, University of Twente, The Netherlands.

Morelissen, R. Hulscher, S.J.M.H., Knaapen, M.A.F., Németh, A.A. and Bijker, R., 2002, Interacting sand waves and pipelines: a data-assimilation based mathematical model, *Coastal Engineering*, in press.

Munoz-Perez, J.J., Enriquez, J., 1998, Litoral dynamic of a complete physiography unit: Sanlucar-Rota, *Rev. Obras Publicas*, Vol. **3375**, pp. 35-44.

Németh, A.A., 1998, Modelling the dynamic behaviour of sand extraction pits and tidal sandbanks, University of Twente en WL | Delft Hydraulics, projectnr.: Z 2471.

Németh, A.A., Hulscher, S.J.M.H. and Van Damme, R.M.J., 2001, Numerical simulation of sand wave evolution in shallow shelf seas, *Proceedings of the fourth conference on coastal dynamics*, Lund, Sweden, editors Hanson, H. & Larson, M., pp. 1048-1057.

Németh, A.A., Hulscher, S.J.M.H. and Vriend, H.J. de, 2002, Modelling sand wave migration in shallow shelf seas, *Continental Shelf Research*, Vol. **22**/18-19, pp. 2795-2806.

Németh, A.A., Hulscher, S.J.M.H. and Vriend, H.J. de, 2003, Offshore sand wave dynamics, engineering problems and future solutions, *Pipeline and Gas Journal*, Vol. **230** (4), pp. 67-69.

Peters, B.G.T.M., 2000, Large-scale sand extraction offshore, The modelling of large-scale sand extraction pits, University of Twente, MSc. Thesis in Civil Engineering, Netherlands.

Richards, K.J. and Taylor, P.A., 1981, A numerical model of flow over sand waves in water of finite depth, *Geophysical Journal of the Royal Astronomical Society*, Vol. **65**, pp. 103-128.

Rommel, M.C., Hulscher, S.J.M.H., Knaapen, M.A.F, 2003, Prediction of sand wave migration in the Gulf of Cadiz, submitted.

Roos, P.C. and Hulscher, S.J.M.H., 2002, Formation of offshore tidal sand banks triggered by a gasmined bed subsidence, *Continental shelf research*, Vol. **22** (18-19), pp. 2807-2818.

Roos, P.C., Hulscher, S.J.M.H., Peters, B.G.T.M. and Németh, A.A., 2001, A simple morphodynamic model for sand banks and large-scale sand pits subject to asymmetrical tides, IAHR-symposium on River, Coastal and Estuarine Morphology (RCEM), Hokkaido, Japan.

Schüttenhelm, R.T.E., 2000, Grainsize variability and crest stability of a North Sea sand wave in space and time, *Marine Sandwave Dynamics*, International Workshop, March 23-24 2000, University of Lille 1, France. Proceedings. Trentesaux A. and Garlan T. Ed, pp. 189-192.

Schielen, R., Doelman, A and Swart, H.E. de, 1993, On the nonlinear dynamics of free bars in straight channels, *Journal of Fluid Mechanics*, Vol. **252**, pp. 325-356.

Soulsby, R.L., 1990, *Ocean Engineering Science: The Sea*, Vol. **9**, Part A, Chapter 15: Tidal-current boundary layers, Le Mehaute, Bernard, Daniel M. Hanes., pp. 523-566.

Stansby, P.K. and Zhou, J.G., 1998, Shallow water flow solver with non-hydrostatic pressure: 2D vertical plane problems, *International Journal of Numerical Methods in Fluids*, No.: **28**, pp. 541-563.

Stolk, A., 2000, The role of sandwaves in the management of the Netherlands Continental Shelf, *Marine Sandwave Dynamics*, International Workshop, March 23-24 2000, University of Lille 1, France. Proceedings. Trentesaux A. and Garlan T. Ed, pp. 193-197.

Terwindt, J.H.J., 1971, Sand waves in the southern Bight of the North Sea, *Marine Geology*, Vol. **10**, pp. 51-67.

Tobias, C.J., 1989, Morphology of sand waves in relation to current, sediment and wave data along the Eurogeul, North Sea; report GEOPRO 1989.01; Dep. Of Physical Geography, University of Utrecht, The Netherlands.

Van Alphen, J.S.L.J. and Damoiseaux, 1989, A geomorphological map of the Dutch shoreface and adjecent part of the continental shelf, *Geologie en Mijnbouw*, Vol. **68**, pp. 433-444.

Van Maren, D.S., 1998, Sand Waves, A state-of-the-art review and bibliography, North Sea Directorate, Ministry of Transport, Public Works and Water Management, the Netherlands, 118 pp.

Van Rijn, L.C., 1993, Handbook of sediment transport by currents and waves, Delft Hydraulics, Delft, The Netherlands.

Van der Molen, J., 2000, Influence of wind-driven flow on the net transport in the North Sea, In: *Proceedings 10th International Biennial Conference On Physics of Estuaries and Coastal Seas*, VIMS, pp. 285-288.

Wever, T.F. and Stender, I.H., 2000, Strategies for and results from the investigation of migrating bedforms in the German Bight, *Marine Sandwave Dynamics*, International Workshop, March 23-24 2000, University of Lille 1, France. Proceedings. Trentesaux A. and Garlan T. Ed, pp. 221-226.

Whitehouse, R.J.S., Damgaard, J.S. and Langhorne, D.N., 2000, Sand waves and seabed engineering: application to submarine cables, *Marine Sandwave Dynamics*, International Workshop, March 23-24 2000, University of Lille 1, France. Proceedings. Trentesaux A. and Garlan T. Ed, pp. 227-234.

Wilkens, J., 1997, Sand waves and possibly related characteristics, Report for Alkyon Hydraulic Consultancy and Research.

Nomenclature

$*$	meaning the parameter is dimensionless	
$\hat{}$	meaning a cluster of different parameters, used to analyse the dimensionless system	
$2DV$	two dimensions: one horizontal and one vertical	
A	matrix on left hand side containing the time dependent terms of the system in the simulation model	
A_{ls}	variable used in least square method	
A_v	kinematic eddy viscosity	$[m^2\ s^{-1}]$
a_0	function incorporating the vertical structure of the non-periodic component of the solution of the horizontal velocity in the stability analysis	$[-]$
a_s, a_c	functions incorporating the vertical structure of the periodic components of the solution of the horizontal velocity in the stability analysis	$[-]$
b	power of transport in the sediment transport formula	$[-]$
B_{ls}	variable used in least square method	
c	propagation velocity of a wave in shallow water	$[m\ s^{-1}]$
c_0	function incorporating the vertical structure of the non-periodic component of the solution of the vertical velocity in the stability analysis	$[-]$
c_s, c_c	functions incorporating the vertical structure of the periodic components of the solution of the vertical velocity in the stability analysis	$[-]$
c_j	weights for approximation methods	$[-]$
d	mean grain size diameter	$[m]$
d_0	function incorporating the position of the water level of the non-periodic component of the solution in the stability analysis	$[-]$
d_s, d_c	functions incorporating the position of the water level of the periodic components of the solution in the stability analysis	$[-]$
D^{11}	first derivative matrix in the horizontal direction	$[-]$
D^{13}	first derivative matrix in the vertical direction	$[-]$
D^{21}	second derivative matrix in the horizontal direction	$[-]$
D^{23}	second derivative matrix in the vertical direction	$[-]$
D_{ij}	derivative matrix containing elements (i, j)	$[-]$

E_v	measure of influence of the viscosity on the water motion	$[-]$
f_j	function value at a grid point	
FGM	fastest growing mode according to a linear analysis	
g	gravitational acceleration	$[m\,s^{-2}]$
h	position of the seabed with respect to the average water depth	$[m]$
h_{sw}	sand wave height based on data	$[m]$
H	average water depth	$[m]$
$I_N f$	interpolation polynomial	
k	wave number sand wave	$[-]$
K_j	cardinal polynomial	
ℓ_m	morphological length scale	$[m]$
L	wavelength tidal motion	$[m]$
L_{sw}	sand wave length	$[m]$
M_0	steady part in water motion	
M_2	sinusoidal tidal motion (primary lunar constituent)	
N^1	number of intervals in the horizontal direction	$[-]$
N^3	number of intervals in the vertical direction	$[-]$
N_{sw}	number of sand waves in the calculation domain	$[-]$
P	cluster of parameters used to make the pressure gradient dimensionless	$[-]$
r	right-hand side containing the time independent terms of the system in the simulation model	
R	function of the square root of the Reynolds number	$[-]$
s	relative density of sediment	$[-]$
S	resistance parameter	$[m\,s^{-1}]$
S_b	volumetric bedload transport	$[kg\,m^{-2}]$
t	time	$[s]$
T_{long}	long slow timescale used to define morphological timescale	$[s]$
T_m	morphological timescale	$[s]$
T_p	Chebyshev polynomials	
u	velocity in the horizontal direction	$[m\,s^{-1}]$
u_r	steady current in the horizontal direction	$[m\,s^{-1}]$
U	maximum depth-averaged flow velocity	$[m\,s^{-1}]$
V_{sw}	migration rate sand wave	$[m\,s^{-1}]$
w	velocity in the vertical direction	$[m\,s^{-1}]$
x	horizontal coordinate	$[m]$
x_l	grid points	$[m]$
Y	the solution vector of the simulation model (u, w, ζ, h)	
z	vertical coordinate	$[m]$

α	proportionality constant in the sediment transport formula	$[s\, m^{-2}]$
β	to vary the ratio of the steady part and the periodic part, in such a way that the maximum velocity always coincides with the velocity used to scale the system	$[-]$
γ	takes into account that during a tidal cycle sediment is not transported when the critical shear stress is too low	$[-]$
δ	stokes layer thickness	$[m]$
ϵ	ratio sand wave amplitude to average water depth	$[-]$
ζ	position water surface	$[m]$
Θ	critical Shields parameter	$[-]$
λ	combined bed slope factor used when investigating infinitely small sand waves	$[m^2\, s^{-2}]$
λ_1	bed slope factor in bed slope term independent of shear stress at the seabed	$[m^2\, s^{-2}]$
λ_2	bed slope factor in bed slope term depending on shear stress at the seabed	$[-]$
ξ^1	horizontal grid points in computational space	$[-]$
ξ^3	vertical grid points in computational space	$[-]$
ρ	density of water	$[kg\, m^{-3}]$
σ	tidal frequency	$[s^{-1}]$
τ_b	shear stress at the seabed	$[m^2\, s^{-2}]$
τ_w	wind induced shear stress at the sea surface	$[m^2\, s^{-2}]$
ϕ_s	friction angle of sediment	$[^\circ]$
φ	phase shift as solution from the least square method	$[-]$
ψ	solution vector of the stability analysis (u, w, ζ, h)	
ω	dimensionless complex growth rate of an infinitely small perturbation	$[-]$
ω_r	real part dimensionless complex growth rate, depicting the dimensionless growth rate of an infinitely small perturbation	$[-]$
ω_i	imaginary part dimensionless complex growth rate, depicting the angular frequency of an infinitely small perturbation	$[-]$
ω_j	weight functions for approximation methods	

About the Author

Attila A. Németh was born in Haskerland, the Netherlands, on the 26^{th} of March 1976. From 1988 to 1994 he attended the R.S.G. in Heerenveen and received here his V.W.O diploma. Subsequently, he started his academic study in Civil Engineering and Management at the University of Twente in 1994. In 1997, he worked for a period of three months at the Észak-Dunántúli Vizügyi Igazgatóság (North-Transdanubian District Water Authority) in Hungary for a traineeship. He conducted his final masters project on tidal sandbanks and sand extraction pits at WL | Delft Hydraulics and the University of Twente for the Rijksinstituut voor Kust en Zee (RIKZ, National Institute for Coastal and Marine Management) and recieved his masters degree in 1998. From the end of 1998 to 2003 he conducted his Ph.D. research at the department of Civil Engineering at the University of Twente and is working there at this moment as a Post Doc.